1982

Irreversible cooperative processes on lattices

David Ray Burgess
Iowa State University

Burgess, David Ray

IRREVERSIBLE COOPERATIVE PROCESSES ON LATTICES

Iowa State University PH.D. 1982

Irreversible cooperative processes on lattices

by

David Ray Burgess

A Dissertation Submitted to the

Graduate Faculty in Partial Fulfillment of the

Requirements for the Degree of

DOCTOR OF PHILOSOPHY

Department: Chemistry
Major: Physical Chemistry

Approved:

Signature was redacted for privacy.

In Charge of Major Work

Signature was redacted for privacy.

For the Major Department

Signature was redacted for privacy.

For the Graduate College

Iowa State University
Ames, Iowa

1982

TABLE OF CONTENTS

1. INTRODUCTION AND LITERATURE REVIEW

This thesis develops kinetic models for irreversible cooperative processes on lattices. The models describe processes on one, two or three dimensional lattices with any finite range cooperative effect. Models of an Ising nature are not applicable since there is no equilibrating mechanism for events (equilibrium is never established).

The microscopic description of poly(methyl vinyl)ketone condensation (1) (see Figure 1.1) is an example of an irreversible process that occurs on a lattice. The one-dimensional (1-D) lattice sites have been chosen in two different ways in Figure 1.1 corresponding to an "atomic" or an "event" lattice description of the process. Occurrence of an event changes the state of a single site on the event lattice, but changes the state of more than one site (simultaneously) on the atomic lattice. The process of Figure 1.1 may be regarded as a dimer filling process since two nearest neighbor (n.n.) atomic sites are simultaneously changed. Notice that a dimer process on the 1-D atomic lattice corresponds to a process where monomer events occur with n.n. blocking on the 1-D event lattice (2).

There are many other processes from diverse areas of chemistry and physics that can be regarded as occurring irreversibly at the sites of a lattice (e.g., see Figure 1.2-1.4). Several of these will be treated in later chapters of this thesis.

For cooperative processes, the probability of an event occurring depends on the state of neighboring lattice sites within the cooperative

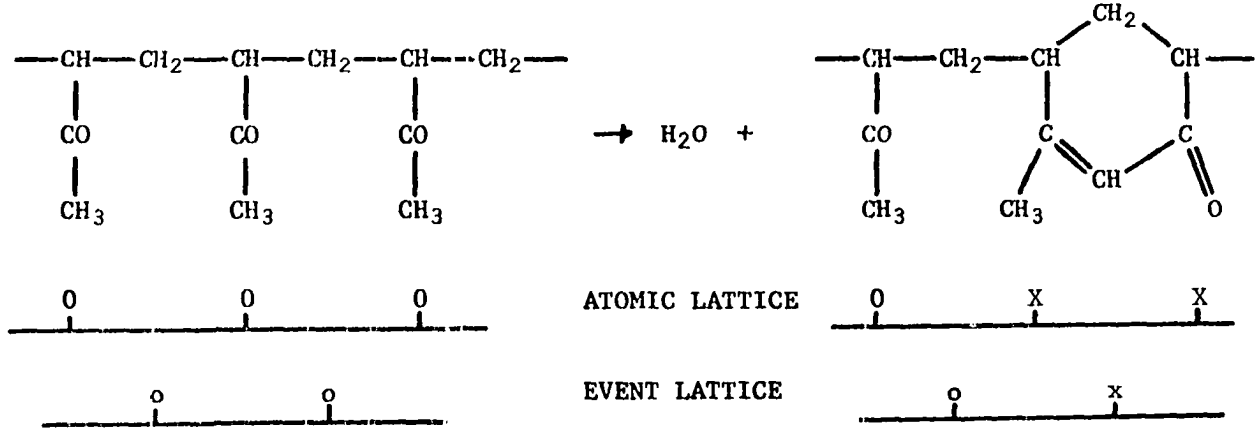

Figure 1.1. Poly(methyl vinyl)ketone condensation (1)

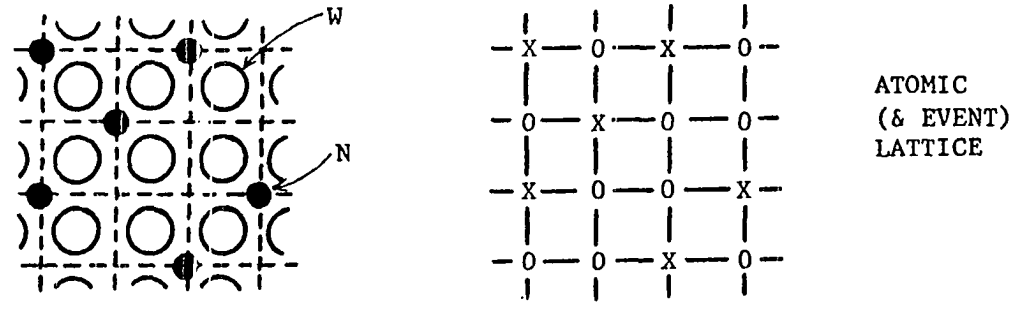

Figure 1.2. Immobile chemisorption of nitrogen on the (100) face of tungsten (3)

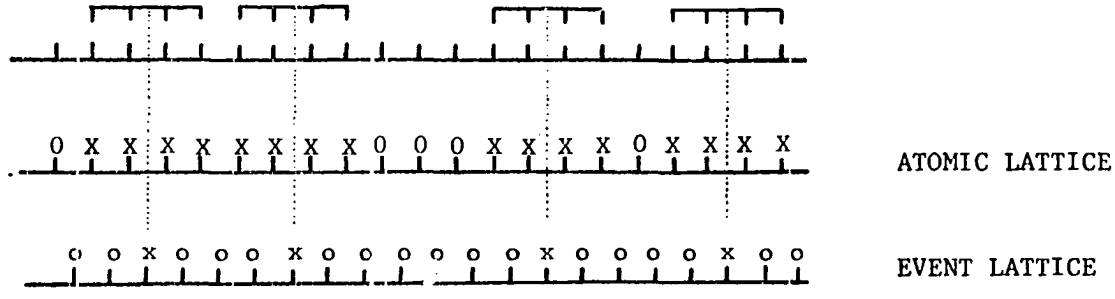

Figure 1.3. Binding of large ligands to polynucleotides and polypeptides (4)

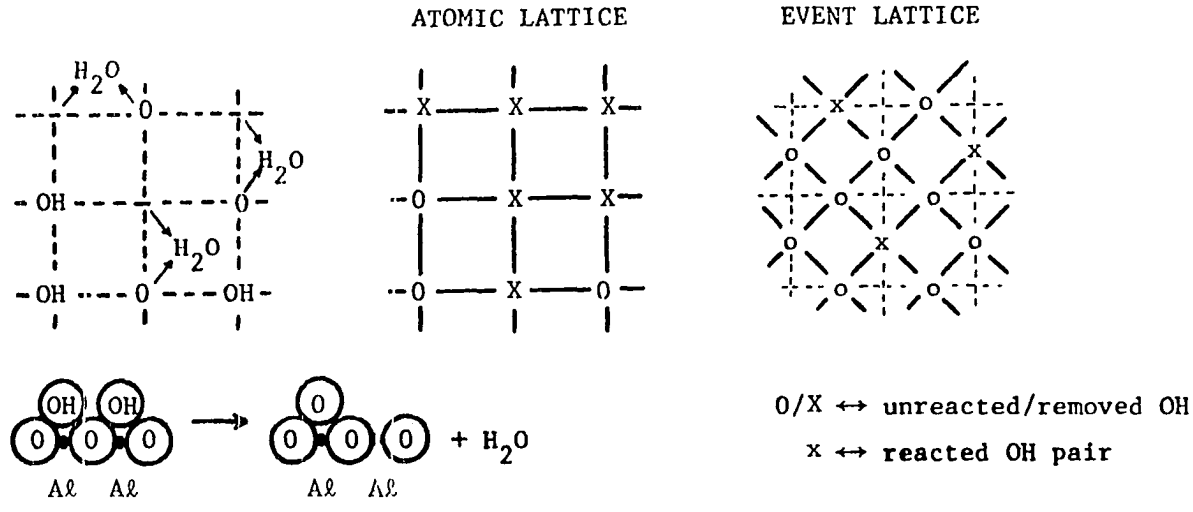

Figure 1.4. Dehydration of γ-alumina (5)

range. Attractive (enhancing) cooperative effects cause clustering of events to occur, while repulsive (inhibiting) cooperative effects also create distinctive distributions which are not random in nature. Various terms will be used to describe the state of a lattice site including reacted/unreacted, occupied(full)/empty, and damaged/undamaged, depending on the physical situation.

The probability of an event taking place on a site is indicated by a rate. The number of rates needed to account for configurational interactions corresponds to the number of different ways full and empty sites can be arranged within the cooperative range (some rates may be the same due to symmetry). On a uniform 1-D event lattice with reflection symmetry and n.n. cooperative effects there are three such rates. These are illustrated in Figure 1.5 where x denotes a full site, o denotes an empty site and • indicates the site to be occupied (always empty). These rates are given the symbols $\tau_{x\bullet x}$, $\tau_{o\bullet x}$ and $\tau_{o\bullet o}$ going from

x•x o•x o•o

Figure 1.5. Possible configurations for R=1 in 1-D

left to right in Figure 1.2, respectively. In general, the cooperative effects are not just n.n. and all sites within the cooperative region, R^i, of the site of interest, i, must be designated empty or full. This configuration about i is given the symbol $\underset{\sim}{g}^i$. In 1-D, it is possible to speak of the configuration of sites on the left of the site of interest,

$\underset{\sim}{\sigma}_L^i$, and the configuration of sites on the right of the site of interest, $\underset{\sim}{\sigma}_R^i$. The total configuration is $\underset{\sim}{\sigma}^i$ as illustrated in Figure 1.6 for R=3.

$\underset{\sim}{\sigma}^i$

$\_\_\_$ oxo•xxo $\_\_\_\_$

$\underset{\sim}{\sigma}_L^i$ i $\underset{\sim}{\sigma}_R^i$

Figure 1.6. One configuration about the site of interest i for R=3

The rate is then written as $\tau_{\underset{\sim}{\sigma}^i}=\tau_{\underset{\sim}{\sigma}_L^i \cdot \underset{\sim}{\sigma}_R^i}$ (e.g., for the specific configuration of Figure 1.6 the rate is written $\tau_{oxo\cdot xxo}$).

In two-dimensions it is possible to designate the cooperative range by the distance through bonds (i.e., the number of lattice vectors) from the site of interest (R^1) or by the actual distance (R^2), depending on the microscopic origin of cooperativity. Figure 1.7 shows the sites within the cooperative ranges $R^1=R^2=1$, $R^1=2$ and $R^2=\sqrt{2}$ for a 2-D square lattice. The rates are again written $\tau_{\underset{\sim}{\sigma}^i}$ where $\underset{\sim}{\sigma}^i$ is the configuration of sites within the interaction range of site i. The extension to three-dimensions is obvious.

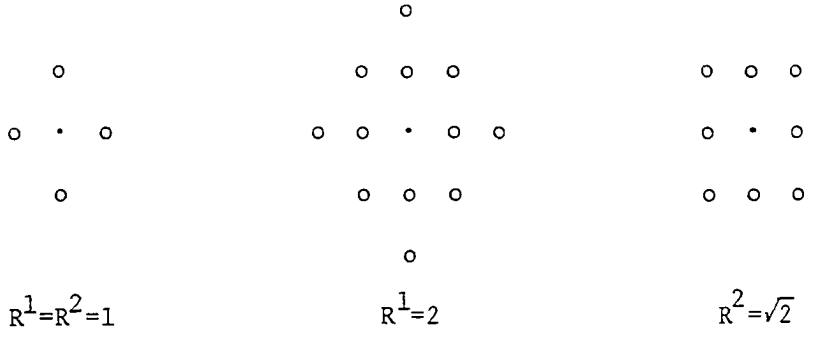

Figure 1.7. Cooperative ranges for $R^1=R^2=1$, $R^1=2$ and $R^2=\sqrt{2}$

Either the probability of finding a configuration $\underset{\sim}{\alpha}$ on the atomic lattice, $P(\underset{\sim}{\alpha})$, or the probability of finding a configuration $\underset{\sim}{\sigma}$ on the event lattice, $f(\underset{\sim}{\sigma})$, may be used to describe the kinetics of a lattice process. Both will be used in this thesis, but the remainder of this section will deal with the event lattice description. The state of a particular site j will be denoted by σ_j where $\sigma_j=x$ indicates a full site and $\sigma_j=o$ indicates an empty site. Further, let i be a filled site in $\underset{\sim}{\sigma}$ and $\underset{\sim}{\sigma}(\sigma_i \to o)$ be the configuration obtained from $\underset{\sim}{\sigma}$ by changing the state of i to empty. The probability of finding $\underset{\sim}{\sigma}$ is increased by an event occurring at the ith site of $\underset{\sim}{\sigma}(\sigma_i \to o)$ and decreased by an event occurring on any empty site in $\underset{\sim}{\sigma}$. The probability of these events occurring is influenced by those sites within the cooperative interaction range. It is possible for some of these influential sites to not be in $\underset{\sim}{\sigma}$, so the symbol $\underset{\sim}{\sigma}^j_*$ is introduced to describe the configuration of sites within the cooperative range of j that are not in $\underset{\sim}{\sigma}$. The kinetic equation describing the change of configurational probability with time is

$$d/dt\ f(\underset{\sim}{\sigma}) = \sum_{\substack{j\in\underset{\sim}{\sigma} \\ \sigma_j=x}} \sum_{\underset{\sim}{\sigma}^j_*} \tau_{\underset{\sim}{\sigma}^j}\ f(\underset{\sim}{\sigma}(\sigma_j\to o) + \underset{\sim}{\sigma}^j_*) \qquad \text{Gain}$$

$$- \sum_{\substack{j\in\underset{\sim}{\sigma} \\ \sigma_j=o}} \sum_{\underset{\sim}{\sigma}^j_*} \tau_{\underset{\sim}{\sigma}^j}\ f(\underset{\sim}{\sigma} + \underset{\sim}{\sigma}^j_*) \qquad \text{Loss}$$

$$= - \sum_{j\in\underset{\sim}{\sigma}} (-1)^{\sigma_j} \sum_{\underset{\sim}{\sigma}^j_*} \tau_{\underset{\sim}{\sigma}^j}\ f(\underset{\sim}{\sigma}(\sigma_j\to o) + \underset{\sim}{\sigma}^j_*) \qquad (1.1)$$

where $(-1)^o \equiv 1$ and $(-1)^x \equiv -1$.

It is often convenient to consider the probabilities as functions of event coverage, $\theta=f(x)$, rather than time. The time dependence is eliminated and the θ dependence introduced when Equation 1.1 is divided by $df(x)/dt$ (i.e., $df(\underset{\sim}{c})/d\theta=df(\underset{\sim}{c})/dt/df(x)/dt$).

It is also often desirable to transform those probabilities of configurations containing full sites to probabilities of configurations with only empty or unspecified sites (2). This can be done by using the following procedure. Let $\{n\}_x$ and $\{n\}_o$ denote a subconfiguration of n sites specified occupied and empty respectively. A general configuration $\underset{\sim}{c}$ may be decomposed as $\underset{\sim}{c}=\{m\}_o + \{n\}_x$ and $f(\underset{\sim}{c})$ may be expressed as

$$f(\{m\}_o + \{n\}_x) = \sum_{\{\ell\}\subset\{n\}} (-1)^{\ell} f(\{m\}_o + \{\ell\}_o) \quad . \tag{1.2}$$

Equation 1.2 follows from conservation of probability. Two specific examples are

$$f(x) = 1 - f(o) \tag{1.3}$$

$$f\left(\overset{x}{\underset{x}{o}}o\right) = f\left(oo\right) - f\left(ooo\right) - f\left(\overset{o}{\underset{o}{o}}o\right) + f\left(o\overset{o}{\underset{o}{o}}o\right) \quad . \tag{1.4}$$

Equation 1.1 provides a set of coupled differential equations. The set is infinite on an infinite lattice and finite on a finite lattice. This thesis treats the structure of these equations and describes the general conditions necessary to exactly solve the hierarchy. Some methods that may be used to approximately truncate the hierarchy and many examples of specific applications are also given.

Chapter two gives a simple illustrative example and then describes some general results. Some other results, mostly of a review nature, are then described to set the stage for later work. Chapter three reports some interesting new results and applications of the 1-D model including correlation functions, nonequilibrium entropy, multi-species adsorption and limited mobility. The hierarchy equations in 2-D will be treated in Chapter four. Chapters five through seven deal with specific physical problems such as polymer reactions, surface phenomena and radiation effects on crystals.

The rest of this chapter reviews the current literature. The review begins with a short description and analysis of the noncooperative case and then describes work on the cooperative models in a chronological manner. Some papers which deal with specific systems will not be reviewed here, but will be discussed in relevant subsequent chapters. If the reader is not interested in such a general review, he may go to Chapter two where a description of the kind of modeling used in this thesis may be found.

1.1. Noncooperative Models

Although this thesis is mainly concerned with cooperative problems it is necessary to discuss some noncooperative models to gain a better perspective into the methods used to solve the cooperative cases. Wolf (2) provides an excellent review of this material. This section will address important aspects of that work and include some references not mentioned by Wolf.

The earliest treatment of a space (lattice) filling problem is Flory's (1) 1939 analysis of the condensation reaction of neighboring ketone groups of poly(methyl vinyl)kentone (see Figure 1.1). He noted that reaction of any neighboring group reduces the original problem to two smaller ones. This reasoning results in a recursion relation for the difference between the average number of unreacted sites per molecule of length n at the end of the reaction and for that of a molecule of length n-1. This allows the problem to be solved for the fraction of unreacted sites at the end of the process. He gave this value as exactly exp(-2) for an infinite lattice.

Cohen and Reiss (6) in 1963 extended the method of Flory to obtain integral equations which may be exactly solved for various empty site configuration probabilities using generation function techniques. Their model for a finite lattice does not properly account for end effects, but gives correct results in the limit of an infinite lattice. Page (7), McQuistan and Lichtman (8), Widom (9), Barron and Boucher (10), Downton (11), Wolf (2) and Olson (12) have also treated the noncooperative dimer problem.

Boucher (13) specifically treated the trimer event problem. He derived kinetic equations for the probabilities of various configurations of empty sites on finite lattices. Recurrence relations, generating functions or a combination of these may be used to solve the equations. Time dependent results are given. He reports the fraction of empty sites to be approximately 0.17635 at the end of the process. He also reports the fraction of paired empty sites at the end of the

process to be exactly $2e^{-3}$. The problem of an n-mer event on a finite lattice has also been treated in a similar manner by Gordon and Hillier (14), Boucher (15), MacKenzie (16) and Wolf (2).

1.2. Cooperative Models

Various polymer reactions have provided motivation to pursue the irreversible, cooperative lattice model. Keller (17), in 1962, observed several polymer reactions which have n.n. effects. He developed equations for the average fractions of unreacted sites having zero, one or two reacted n.n. The equations were closed by assuming the rate of reaction of the end site of three consecutive empty sites as a weighted average of the cases where the end site has an unreacted n.n. and where it has a reacted n.n.

In 1963, Alfrey and Lloyd (18) considered the cooperative, irreversible model on a finite "ring" lattice by introducing a complete set of equations describing unreacted sequences of varying length. They also considered the infinite chain model, exactly solved it for one special case and presented approximate methods of solution for other cases.

Arends (19), in a companion paper to that of Alfrey and Lloyd, obtained an exact solution for the kinetic equations describing the rate of change in the numbers of the various sequence lengths and the number of unreacted sites. He gave the particularly simple expression, $\exp[-\tau_{o\cdot o}t]$, for the conditional probability of finding an empty site at the right of two consecutive empty sites, where $\tau_{o\cdot o}$ is the rate for an event ocurring between two empty sites. This significant result will

appear in most of the models discussed in this section. Keller (20), also in 1963, published a second paper showing that Arends' solution can be obtained by solving Alfrey and Lloyd's equations and that all of these results verified the hypothesis of his previous paper.

In 1965, McQuarrie et al. (21) described the irreversible kinetics of denaturation or renaturation in an exact manner using a n.n. cooperative model as suggested by the Zimm and Bragg (22) statistical mechanical treatment of the equilibrium thermodynamic properties of polypeptides. They exactly solved the hierarchy of equations for the total number of n-tuples (configurations of n consecutive empty sites). The solutions are given succinctly in terms of incomplete gamma functions.

Six years later, in 1971, Schwartz (23) analyzed the general cooperative kinetics on a linear Ising lattice. In his discussion of the nonequilibrium case, he postulated the "triplet closure rule" which has been shown to be only an approximation for truncating conditional probabilities (2). Schwartz also emphasized the the Gō-Kikuchi theory (24,25) (a path integral formalism) is essentially equivalent to the (approximate) triplet closure rule.

Boucher (26), in 1972, extended the irreversible finite lattice model with n.n. cooperative effects from monomer to n-mer events. An asymptotic analysis provided results for the infinite lattice. A table listing the fraction of sites left vacant at the end of the filling process for selected n-mer events is given.

In 1974, Gonzalez et al. (27) again solved the n-mer event problem. They modeled the process as an event occurring which blocked a specified number of nearby sites, n-1, from reacting and was influenced by the

state of the n-th site. This corresponds to an n-mer event with n.n. cooperative interaction. They directly solve a hierarchy of kinetic equations for the average densities of various length sequences of unreacted sites. Finite lattice effects are also examined by using a generating function technique. Special cases for n.n. effects are analyzed and the continuum limit of Renyi is obtained.

By the mid-1970s, it was realized that probability distributions for occupied sites were not obtainable from those for empty n-tuples. Several authors (28-33) proposed models to obtain these filled distributions. Of this group only Platé et al. (32) correctly described the general procedure for obtaining all probabilities for a n.n. cooperative process which are needed to exactly find occupied site probabilities. As an example, to calculate P(oxo) it is necessary to know P(o_o) which in turn requires P(oo_o) and P(oo_oo). After truncation, the three kinetic equations for these probabilities are closed upon themselves and the consecutively empty configurations previously described. To calculate other occupied probabilities the hierarchy must again be extended to include configurations with two unspecified sites between the empty sites by adding the equations for P(o_ _o), P(oo_ _o) and P(oo_ _oo). This process may be continued to describe any singly disconnected configurations in analytic form. This process of hierarchy extension is diagramed in Figure 1.8 where the equations for all configurations above and to the left of a configuration of interest must be known. (To calculate P(oo_o) requires P(oo_oo), P(ooo), P(oo) and P(o) to be known but not P(o_o).) It is pointed out

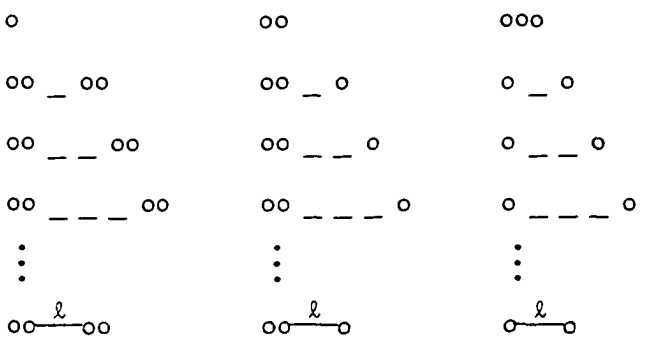

Figure 1.8. Configuration hierarchy for singly disconnected clusters of empty sites (see text)

by Platé et al. (32) that configurations with multiple disconnections (e.g., o_o_o) require repeated recursive integration to determine their probabilities. The recursive integration is performed on hierarchies of kinetic equations for multiply disconnected configurations which are extended as in the singly disconnected case and require all previously determined configurations. Platé et al. also discuss Markovian approximations and show all but the first order Markovian approximation to be quite accurate when compared to the exact result.

One way to generalize the above problem is to allow more than one kind of event to occur. This general topic is treated in Chapter three. One special case of this generalization where an initial event (A) takes place and terminates then a second event (B) is allowed to occur was discussed by Hemmer and Gonzalez (34) in 1977 to describe neighboring group effects in repeated oxidations of polysaccharides. They performed a periodate oxidation experiment with polysaccharides which cause inhibitory effects due to hemiacetal formation. This was event A. They then removed the hemiacetals allowing further oxidation on the unreacted

sites but not allowing any second reactions on the initially reacted sites. The second oxidation was then performed (event B) without any cooperative effects from the sites reacted by event A. Only n.n. cooperative effects were considered in their model. These workers use an exact method called the "principle of independence of unreacted neighbors" to truncate the hierarchy. This principle is applicable to finite, semi-infinite or infinite lattices with n.n. cooperative effects. For single event processes, it may be stated as follows:

> The probability of any subconfiguration with two consecutive empty sites is a product of probabilities for the corresponding subconfigurations on the smaller lattices obtained by a partition of the original lattice between the unreacted site.

It is important to appropriately describe the rate of an event occurring on the newly created end site when using this rule.

Another generalization of the basic lattice model is to consider the lattice to be composed of more than one kind of site. This model has been treated by Gonzalez and Hemmer (35-38) to describe n.n. cooperative reactions on copolymers. They consider periodic and nonperiodic sequences. For the nonperiodic lattices, they consider random, Markovian and second-order Markovian copolymers. They also separately consider the cases where only one monomer event is cooperative and where both types of units exert different cooperative effects.

The most recent articles describing these kinetic models were written by Epstein (4,39) (in 1979) and Wolf et al. (3) (in 1980). They both consider hierarchies with only empty site configurations. Epstein considered large-ligand binding and analyzed both the non-

cooperative and cooperative cases on an infinite lattice. His approach was the same as Cohen and Reiss, including the same incorrect description of end effects on the finite lattice. In his work, concise expressions are given, including the general expression for the final covering fraction. The role of the shielding condition in the solvability may also be clearly seen. The case of competitive binding of different size ligands is also treated.

The continuous analog of these problems has also been considered (the so-called "parking problem"). In this case, intervals of fixed length, r, are placed randomly on a continuous line (as opposed to a discrete lattice). This may be thought of as decreasing the spacing between lattice sites while keeping the blocking length constant. This clearly shows the continuous case to be a limit of the discrete case (2). Rényi (40) first treated the parking problem by direct analysis of the distributions.

The number of 2-D and 3-D analyses is significantly smaller than the volume of 1-D studies just discussed. The random dimer filling problem on a square lattice has been studied by Peri (41), Rossington and Borst (42) and Vette et al. (43) who give the final surface coverages as 0.904, 0.909 and 0.902, respectively. Vette et al. also report values for the hexagonal (0.880) and triangular (0.915) lattices. The relationship between adsorption of squares on a square lattice and n-mers on a linear lattice has been examined by Blaisdell and Solomon (44). They found that the generalized Palasti conjecture (45), which says that the packing density for the 2-D problem is the square of that

for the 1-D lattice, is only approximate. Other 2-D work dealing with specific physical system will be discussed in Chapter six.

Jackson and Montroll (46) considered random dimer formation in 3-D. They used a simplified statistical model where average concentrations of unreacted sites are calculated. They report the fraction of unreacted sites to range from 0.14 for a simple cubic lattice to 0.10 for a face-centered cubic lattice.

Wolf et al. (3) describe the immobile adsorption of nitrogen atoms from an energetic precursor state onto the (100) face of tungsten. They introduce conditional probabilities and clearly demonstrate the relationship between truncation of the hierarchy and the shielding condition which will be further discussed in Chapter two. An ordered filling limit which causes all sites without any nearest neighbors to fill before sites with one n.n. and sites with only one n.n. to fill before sites with two n.n. is thoroughly discussed. The corresponding 2-D problem is also considered. An extensive review of the methods used by Wolf (2) and extensions of this theory are given in Chapter two.

Very little has been published about irreversible, cooperative lattice models in higher dimensions. Hoffman (47) has derived and solved kinetic equations governing the distribution of adatoms resulting from irreversible, dissociative adsorption of homonuclear diatoms onto a 2-D lattice. The rate constants were assumed to be of an Arrhenious form and the solution is expressed as a power series in the covering fraction with

coefficients involving molecular cluster diagrams similar to those in equilibrium virial expansions. An analysis of many features of the general model, including shielding, has recently been given (48).

2. GENERAL MODEL

The irreversible cooperative models of Section 1.2 have many applications. Some of these have been treated previously, but in some cases the workers seem to not be aware of one another's efforts. This chapter will cover three areas. First, a simple example of the kinetic equations for certain 1-D, irreversible cooperative lattice processes and various modifications of these will be given. The second section will present some general results that will place the approaches previously discussed into a common framework and extend their applicability. The last section will briefly outline the cases where solutions can be extracted using a shielding condition.

2.1. The 1-D Lattice with n.n. Cooperative Effects

The presentation of this example is essentially the same as that given by Wolf (2), thus some details have been omitted. The reader is referred to Reference 2 for those details.

Consider an infinite linear lattice composed of equivalent, equally spaced sites where a single type of irreversible event occurs with n.n. cooperative effects. Also assume that the probability of an event occurring on a site within time dt can be written as $\rho(t)\tau_{\sigma\cdot\sigma'}\,dt$, where $\rho(t)$ is the source density (e.g., procursor density of adatoms for chemisorption) and $\tau_{\sigma\cdot\sigma'}$ is time independent. Reflection symmetry is assumed in this example so that $\tau_{\sigma\cdot\sigma'}=\tau_{\sigma'\cdot\sigma}$. A transformation to the chemical time scale $d\hat{t}=\rho(t)\,dt$ is assumed throughout this thesis.

Wolf assumes the lattice to be initially empty. Thus, at t=0 the probability of any configuration of empty sites is unity. This corresponds, for example, to a completely unreacted polymer chain. The time rate of change for the probability of finding a single empty site is (cf., Equation 1.1)

$$d/dt\ f(o) = -\tau_{o\cdot o} f(ooo) - 2\tau_{o\cdot x} f(oox) - \tau_{x\cdot x} f(xox) \qquad (2.1)$$

where the condition of each site is indicated in parentheses. The kinetic equations for probabilities of n consecutive empty sites are (after using Equation 1.2 to transform to all empty configurations)

$$d/dt\ f(1) = -\tau_{o\cdot o} f(3) - 2\tau_{o\cdot x}[f(2)-f(3)] - \tau_{x\cdot x}[1-2f(2)+f(3)] \qquad (2.2)$$

and

$$d/dt\ f(n) = -(n-2)\tau_{o\cdot o} f(n) - 2\tau_{o\cdot x} f(n) - 2(\tau_{o\cdot o}-\tau_{o\cdot x}) f(n+1),\ n\geq 2, \qquad (2.3)$$

where f(n) is the probability for an empty n-tuple of sites. Note that for every n the equation for f(n) has a term involving f(n+1). Equation 2.6 is thus an infinite set of coupled differential equations.

This infinite set of equations can be truncated by introducing the conditional probability

$$q_n = f(n+1)/f(n) \qquad (2.4)$$

which is the probability of an empty site given n adjacent empty sites.

Equations 2.2 and 2.3 can now be written in terms of conditional probabilities as

$$d/dt\ q_1 = -2(\tau_{o\cdot x}-\tau_{x\cdot x})q_1-2(\tau_{o\cdot o}-\tau_{o\cdot x})q_1q_2+2(\tau_{o\cdot x}-\tau_{x\cdot x})q_1^2$$
$$+(\tau_{o\cdot o}-2\tau_{o\cdot x}+\tau_{x\cdot x})q_1^2q_2 \qquad (2.5)$$

and

$$d/dt\ q_n = -\tau_{o\cdot o}q_n-2(\tau_{o\cdot o}-\tau_{o\cdot x})(q_nq_{n+1}-q_n^2),\ n\geq 2\ . \qquad (2.6)$$

It is clear that given the boundary conditions ($q_n=q_2=1$ at $t=0$) $q_n=q_2$, $n\geq 2$, is a unique solution of these equations. This independence of n will be referred to as shielding (the idea of shielding is illustrated by letting $q_n=qo[n]$ and observing that $qo[oo\underset{\sim}{g}]=qo[oo]$ independent of $\underset{\sim}{g}$).

Substituting $q_n=q_2$ for $n\geq 2$ into Equation 2.6 gives

$$q_2 = \exp(-\tau_{o\cdot o}t)\ . \qquad (2.7)$$

This is the same result originally found by Arends (19) and allows q_1 and all other probabilities to be expressed analytically.

2.2. General Results for Empty Site Configurations

General results for empty site configurations on lattices of general dimension and general cooperative effects are now developed. The set of kinetic equations for configurations where only empty or

unspecified sites appears on the left hand side is (cf., Equation 1.1)

$$d/dt\ f(\underset{\sim}{\sigma}) = -\sum_{\substack{j\in\underset{\sim}{\sigma} \\ \sigma_j=0}} \sum_{\underset{\sim}{\sigma}^j_*} \tau_{\underset{\sim}{\sigma}j}\ f(\underset{\sim}{\sigma} + \underset{\sim}{\sigma}^j_*) \ . \tag{2.8}$$

An equivalent hierarchy can be written by using

$$q\ \underset{\sim}{\sigma}[\underset{\sim}{\sigma}'] = f(\underset{\sim}{\sigma} + \underset{\sim}{\sigma}')/f(\underset{\sim}{\sigma}') \tag{2.9}$$

which is the conditional probability of configuration $\underset{\sim}{\sigma}$ given the adjacent configuration $\underset{\sim}{\sigma}'$. The expression $\underset{\sim}{\sigma} + \underset{\sim}{\sigma}'$ means the union of the two individual configurations. Also, $\underset{\sim}{\sigma}$ is called the conditioned configuration and $\underset{\sim}{\sigma}'$ is called the conditioning configuration.

Differentiating the natural logarithm of Equation 2.9 with respect to time yields

$$d/dt\ \ell n\ q\ \underset{\sim}{\sigma}[\underset{\sim}{\sigma}'] = \frac{1}{f(\underset{\sim}{\sigma}+\underset{\sim}{\sigma}')}\ d/dt\ f(\underset{\sim}{\sigma}+\underset{\sim}{\sigma}') - \frac{1}{f(\underset{\sim}{\sigma}')}\ d/dt\ f(\underset{\sim}{\sigma}') \ . \tag{2.10}$$

Equation 2.8 then gives

$$d/dt\ \ell n\ q\ \underset{\sim}{\sigma}[\underset{\sim}{\sigma}'] = -\sum_{j\in\underset{\sim}{\sigma}+\underset{\sim}{\sigma}'} \sum_{\underset{\sim}{\sigma}^j_*} \tau_{\underset{\sim}{\sigma}j}\ \frac{f(\underset{\sim}{\sigma}+\underset{\sim}{\sigma}'+\underset{\sim}{\sigma}^j_*)}{f(\underset{\sim}{\sigma}+\underset{\sim}{\sigma}')}$$

$$+ \sum_{j\in\underset{\sim}{\sigma}'} \sum_{\underset{\sim}{\sigma}^j_*} \tau_{\underset{\sim}{\sigma}j}\ \frac{f(\underset{\sim}{\sigma}'+\underset{\sim}{\sigma}^j_*)}{f(\underset{\sim}{\sigma}')} \ . \tag{2.11}$$

The ratios of probabilities can be expressed as conditional probabilities to obtain

$$d/dt\ \ell n\ q\ \underset{\sim}{\sigma}[\underset{\sim}{\sigma}'] = -\sum_{j\varepsilon\underset{\sim}{\sigma}+\underset{\sim}{\sigma}'}\ \sum_{\underset{\sim}{\sigma}^j_*}\ \tau_{\underset{\sim}{\sigma}j}\ q\ \underset{\sim}{\sigma}^j_*[\underset{\sim}{\sigma}+\underset{\sim}{\sigma}']$$

$$+\sum_{j\varepsilon\underset{\sim}{\sigma}'}\ \sum_{\underset{\sim}{\sigma}^j_*}\ \tau_{\underset{\sim}{\sigma}j}\ q\ \underset{\sim}{\sigma}^j_*[\underset{\sim}{\sigma}'] \ . \qquad (2.12)$$

This result is used extensively in Chapter four where the 2-D system is discussed. Any conditional probabilities that may arise on the right hand side of Equation 2.12 with full conditioned sites may be transformed to expressions with only empty sites using Equation 1.2. As an illustration of Equation 2.12, the equation for qo[oo] is written for n.n. cooperative effects in 1-D as

$$d/dt\ \ell n\ qo[oo] = -\tau_{o\cdot o}-2(\tau_{o\cdot o}qo[ooo]+\tau_{o\cdot x}qx[ooo])$$

$$+2(\tau_{o\cdot o}qo[oo]+\tau_{o\cdot x}qx[oo]) \ . \qquad (2.13)$$

After setting qx[ooo]=1-qo[ooo], qx[oo]=1-qo[oo] and rearranging, Equation 2.13 is found to be Equation 2.6 for n=2. Equation 2.12 is, of course, general and independent of dimension and cooperative interaction range.

The shielding condition will now be discussed in a more general context. It is possible to show from the hierarchy equations that in systems with finite range cooperative effects, an exact "shielding condition" exists for walls of sites specified empty. This condition has the following general form:

> Consider a wall of sites specified empty dividing the system into two disconnected regions. Suppose the wall is sufficiently thick that an event occurring at a site within the wall is not simultaneously affected by the state of sites on both sides. Such a wall shields sites on one side from the influence of those on the other (provided the initial conditions incorporate this independence).

For certain 1-D systems, this condition leads to exact truncation and solution in closed form of the hierarchy as previously shown. For other systems, it provides a basis for approximate truncation of the infinite hierarchy. If, in the 1-D model, cooperative effects are specified to be of range R, then a shielding wall of thickness 2R is required. This terminology is used in higher dimensions even though the definition of wall thickness must be made explicit for each lattice geometry and rate specification. A shielding condition is not available for occupied sites (this sort of asymmetry between empty and occupied sites is not present in equilibrium distributions as discussed in Section 3.2).

In order to firmly establish the shielding condition concept, some examples will now be given. The simplest cases occur in 1-D. Equations 2.14 illustrate shielding for R=1, R=2 and R=3 in 1-D.

$$\begin{aligned} &q_o[oooxo] = q_o[oo], \quad R=1 \\ &q_o[ooooxxo] = q_o[oooo], \quad R=2 \\ &q_o[oooooooxox] = q_o[oooooo], \quad R=3 \end{aligned} \tag{2.14}$$

For a ring lattice, it is necessary to have two blocks of 2R consecutive empty sites in order to completely disconnect the lattice. Equations 2.15 provide examples for the ring lattice when R=1 and R=2. The site

outside of the brackets is the conditioned site and the sites within the brackets are the conditioning sites.

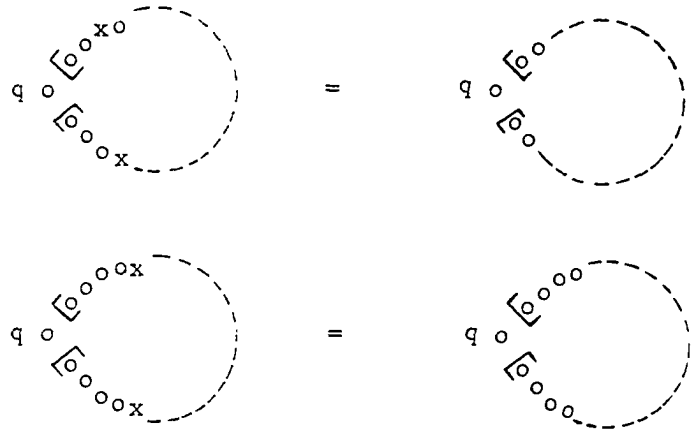

(2.15)

In 2-D, the shielding wall must be of infinite length or connect back on itself. Figure 2.1a illustrates a shielding wall for the 2-D $R^1=1$ case, while Figure 2.1b illustrates a portion of a shielding wall for 2-D $R^1=2$ and $R^2=\sqrt{2}$. That an event within the wall is not influenced simultaneously by sites on both sides of the wall is also pointed out in Figure 2.1b for the $R^2=\sqrt{2}$ case (above) and the $R^1=2$ case (below).

The geometry of the lattice will dictate characteristic shapes of the shielding wall. Some generic examples are given in Figure 2.2. Isolated sublattices such as the one in the center of the 2R shielding wall of Figure 2.2b are described by a finite number of conditional probability equations. It is of interest that the configuration of the surrounded sites has no influence on the rest of the lattice. In the same way, the edge of a semi-infinite lattice will not affect interior sites if a shielding wall is present along the edge (see Figure 2.2d).

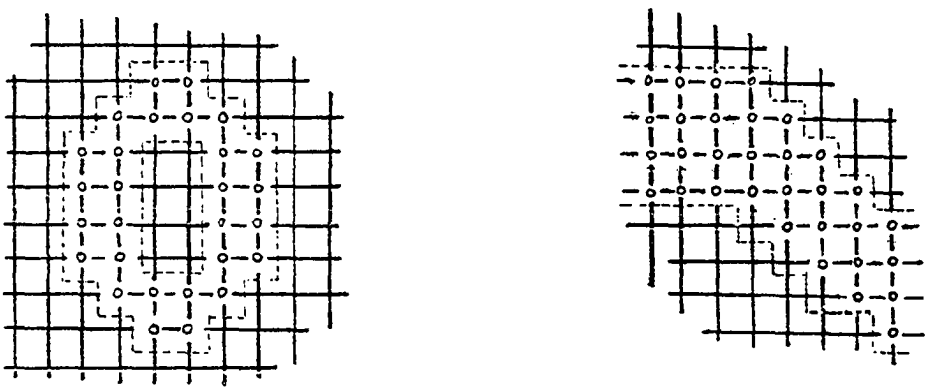

(a) (b)

Figure 2.1. Shielding walls for the 2-D R'=1 case (a) and the R'=2 and $R^2=\sqrt{2}$ (b) cases

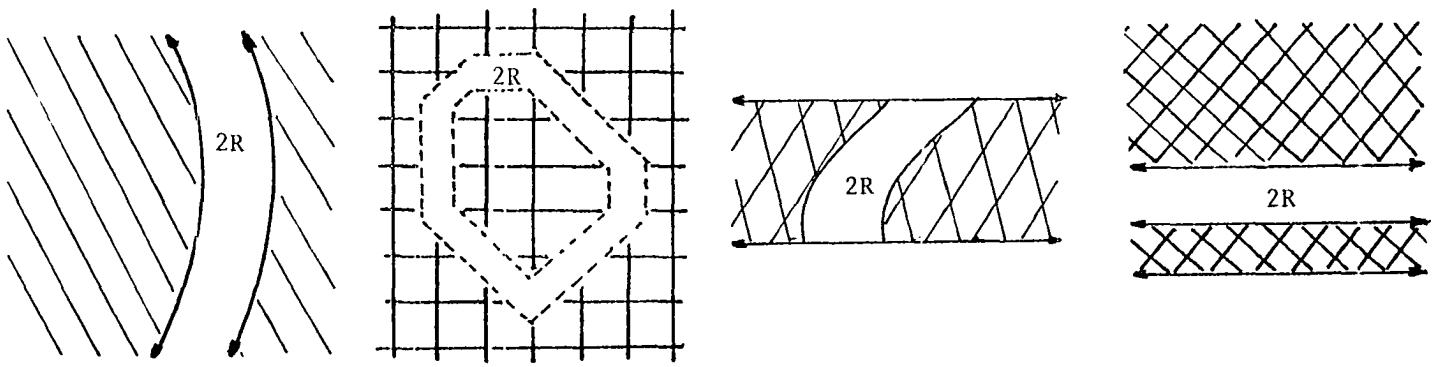

Figure 2.2. Examples of shielding walls for various lattice geometries

On a torus shaped lattice there must be two shielding walls about the same axis in order to completely disconnect the lattice.

In 3-D, the lattice may be disconnected by a set of consecutive infinite planes with thickness 2R. Alternatively, any surface of thickness 2R which completely encloses a portion of the 3-D lattice would shield since an event on an enclosed site would not influence nor be influenced by events that were not in the enclosed sublattice.

The general proof of the shielding condition is not given, but the spirit is illustrated by the following examples for 1-D and R=1. From Equation 2.12

$$d/dt\ \ln q_o[oox] = -\tau_{o\cdot x} q_x[oox] - \tau_{o\cdot o} q_o[oox] - \tau_{o\cdot x} - \tau_{o\cdot o} + \tau_{o\cdot x} q_x[oox] + \tau_{o\cdot o} q_o[oox] + \tau_{o\cdot x} \quad . \tag{2.16}$$

After application of the shielding condition, all terms of Equation 2.16 will cancel except $-\tau_{o\cdot o}$ and $q_o[oox]=e^{-\tau_{o\cdot o}t}$. If the equation is written for $q_o[ooxo]$ it is found that

$$\begin{aligned} d/dt\ \ln q_o[ooxo] = {} & -\tau_{o\cdot x} q_x[oooxo] - \tau_{o\cdot o} q_o[oooxo] - \tau_{o\cdot x} q[oooxo]o \\ & - \tau_{x\cdot x} q[oooxo]x - \tau_{o\cdot x} - \tau_{o\cdot o} + \tau_{o\cdot x} q_x[ooxo] \\ & + \tau_{o\cdot o} q_o[ooxo] + \tau_{o\cdot x} q[ooxo]o - \tau_{x\cdot x} q[ooxo]x + \tau_{o\cdot x} \quad . \end{aligned} \tag{2.17}$$

It is again seen that application of the shielding condition results in cancellation of all terms except $-\tau_{o\cdot o}$ and $q_o[ooxo]=e^{-\tau_{o\cdot o}t}$. This is,

of course, the same result which establishes the shielding obtained for $q_o[oo]$(cf., Equation 2.7).

The general proof follows the reasoning established above except, rather than showing that all terms other than $\tau_{o \cdot o}$ cancel, it is shown than even though there may be terms that do not cancel, those terms are independent of the condition of sites on the opposite side of the shielding wall (i.e., the argument is one of self-consistency).

The shielding condition automatically establishes relationships between various probabilities. For example, P(ooox)/P(oox)= P(oooxo)/P(ooxo) (as shown above $q_o[oox]=q_o[ooxo]$ in 1-D and for R=1). Analogous equalities also hold in other dimensions.

2.3. Exactly Soluble Systems

Even though a shielding condition can be described for all dimensions and finite cooperative effects, there are only a few systems having shielding conditions that allow exact truncation of the kinetic equations (in closed form). Only a limited number of 1-D systems and no systems of dimension greater than one are exactly soluble (in closed form).

The exactly solvable 1-D, R=1 case has been treated by several authors in a variety of contexts. Platé et al. (32,33) and Wolf (2) give a method for obtaining the nested sets of disconnected empty site configurations described in Section 1.2. Chapter three will give an alternative method tailored to analyze the large separation behavior of correlation functions.

Wolf (2) has shown that a process with sites 1,2,$\cdots$,r (from the site of interest) blocking and sites r+1,r+2,$\cdots$,2r+1 having cooperative effects can be exactly solved. Epstein (4,39) also discussed this for the simplest case. Other exactly soluble systems include certain cases of multi-event processes and certain cases involving limited mobility. These and other interesting examples are discussed in detail in Chapter three.

The corresponding semi-infinite systems can also be exactly solved. Wolf (2) has discussed several aspects of these lattice problems in 1-D including both noncooperative and cooperative irreversible events. He gives both an iterative and a transform solution for the cooperative case. Specific rates for landing on the end (1st) site with an empty n.n., $\tau_{o\cdot 1}$ and for landing on the end site with an occupied n.n., $\tau_{x\cdot 1}$ besides the usual rates $\tau_{o\cdot o}$, $\tau_{o\cdot x}$ and $\tau_{x\cdot x}$ must be identified for 1-D and R=1. For this reason, special equations for the end sites are needed. For longer range cooperative effects, more rates must be identified to account for those situations. Figure 2.3 shows how the difference between finding site i, near the end, empty and finding an interior site empty, $f_i(o)-f(o)$, changes going toward the interior from the end site (labeled one). These calculations are for the 1-D, R=1 semi-infinite lattice where $\tau_{o\cdot 1}=1.5$, $\tau_{x\cdot 1}=0.5$, $\tau_{o\cdot x}=0.3$ and $\tau_{x\cdot x}=0.09$. This choice of rates corresponds to a small repulsive cooperative effect for all interior sites, a slightly less repulsive effect for landing on the end site with a n.n. and an

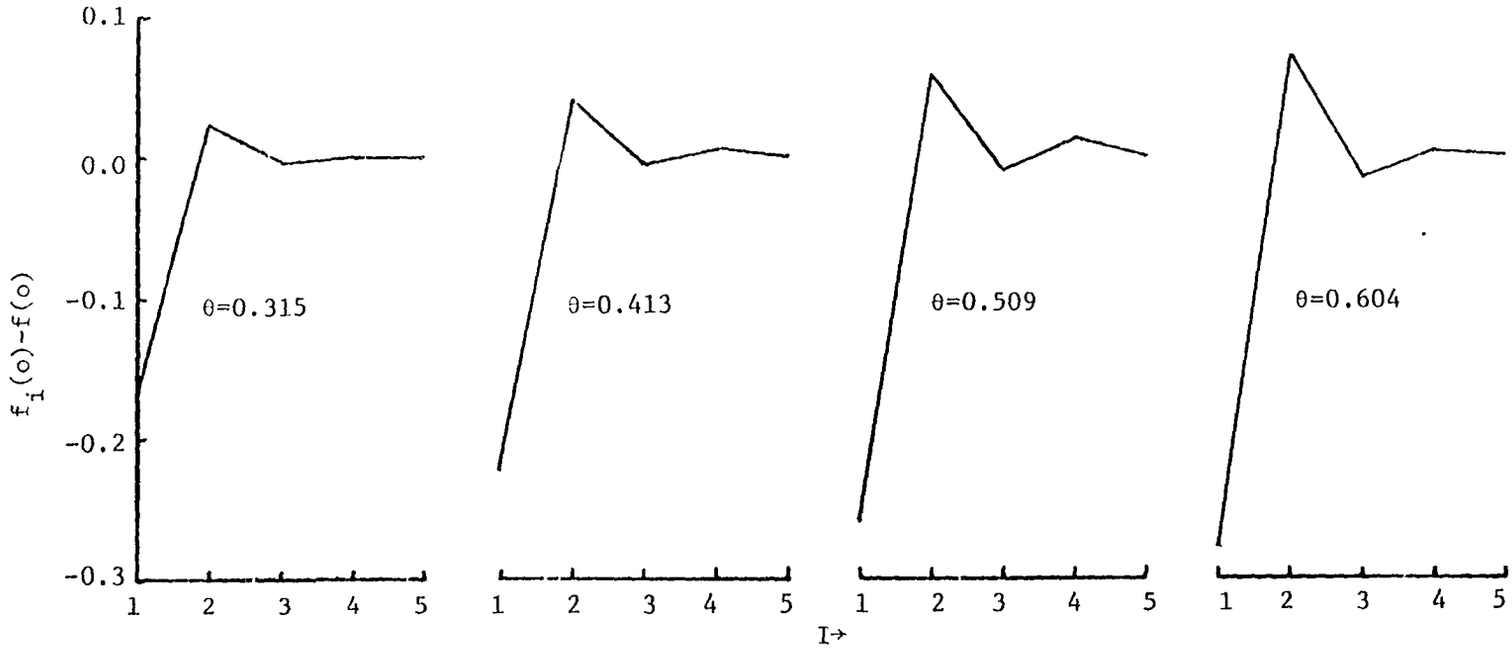

Figure 2.3. The difference between the probability of finding an empty site near the end of a 1-D semi-infinite lattice and the probability of finding an empty interior site as a function of the distance from the end site (labeled one). Here $\tau_{o\cdot 1}=1.5$, $\tau_{x\cdot 1}=0.5$, $\tau_{o\cdot x}=0.3$ and $\tau_{x\cdot x}=0.09$

enhanced rate for landing on the end site without a n.n. The results indicate that for this case the end effects are very small beyond five sites from the end. In many instances, end effects may not be important when describing reactions on long lattices (e.g., long polymer chains) and infinite lattice models may be effectively used to describe these processes.

3. 1-D MODELS

The 1-D case of the general theory presented in Chapter two is interesting because a) irreversible 1-D processes (e.g., many polymer reactions) are described by this model, b) some results are exact and can be used as a tool to test approximations from models that are not exactly soluble and c) the procedures developed in 1-D often extend to higher dimensions.

3.1. Single Site Cooperative Tail beyond r n.n. Blocking Sites

A process with sites $1,2,\cdots,r$ (from the site of interest) blocking and site r+1 cooperative tail which begins on a completely empty lattice will be treated in this section. The four rates needed to describe this process are τ_{oo}, τ_{ox}, τ_{xo}, and τ_{xx}, where τ_{oo} is the rate of an event occurring on a site flanked on both sides by r+1 consecutive empty sites, τ_{ox} is the rate of an event occurring on a site flanked on the left by r+1 consecutive empty sites and flanked on the right by r consecutive empty sites and then one full site, $\tau_{xo}=\tau_{ox}$ (throughout this chapter reflection symmetry is assumed) and τ_{xx} is the rate of an event occurring on a site flanked on both sides by r consecutive empty sites and then one full site. Reduced rates will be denoted in the same manner (e.g., $\rho_{ox}=\tau_{ox}/\tau_{oo}$).

After converting the configurations of Equation 1.1 to only include empty sites, it is found in this case that

$$-d/dt\ f(n) = n[\tau_{xx}f(2r+1)+2(\tau_{ox}-\tau_{xx})f(2r+2)+(\tau_{oo}-2\tau_{ox}+\tau_{xx})f(2r+3)],$$

$$1 \leqslant n \leqslant r+1\ , \tag{3.1}$$

$$-d/dt\ f(r+1+k) = 2\sum_{\ell=1}^{k}[\tau_{ox}f(2r+k-\ell+2)+(\tau_{oo}-\tau_{ox})f(2r+k-\ell+3)]$$

$$+(r+1-k)[\tau_{xx}f(2r+1)+2(\tau_{ox}-\tau_{xx})f(2r+2)$$

$$+(\tau_{oo}-2\tau_{ox}+\tau_{xx})f(2r+3)],\quad 1 \leqslant k \leqslant r+1\ , \tag{3.2}$$

$$-d/dt\ f(2r+2+k) = 2\sum_{\ell=1}^{r+1}\{\tau_{ox}[f(3r+k-\ell+3)-f(3r+k-\ell+4)]+\tau_{oo}f(3r+k-\ell+4)\}$$

$$+k\tau_{oo}f(2r+2+k),\quad k \geqslant 0\ . \tag{3.3}$$

Application of the shielding condition leads to $q_o[2r+2+k]=q_o[2r+2]\equiv q$ which implies

$$q = e^{-\tau_{oo}t} \tag{3.4}$$

and

$$f(2r+2+k) = q^k\ f(2r+2)\ ,\quad k \geqslant 0\ . \tag{3.5}$$

Converting to functions of θ gives

$$-d/d\theta\ f(n) = n\ ,\quad 1 \leqslant n \leqslant r+1 \tag{3.6}$$

$$-d/d\theta\ f(r+1+k) = \frac{2[\rho_{ox}+(1-\rho_{ox})q]\left[\sum_{\ell=0}^{k-1} q^{\ell}\right]f(2r+2)}{F(f(2r+1),f(2r+2),q)}+r+1-k,$$

$$1 \leqslant k \leqslant r+1\ , \tag{3.7}$$

and

$$-d/d\theta\ q = \frac{q}{F(f(2r+1),f(2r+2),q)}\ , \tag{3.8}$$

where

$$F(f(2r+1),f(2r+2),q) = \rho_{xx}f(2r+1)+\{2(\rho_{ox}-\rho_{xx})+(1-2\rho_{ox}+\rho_{xx})q\}f(2r+2)\ . \tag{3.9}$$

These equations form a closed, coupled set which may be solved for the various probabilities. Of particular interest is the saturation value of θ,θ^*. Integrating Equation 3.8 from q=0 to 1 and making use of the fact that q=0 at $\theta=\theta^*$ gives

$$\theta^* = \int_0^1 dq'\ \frac{F(f(2r+1),f(2r+2),q')}{q'} \tag{3.10}$$

where f(2r+1) and f(2r+2) are functions of q'.

3.1.1. Examples of tail interactions for r=1

Four examples follow to show how the process changes as the cooperative effect of the tail is varied from very attractive to very repulsive.

(1) Infinitely strong attractive tail. For n.n. blocking and infinitely strong attractive second n.n. events will occur in a totally ordered fashion as shown in Figure 3.1. In this case, all probabilities of consecutive empty sites greater than one go to zero when the covering

$\cdots\overset{\downarrow}{o}oxoxoxoxoxoxo\overset{\downarrow}{o}\cdots$

Figure 3.1. Totally ordered filling of a 1-D lattice

fraction equals 0.5. The conditional probability, $q=q_o[oo]$, remains one until $\theta=0.5$ and then it is zero. See Figure 3.2.

(2) Strong attractive tail. If the attractiveness of the second n.n. is relaxed then ordered clusters, or islands, of the type shown in Figure 3.1 will form. The length of these islands will increase with ρ_{ox}. As $\rho_{ox}\to\infty$ (attractive limit) the lattice becomes one long cluster of perfectly ordered events as discussed earlier and $\theta^*=0.5$. As ρ_{ox} gets smaller the island size decreases and more doublets, separating islands, occur. This results in θ^* being less than 0.5. Some probabilities are graphed against θ for this case in Figure 3.3.

(3) No cooperative tail. When the second n.n. has no cooperative effect the process is n.n. blocking where $r=0$ and $\rho_{ox}=\rho_{xx}=0$. For such a process Equations 3.7 and 3.8 give

$$f(2) = e^{2(q-1)} \quad . \tag{3.11}$$

At the end of the process $q=0$, $f(2)=e^{-2}$ (the Flory result) and $\theta=\theta^*=1/2(1-e^{-2})=.43233\cdots$. This case is illustrated in Figure 3.4.

(4) Infinitely strong repulsive tail. The last case that will be considered is when the second n.n. is in the strongly repulsive limit. When $\rho_{oo}\gg\rho_{ox}\gg\rho_{xx}$ the process will proceed in three stages corresponding to events occurring with no occupied second n.n., one occupied second n.n. and two occupied second n.n.

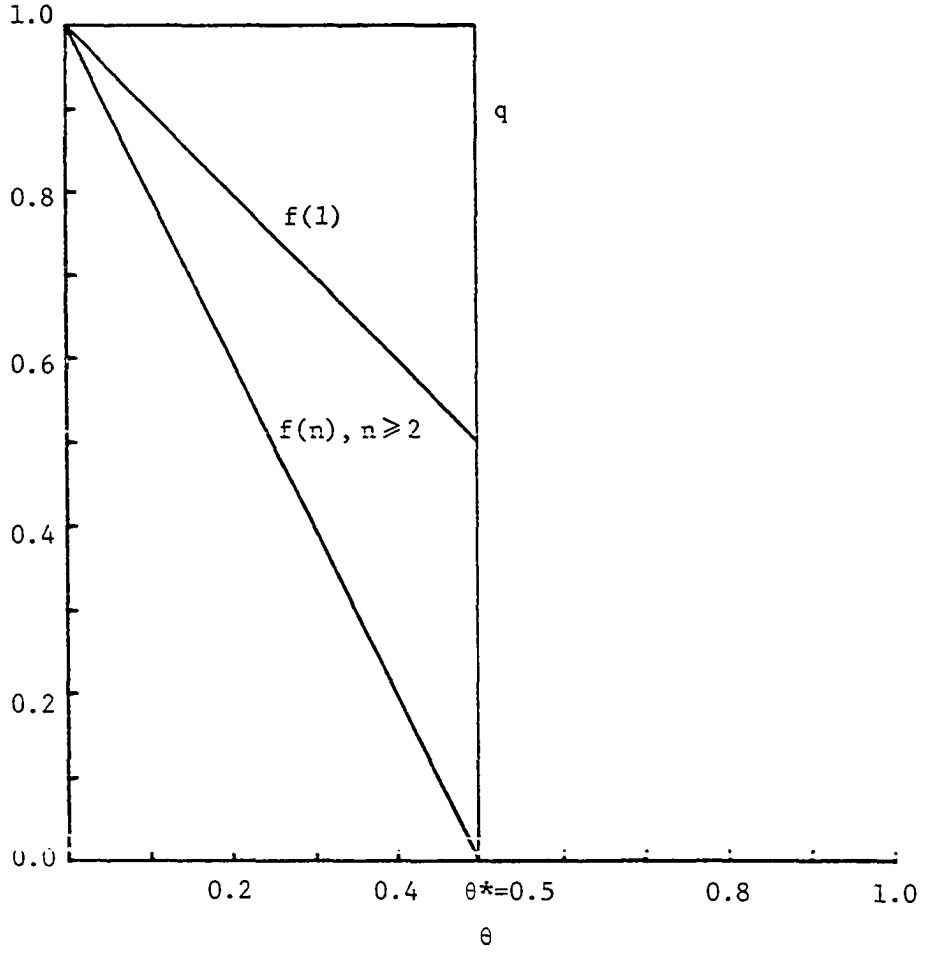

Figure 3.2. The probabilities f(n) and q as a function of θ for n.n. blocking and second n.n. infinitely attractive

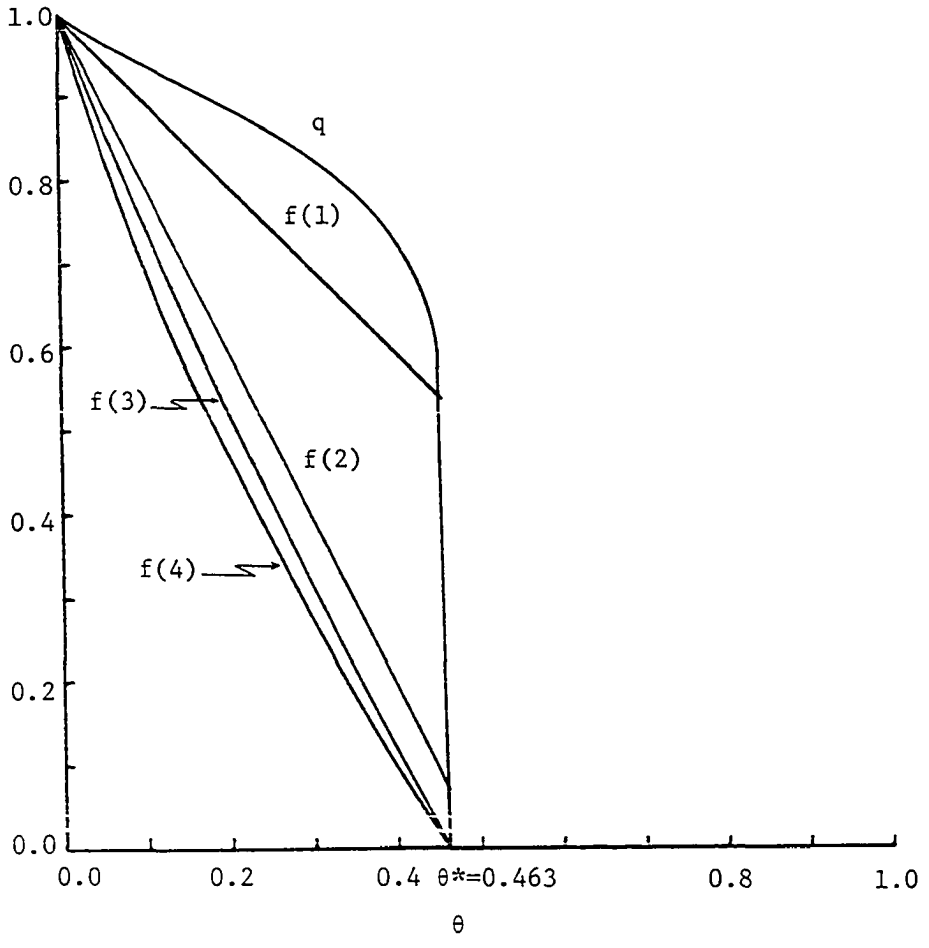

Figure 3.3. The probabilities f(n), $1 \leqslant n \leqslant 4$, and q as a function of θ for n.n. blocking and second n.n. moderately attractive

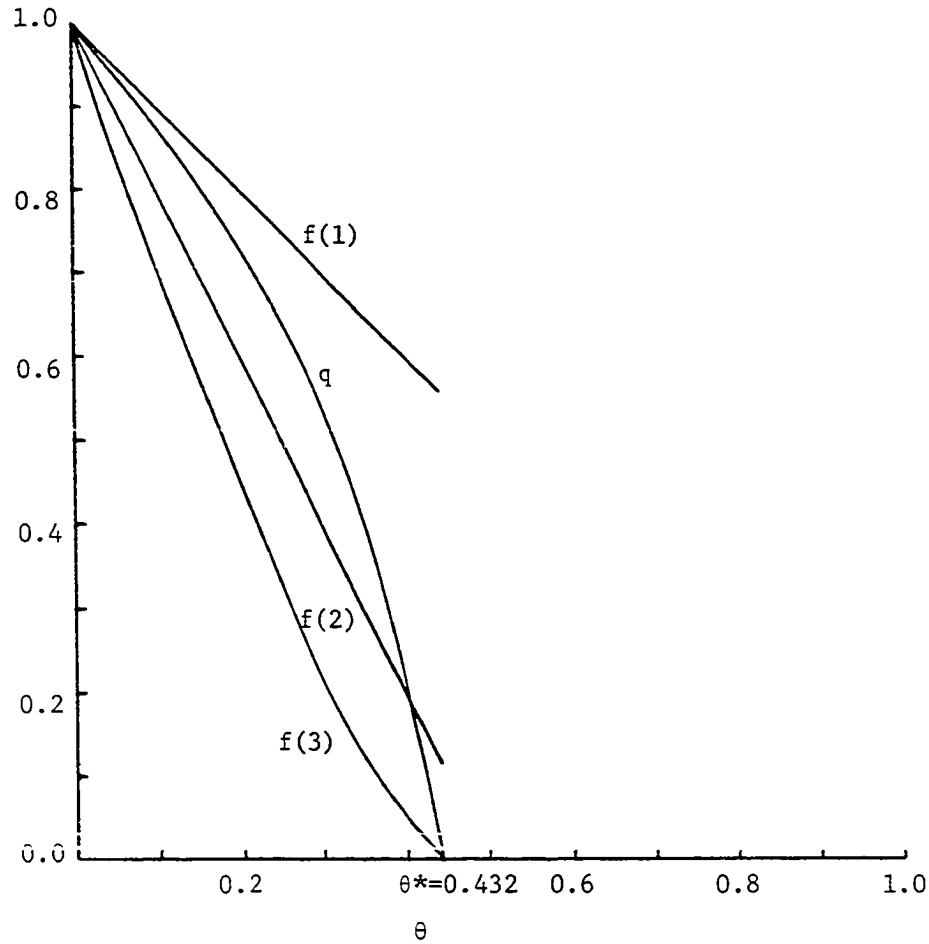

Figure 3.4. The probabilities f(n), $1 \leqslant n \leqslant 3$, and q as a function of θ for n.n. blocking and no second n.n. cooperative effect

During the first stage $d/d\theta\ f(2)=-2$, $d/d\theta\ f(3)=-3$, and $f(n)\rightarrow 0$ for $n\geqslant 5$ as $\theta\rightarrow\theta^*(1)$, where $\theta^*(1)$ is the event coverage at the end of the first stage. The value of $\theta^*(1)$ may be obtained using Equations 3.7 and 3.10 where ρ_{ox} and ρ_{xx} are set to zero. This allows Equation 3.10 to be expressed in terms of Dawson's integral (49) as

$$\theta^*(1) = D(2)-e^{-3}D(1) \cong 0.27455 \ . \tag{3.12}$$

Also, Equation 3.7 can be used to find that

$$f(4)\big|_{\theta^*(1)} = e^{-3} \ . \tag{3.13}$$

During the second stage $\theta^*(1)\leqslant\theta\leqslant\theta^*(2)$, $d/d\theta\ f(2)=-2$, $d/d\theta\ f(3)=-2$ and $d/d\theta\ f(4)=-1$. At the end of this stage $f(4)$ equals zero and by using the geometric construction shown in Figure 3.5

$$\theta^*(2) = \theta^*(1)+f(4)\big|_{\theta^*(1)} \cong 0.32434 \ . \tag{3.14}$$

Other values of interest may also be determined analogously to Equation 3.14. For example,

$$f(3)\big|_{\theta^*(2)} = 1-3\theta^*(1)-2[\theta^*(2)-\theta^*(1)] \cong 0.07677 \ . \tag{3.15}$$

During the final stage $\theta^*(2)\leqslant\theta\leqslant\theta^*(3)$, $d/d\theta\ f(2)=-2$, $d/d\theta\ f(3)=-1$ and, at $\theta=\theta^*(3)$, $f(3)=0$. The expression for $\theta^*(3)$ is

$$\theta^*(3) = \theta^*(2)+f(3)\big|_{\theta^*(2)} \cong 0.40111 \ . \tag{3.16}$$

This case is graphically illustrated in Figure 3.6.

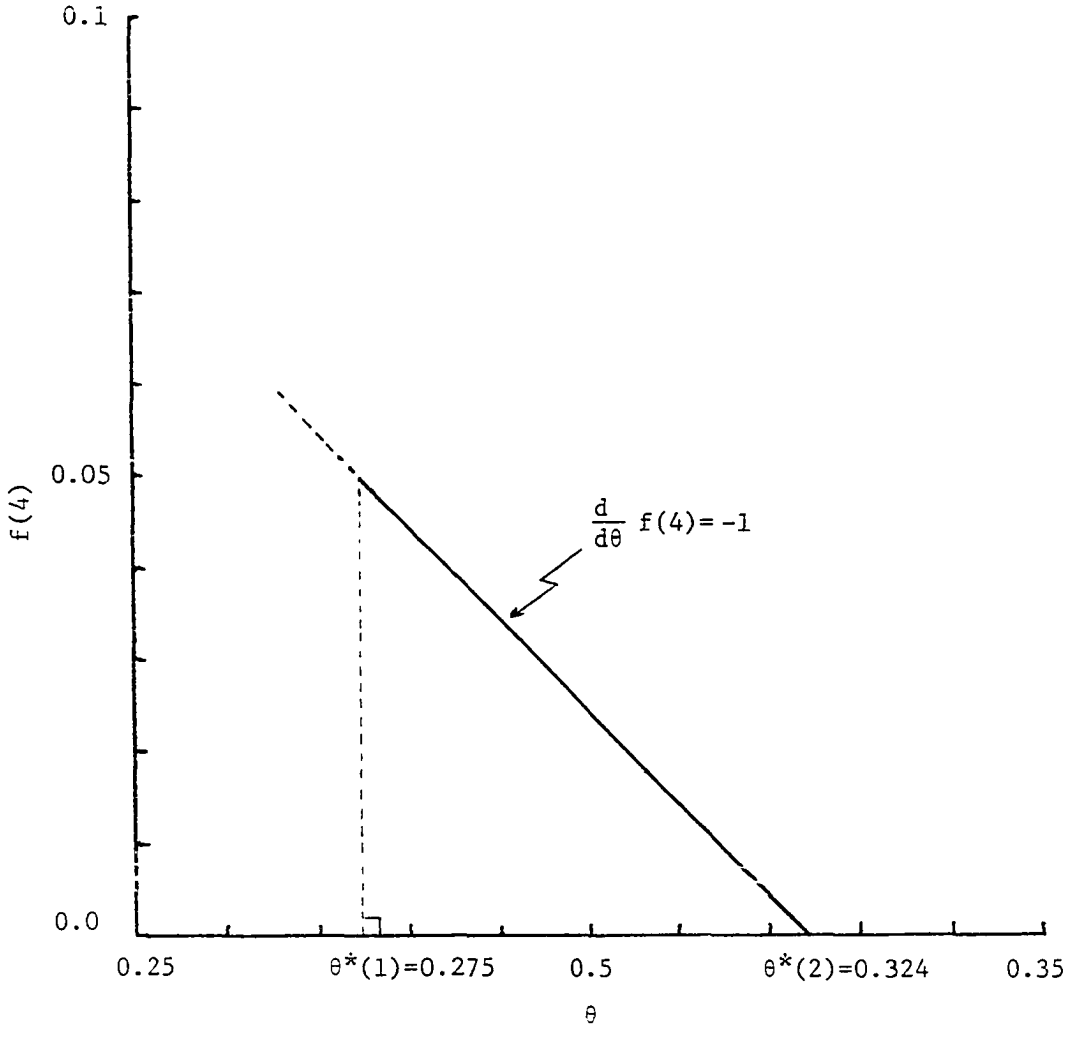

Figure 3.5. Geometric construction for determination of $\theta^*(2)$

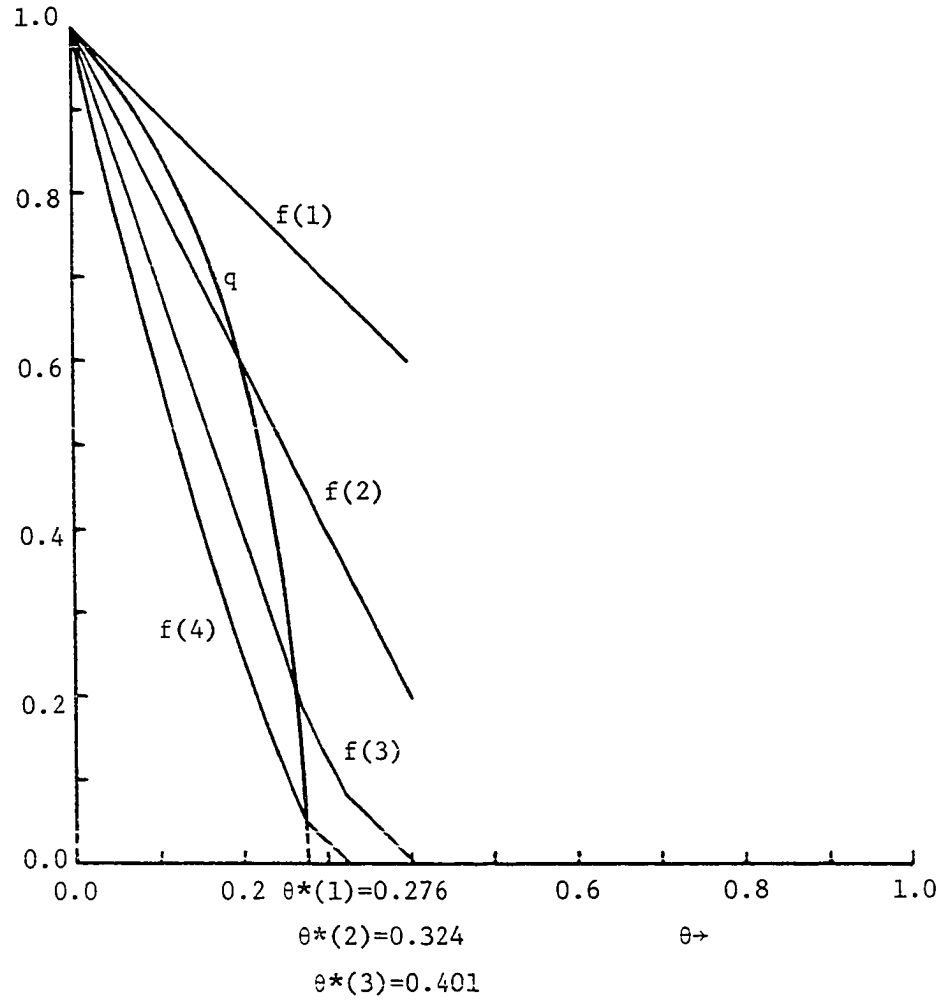

Figure 3.6. The probabilities f(n), $1 \leqslant n \leqslant 4$, and q as a function of θ for n.n. blocking and second n.n. strongly repulsive

3.1.2. Saturation coverage as a function of tail interaction for r=1

The behavior of θ^*, as the second n.n. cooperative tail is varied from very repulsive to very attractive, is shown in Figure 3.7. As $\rho_{ox} \to 0$ the three stages discussed in the last section become more distinct, but the process continues through all stages as long as $\rho_{ox} \neq 0$ (assuming $\rho_{xx}=\rho_{ox}^2$). It should be noted, however, that if $\rho_{ox}=0$ the maximum coverage is 0.27455 since $0 \leqslant \theta \leqslant \theta^*(1)$. It is also possible to have a process where $\rho_{ox} \neq 0$ (but $\rho_{oo} \gg \rho_{ox}$) and $\rho_{xx}=0$ which would result in a final coverage of 0.32434 as previously shown. Interpretation of experimental data for irreversible processes with repulsive cooperative effects must be done with caution since any of the above (or other) final coverages may be observed due to time constraints or due to competing reactions.

The results of this section could have also been obtained in a manner similar to that of Wolf et al. (3) from the solution of the most general problem (2). Their method starts with an analytical solution for general rates from which limits for various ratios of those rates are taken (e.g., $\tau_{ox}/\tau_{oo} \to 0$).

3.2. Filling in Stages for Highly Repulsive Interactions

General filling in stages and an extension of exact solutions using this concept will be treated next. Certain symmetry considerations for probability functions in the highly repulsive case and perturbation from the repulsive limit will then be discussed.

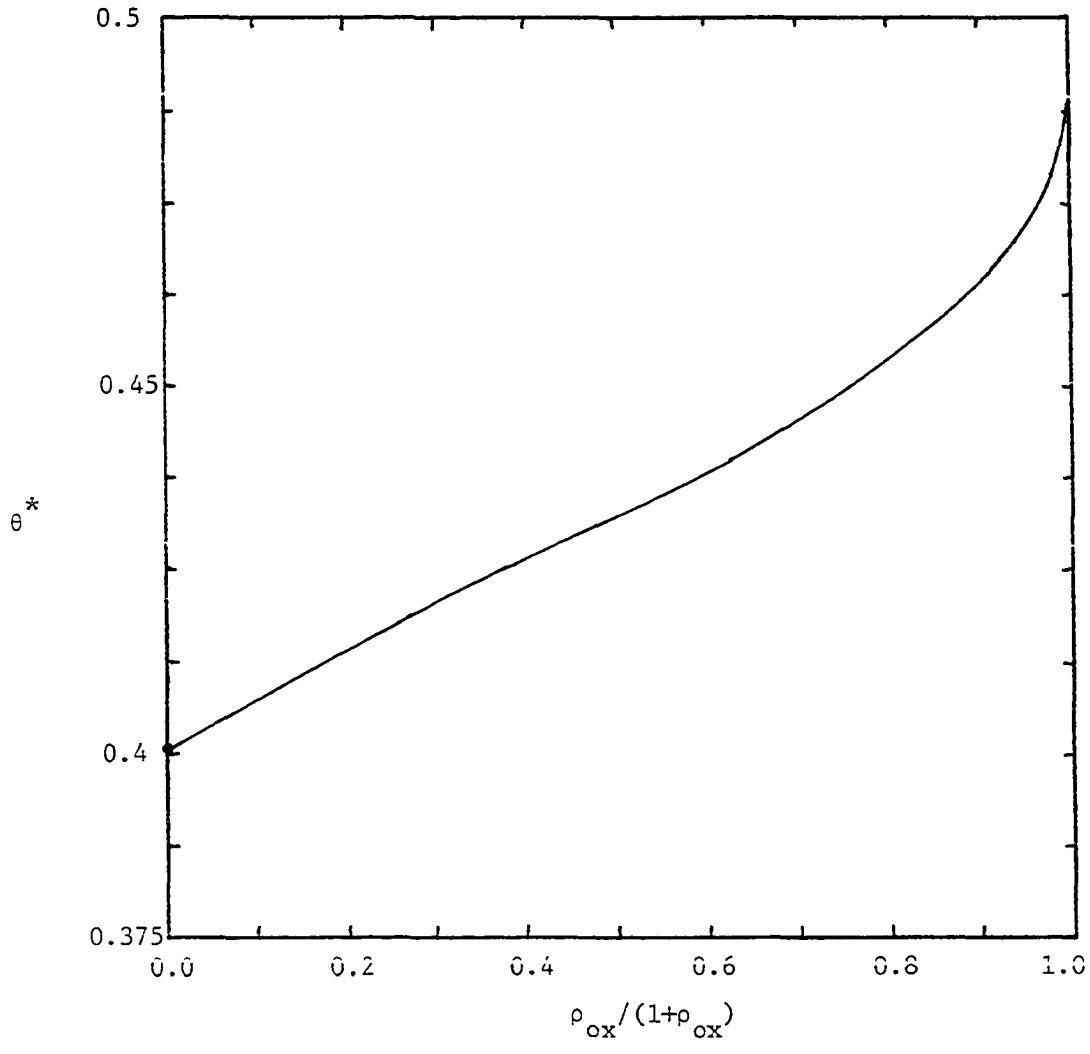

Figure 3.7. Saturation coverage as a function of ρ_{ox}

3.2.1. Analysis of filling in stages

The problem of arbitrary cooperative effects for sites within a total range R is not exactly solvable. If, however, the cooperative effects are such that stages occur, each having a characteristic rate, then exact results can be obtained for the process using the method introduced in the last section. In that section, three stages were found for an R=2 process with n.n. blocking and highly repulsive second n.n. If the n.n. blocking is relaxed, two more stages appear, the first of these filling sites with one occupied n.n. and the second filling sites with two occupied n.n. Table 3.1 summarizes these stages for R=1 (3) and R=2.

This same kind of analysis can be applied to any process displaying a behavior of filling in stages (for arbitrary, but finite, R). In order to understand this in a more general way, consider a strongly repulsive cooperative effect of range R where the repulsive cluster increases with decreasing distance (e.g., $\tau_{o\cdot x} < \tau_{oo\cdot ox} < \tau_{ooo\cdot oox}$, etc.). The lattice filling process will then occur in an ordered manner and may be described by the following stages:

(1) $0 \leqslant \theta \leqslant \theta^*(1)$, $\underbrace{oo\cdots o}_{R}\dot{o}\underbrace{o\cdots oo}_{R}$

$$d/d\theta\ f(n) = -n\ , \quad n = 1, 2, \cdots, R+1$$

$$f(n) \to 0 \text{ for } n \geqslant 2R+1 \text{ as } \theta \to \theta^*(1)$$

$$\theta^*(1) = \int_0^1 \exp\left[-2 \sum_{\ell=1}^{r+1} \frac{1-q^{\ell}}{\ell}\right] dq$$

Table 3.1. Stages for highly repulsive neighbors when R=1 and R=2

A. R=1, highly repulsive n.n.

I.	$0 \leqslant \theta \leqslant \theta^*(1)=0.43233$,	$o\overset{\downarrow}{o}o$,	$d/d\theta f(2)=-2$, $f(3)\to 0$
II.	$\theta^*(1) \leqslant \theta \leqslant \theta^*(2)=0.56767$,	$x\overset{\downarrow}{o}o$,	$d/d\theta f(2)=-1$, $f(2)\to 0$
III.	$\theta^*(2) \leqslant \theta \leqslant 1.00000$,	$x\overset{\downarrow}{o}x$,	$d/d\theta f(2)=0$, $f(1)\to 0$

B. R=2, highly repulsive first and second n.n.

I.	$0 \leqslant \theta \leqslant \theta^*(1)=0.27455$,	$oo\overset{\downarrow}{o}oo$,	$d/d\theta f(3)=-3$, $f(5)\to 0$
II.	$\theta^*(1) \leqslant \theta \leqslant \theta^*(2)=0.32434$,	$xo\overset{\downarrow}{o}oo$,	$d/d\theta f(3)=-2$, $f(4)\to 0$
III.	$\theta^*(2) \leqslant \theta \leqslant \theta^*(3)=0.40111$,	$xo\overset{\downarrow}{o}ox$,	$d/d\theta f(3)=-1$, $f(3)\to 0$
IV.	$\theta^*(3) \leqslant \theta \leqslant \theta^*(4)=0.59889$,	$x\overset{\downarrow}{o}o$,	$d/d\theta f(3)=0$, $f(2)\to 0$
V.	$\theta^*(4) \leqslant \theta \leqslant \theta^*(5)=1.00000$,	$x\overset{\downarrow}{o}x$,	$d/d\theta f(3)=0$, $f(1)\to 0$

---

(2) $\theta^*(1) \leqslant \theta \leqslant \theta^*(2)$, $xo\cdots o\overset{\downarrow}{o}o\cdots oo$ (R-1, R)

$d/d\theta\ f(n)=-n$, $n=1,2,\cdots,r$

$d/d\theta\ f(r+k)=k-r-1$, $k=1,2,\cdots,r$

$f(2R)\to 0$ as $\theta\to\theta^*(2)$

$\theta^*(2)=\theta^*(1)+f(2R)\big|_{\theta^*(1)}$

(3) $\theta^*(2) \leqslant \theta \leqslant \theta^*(3)$, $xo\cdots o\overset{\downarrow}{o}o\cdots ox$ (R-1, R-1)

$d/d\theta\ f(n)=-1$, $n=1,2,3,\cdots,r$

$d/d\theta\ f(R+k)=k-R$, $k=1,2,\cdots,r-1$

$f(2R-1)\to 0$ as $\theta\to\theta^*(3)$

$\theta^*(3)=\theta^*(2)+f(2R-1)\big|_{\theta^*(2)}$

(4) $\theta^*(3) \leqslant \theta \leqslant \theta^*(4)$, $xo\cdots o\overset{\downarrow}{o}o\cdots ox$ (R-2, R-1)

$d/d\theta\ f(n)=-n$, $n=1,2,\cdots,R-1$

$d/d\theta\ f(R+k)=k+1-R$, $k=0,1,\cdots,R-2$

$f(2R-2)\to 0$ as $\theta\to\theta^*(4)$

$\theta^*(4)=\theta^*(3)+f(2R-2)\big|_{\theta^*(3)}$

$\vdots$

(2R+1) $\theta^*(2R) \leqslant \theta \leqslant \theta^*(2R+1)=1$, $x\overset{\downarrow}{o}x$

Figures 3.8, 3.9 and 3.10 graphically show the cases R=2, R=3 and R=4 respectively.

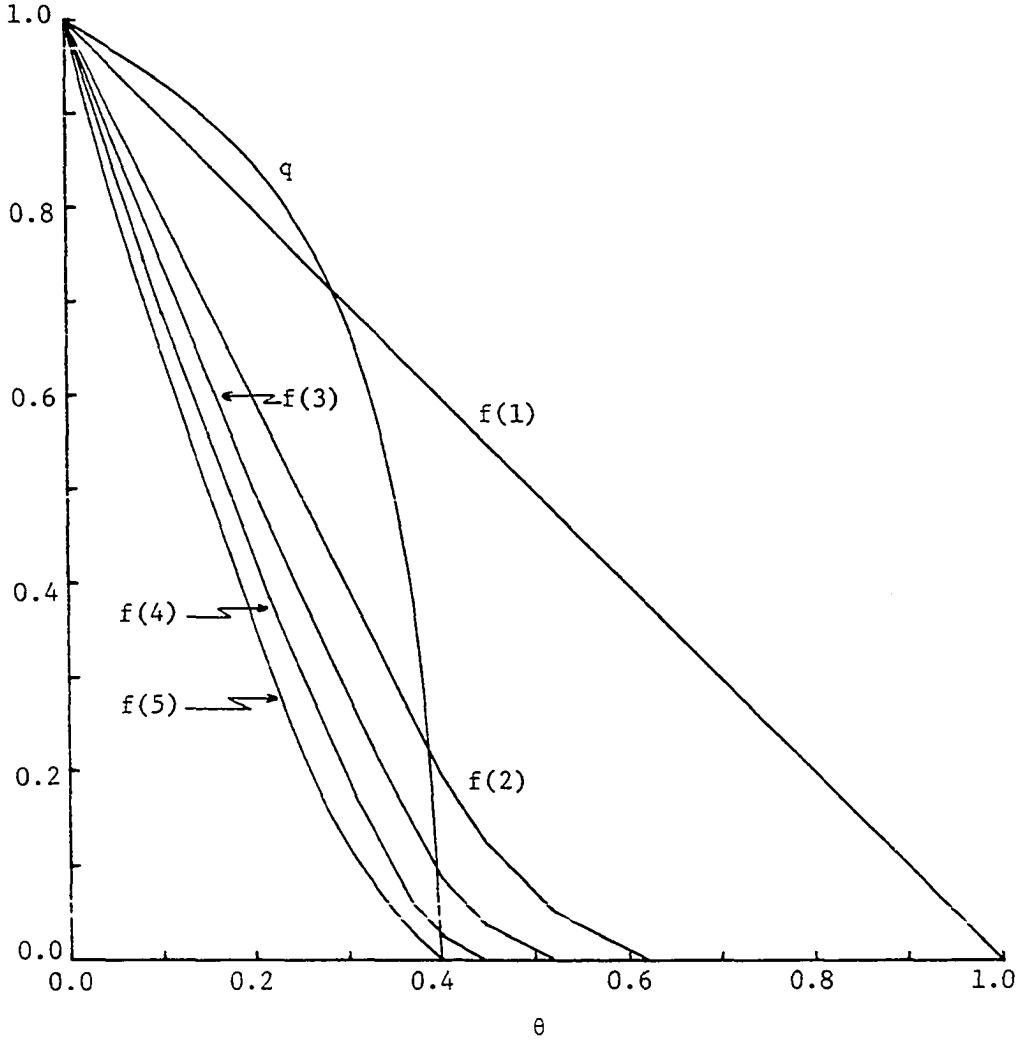

Figure 3.8. The probabilities f(n), $1 \leqslant n \leqslant 5$, and q for filling in stages when R=2

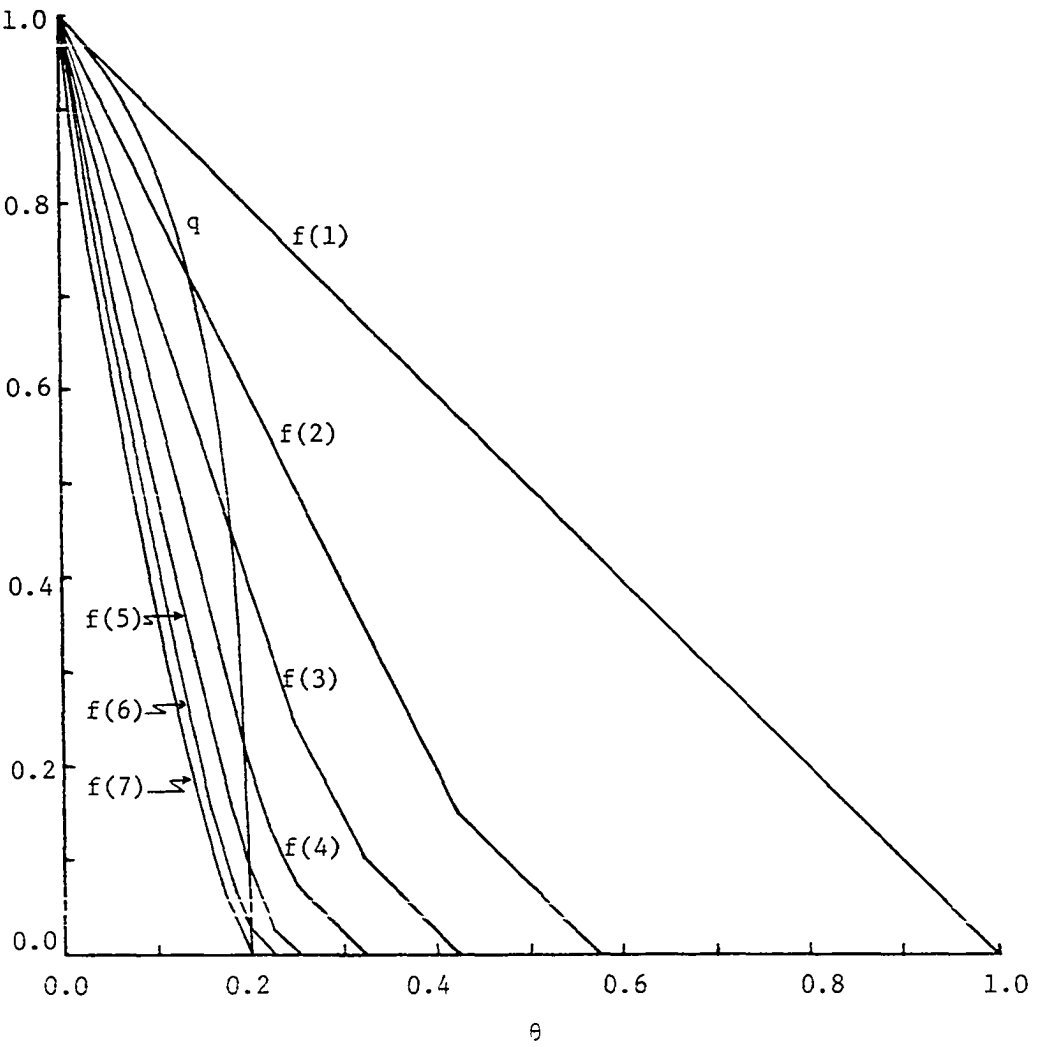

Figure 3. 9. The probabilities f(n), $1 \leqslant n \leqslant 7$, and q for filling in stages when R=3

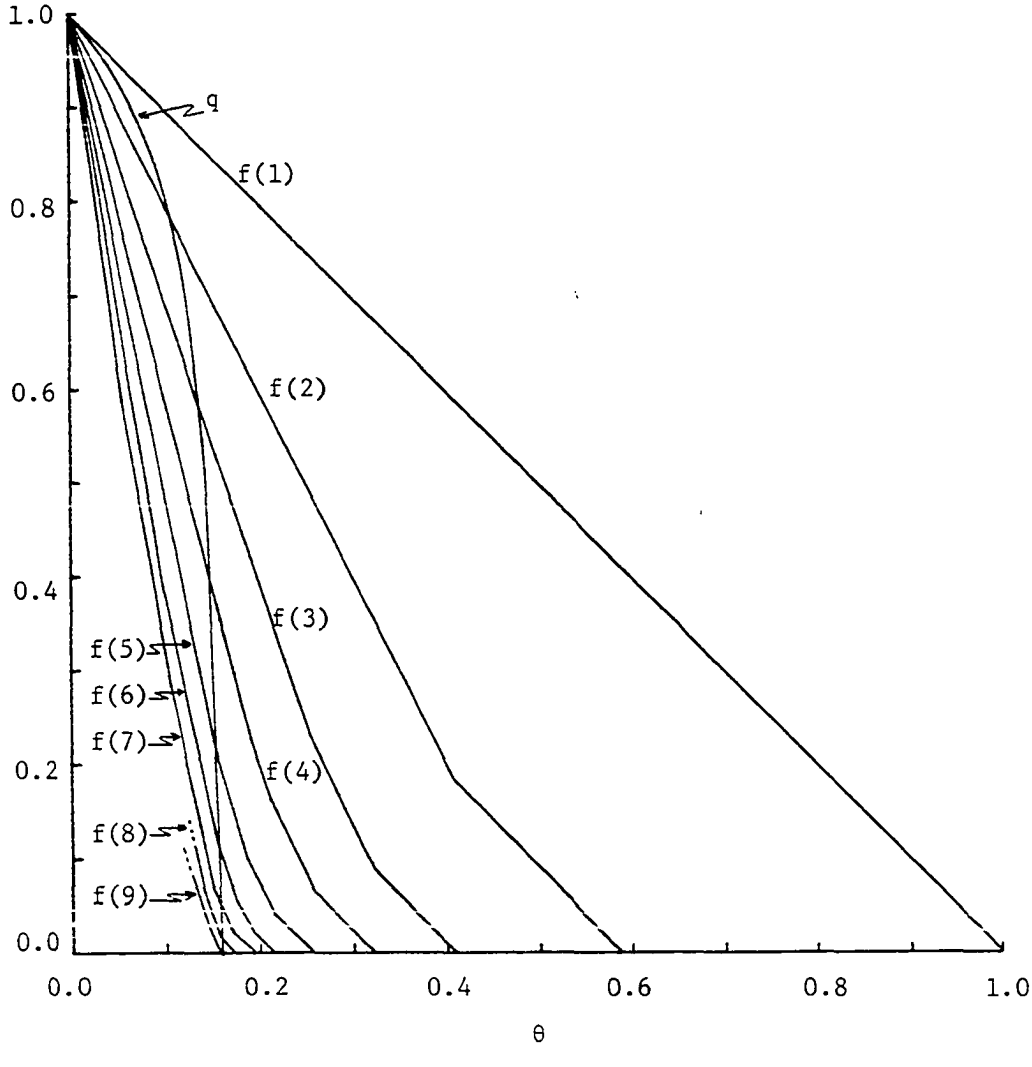

Figure 3.10. The probabilities f(n), $1 \leqslant n \leqslant 9$, and q for filling in stages when R=4

3.2.2. Nonsymmetry of certain probability functions for highly repulsive interactions

Equilibrium processes with pairwise interactions have the symmetry property

$$f(\underset{\sim}{\sigma})\big|_{\theta} = f(\underset{\sim}{\sigma}^*)\big|_{1-\theta} \tag{3.17}$$

where the empty (full) sites in $\underset{\sim}{\sigma}$ have been changed to full (empty) sites to form $\underset{\sim}{\sigma}^*$. Certain probability functions (e.g., $f(2)+\theta$) in the irreversible R=1 case (in 1-D) also have this symmetry. The symmetry might seem to follow from some kind of time reversal argument (e.g., by emptying a filled lattice and filling an empty lattice to the same configuration by means which can be put in one-to-one correspondence). It is, therefore, interesting to consider this question in more detail.

In the one dimensional equilibrium case,

$$f(\underset{\sim}{\sigma}) = f(\sigma_1)q^{k}o[o]q^{\ell}x[x]q^{m}o[x]q^{n}x[o] \tag{3.18}$$

where σ_1 is the condition of the first site of $\underset{\sim}{\sigma}$ and k, ℓ, m and n are the number of n.n. pairs of the indicated q configurations (see Section 3.3.2 for an explanation of the equilibrium Markovian behavior). Expressions for the conditional probabilities are shown using conservation of probability to be

$$qo[o] = \frac{f(2)}{1-\theta}$$

$$qx[x] = \frac{f(2)+2\theta-1}{\theta}$$

$$qo[x] = \frac{1-\theta-f(2)}{\theta}$$

$$qx[o] = \frac{1-\theta-f(2)}{1-\theta} \quad . \tag{3.19}$$

The expression for f(2) is (50)

$$f(2) = 1-\theta - 2\theta(1-\theta)/\{[1+4\theta(1-\theta)B(T_s)]^{\frac{1}{2}}+1\} \tag{3.20}$$

where $B(T_s)=(e^{-w/k\ T_s}-1)$ and w is the repulsive interaction energy between n.n. events. Substitution of $\theta=1-\theta$ into Equations 3.19 shows that

$$\begin{aligned} qo[oo]|_{\theta} &= qx[xx]|_{1-\theta} \\ qo[x]|_{\theta} &= qx[o]|_{1-\theta} \quad . \end{aligned} \tag{3.21}$$

Equations 3.21 and $f(\sigma_1)|_{\theta}=f(\sigma_1^*)|_{1-\theta}$ show that Equation 3.17 is always true in the one dimensional equilibrium case.

In the irreversible case, however, Equation 3.17 is not true for all configurations. For example, consider $f(ooo)|_{\theta}$ and $f(xxx)|_{1-\theta}$ for R=1 processes in the highly repulsive regime (in 1-D). During the second stage of filling f(ooo)=0 (all sites with no n.n. are full), but $f(xxx)\neq 0$ since events can occur on both sides of a full site (during the second stage sites with one n.n. are filled). Any choice of θ between 0.432 and 0.568 will, therefore, contradict Equation 3.17.

As mentioned earlier there are some functions, such as $f(2)+\theta$, that display the symmetry property in the repulsive limit of the

irreversible case. The symmetry is "quickly" broken, however, when the infinite repulsive limit is relaxed. For finite interactions the minimum of f(2)+θ varies according to the interaction. Figure 3.11 is a plot of θ_{min} (θ where the minimum occurs) against the interaction function $\rho_{ox}/(1+\rho_{ox})$ (R=1).

Figure 3.11 shows that a perturbation from the repulsive limit causes a minimum in the P(2)+θ verses θ graph to occur close to θ=0.432. An analysis of the slope during the second stage (the slope is zero during the second stage in the repulsive limit for R=1) for a perturbation from the repulsive limit will now be given. This is motivated by a desire to do a similar analysis in the analogous 2-D case because of the significance of this quantity in surface applications (see Chapters four and six).

The equation for d/dθ (f(2)+θ) is

$$d/d\theta(f(2)+\theta) = \frac{-2[\rho_{ox}f(2)+(1-\rho_{ox})f(3)]}{[\rho_{xx}f(1)+2(\rho_{ox}-\rho_{xx})f(2)+(1-2\rho_{ox}+\rho_{xx})f(3)} + 1 \ . \tag{3.22}$$

For a perturbation $0<\varepsilon=\rho_{xx}/\rho_{ox}\ll 1$ during the second stage, since $P(3)\ll\varepsilon$ (from Equation 2.3,

$$P(3)=\exp\{-\frac{1}{\varepsilon}[2\rho_{xx}(\rho_{xx}^{-1}-1)(1-q)+(2\tau_{xx}+\varepsilon\tau_{oo})t]\}) \ , \tag{3.23}$$

Equation 3.22 reduces to

$$d/d\theta(f(2)+\theta) = 1 - \frac{1}{1+g(\theta)} \cong g(\theta) \tag{3.24}$$

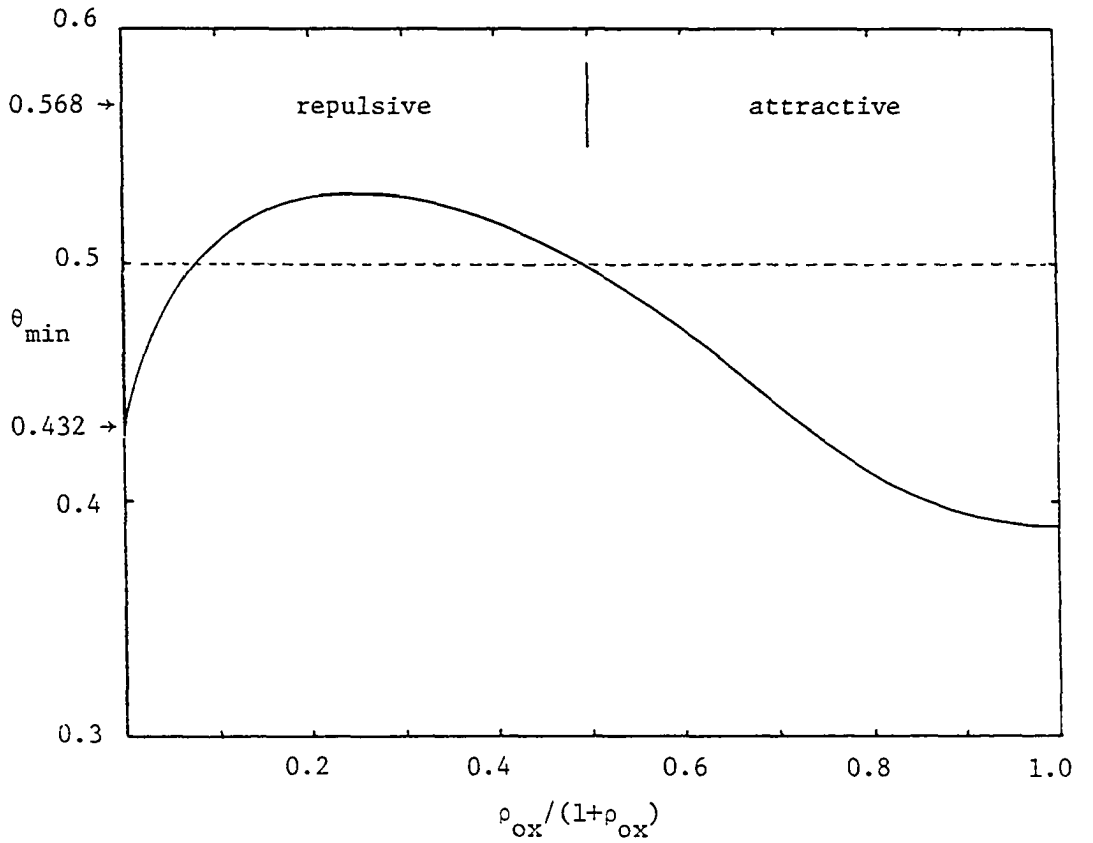

Figure 3.11. Coverage where f(2)+θ is minimum (θ_{min}) as a function of interaction

where $g(\theta)=(\frac{1}{2}f(1)/f(2)-1)\varepsilon$. To first order in ε, $g(\theta)$, evaluated using $f(1)$ and $f(2)$ from the repulsive limit, is positive. Using this expression for $g(\theta)$ and $\varepsilon=0.01$, Equation 3.24 is integrated for $f(2)+\theta$ to obtain Figure 3.12. This analysis is consistent with Figure 3.11 and the fact that only one minimum is obtained under these conditions.

3.3. Correlation Functions

For 1-D systems, two cluster correlation functions may be defined as

$$c(\underset{\sim}{\sigma}\overset{\ell}{\text{---}}\underset{\sim}{\sigma}') = f(\underset{\sim}{\sigma}\overset{\ell}{\text{---}}\sigma')-f(\sigma)f(\sigma') \ , \tag{3.25}$$

where $\overset{\ell}{\text{---}}$ denotes ℓ consecutive unspecified sites. Exact expressions for the three functions $c(oo\overset{\ell}{\text{---}}oo)$, $c(oo\overset{\ell}{\text{---}}o)$ and $c(o\overset{\ell}{\text{---}}o)$ are derived below for R=1, cooperative, irreversible processes using both z-transform and recursive methods. The section ends by presenting expressions for the corresponding equilibrium correlation functions and comparing them with the irreversible results.

3.3.1. Correlation functions for 1-D, R=1 irreversible processes

For fixed configurations $\underset{\sim}{\sigma}$ and $\underset{\sim}{\sigma}'$, define

$$\tilde{f}(\underset{\sim}{\sigma},\underset{\sim}{\sigma}',z) = \sum_{\ell=1}^{\infty} z^{\ell} \, f(\underset{\sim}{\sigma}\overset{\ell}{\text{---}}\underset{\sim}{\sigma}') \tag{3.26}$$

so

$$f(\underset{\sim}{\sigma}\overset{\ell}{\text{---}}\underset{\sim}{\sigma}') = \frac{1}{\ell!}\frac{d^{\ell}}{dz^{\ell}} \, \tilde{f}(\underset{\sim}{\sigma},\underset{\sim}{\sigma}',z)\Big|_{z=0} = \frac{1}{2\pi i}\oint dz \, z^{-n}\tilde{f}(\underset{\sim}{\sigma},\underset{\sim}{\sigma}',z) \ , \tag{3.27}$$

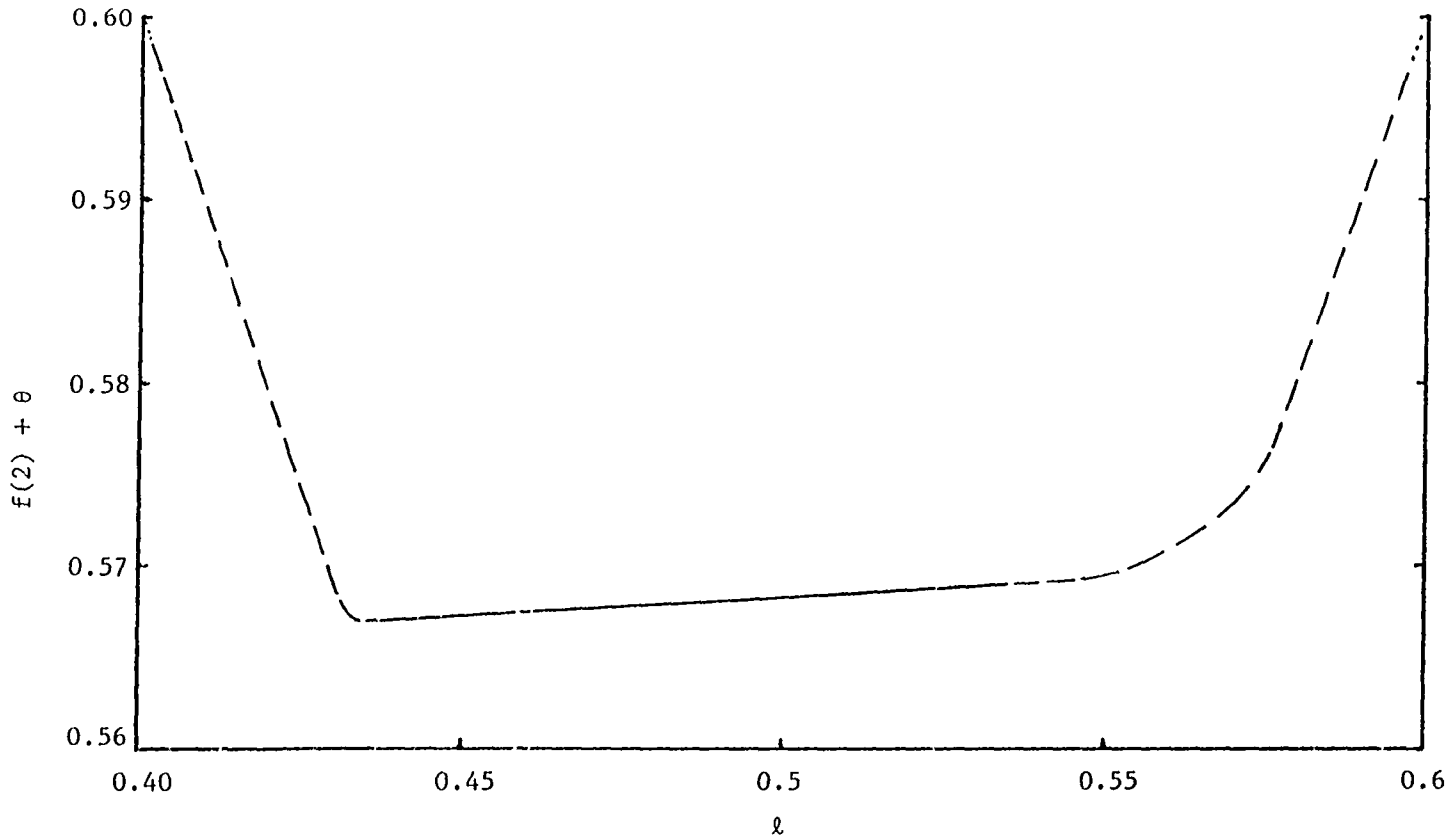

Figure 3.12. First term perturbation from the repulsive limit in 1-D (see text)

where the integration contour encloses the origin. In this treatment, at t=0 $f(\underset{\sim}{g}\overset{\ell}{\text{---}}\underset{\sim}{g}')=1$ if $\underset{\sim}{g}$ and $\underset{\sim}{g}'$ are composed of only empty sites, and zero otherwise.

Let m, and n denote blocks of consecutive empty sites, then

$$d/dt\ \tilde{f}(m,n,z)+[\alpha(t)+\beta(t)z]\tilde{f}(m,n,z)=\gamma(t)z+[\delta(t)+\varepsilon(t)z]f(m\overset{1}{\text{---}}n+1)\ , \tag{3.28}$$

where m,n=1,2 ($m\geq n$) and the coefficients are implicitly dependent upon m and n (see Table 3.2). Integrating and applying the inverse transform (Equation 3.27) to Equation 3.28 yields

$$f(m\overset{\ell}{\text{---}}n)=e^{-[A(t)+B(t)]}\left[1+\int_{s=0}^{t} ds\, e^{[A(s)+B(t)]}f(m)f(n+1)\{\delta(s)e^{[B(s)-B(t)]}+\varepsilon(s)\ e^{[B(s)-B(t)]}\}\right]+c(m\overset{\ell}{\text{---}}n) \tag{3.29}$$

where

$$\begin{aligned} c(m\overset{\ell}{\text{---}}n)=e^{-A(t)}&\int_{s=0}^{t} ds\ e^{A(s)}\ \frac{1}{(\ell-1)!}\gamma(s)[B(s)-B(t)]^{\ell-1} \\ &+\delta(s)\sum_{j=0}^{\ell}\frac{[B(s)-B(t)]^{j}}{j!}[f(m\overset{\ell-j}{\text{---}}n+1)-f(m)f(n+1)] \\ &+\varepsilon(s)\sum_{k=0}^{\ell-1}\frac{[B(s)-B(t)]^{k}}{k!}[f(m\overset{\ell-k-1}{\text{---}}n+1)-f(m)f(n+1)]\ . \end{aligned} \tag{3.30}$$

The f's appearing in Equations 3.29,30 are functions of s, $A(t)=\int_{t=0}^{t}\alpha(t)dt$ and $B(t)=\int_{t=0}^{t}\beta(t)dt$. The first term of Equation 3.29 is just $f(m)\cdot f(n)$.

Table 3.2. Expressions needed in Equations 3.28-3.30

$f(oo\overset{\ell}{---}oo)$:	$A_{22}(t)=4\tau_{ox}t-2(1-\rho_{ox})(q-1)$
(m=n=2)	$B_{22}(t)=-2(1-\rho_{ox})(q-1)$
	$\alpha_{22}(t)=4\tau_{ox}+2(\tau_{oo}-\tau_{ox})q$
	$\beta_{22}(t)=2(\tau_{oo}-\tau_{ox})q$
	$\gamma_{22}(t)=-2(\tau_{oo}-\tau_{ox})f(2)q^3$
	$\delta_{22}(t)=0.0$
$f(oo\overset{\ell}{---}o)$:	$A_{21}(t)=(2\tau_{ox}+\tau_{xx})t-(1-\rho_{ox})(q-1)$
(m=2,n=1)	$B_{21}(t)=-(1-\rho_{ox})(q-1)$
	$\alpha_{21}(t)=2\tau_{ox}+\tau_{xx}+(\tau_{oo}-\tau_{ox})q$
	$\beta_{21}(t)=(\tau_{oo}-\tau_{ox})q$
	$\gamma_{21}(t)=-q^2f(2)[\tau_{ox}-\tau_{xx}+(\tau_{oo}-\tau_{ox})q+(\tau_{oo}-2\tau_{ox}+\tau_{xx})q]$
	$\delta_{21}(t)=\tau_{xx}-\tau_{ox}$
	$\varepsilon_{21}(t)=-[\tau_{ox}-\tau_{xx}+(\tau_{oo}-2\tau_{ox}+\tau_{xx})q]$
$f(o\overset{\ell}{---}o)$:	$A_{11}(t)=2\tau_{xx}t$
(m=n=1)	$B_{11}(t)=0.0$
	$\alpha_{11}(t)=2\tau_{xx}$
	$\beta_{11}(t)=0.0$
	$\gamma_{11}(t)=-2qf(2)[\tau_{ox}-\tau_{xx}+(\tau_{oo}-2\tau_{ox}+\tau_{xx})q]$
	$\delta_{11}(t)=2(\tau_{xx}-\tau_{ox})$
	$\varepsilon_{11}(t)=-2[\tau_{ox}-\tau_{xx}+(\tau_{oo}-2\tau_{ox}+\tau_{xx})q]$

From Table 3.2 and Equation 3.30,

$$c(oo\overset{\ell}{\text{---}}oo)= \frac{e^{-A(t)}e_{\ell}^{-B(t)}}{(\ell-1)!}\int_{s=0}^{t} ds\ e^{A(s)}\ e_{\ell-1}^{B(s)}\ \gamma(s)[B(s)-B(t)]^{\ell-1}\ , \tag{3.31}$$

where $e_{\ell}^{x}=\sum_{i=0}^{\ell}\frac{x^{i}}{\ell!}$. Examination of Equation 3.31 along with Table 3.2 shows that the dominant decay for this correlation function is $\frac{1}{(\ell-1)!}$ as $\ell\to\infty$.

The nature of the decay of $c(oo\overset{\ell}{\text{---}}o)$ is seen by substituting $c(oo\overset{\ell-j}{\text{---}}oo)=f(m\overset{\ell-j}{\text{---}}n+1)-f(m)f(n+1)$ and $c(oo\overset{\ell-k-1}{\text{---}}oo)=f(m\overset{\ell-k-1}{\text{---}}n+1)-f(m)f(n+1)$ into Equation 3.30. Looking only at the term multiplied by $\delta(s)$, and using $a(s)=B(s)-B(t)$ and $a(t')=B(t')-B(s)$, gives

$$\frac{e^{-A(s)}}{(\ell-1)!}\int_{t'=0}^{t} dt'\ e^{A(t')}\ \delta(t')\ \sum_{j=0}^{\ell}\frac{(\ell-1)!}{j!(\ell-1-j)!}\ a(s)^{j}\ a(t')^{\ell-1-j}$$

$$=\frac{e^{-A(s)}}{(\ell-1)!}\int_{t'=0}^{t} dt'\ e^{A(t')}\ \gamma(t')[a(t')+a(s)]^{\ell-1}\ . \tag{3.32}$$

The $\frac{1}{(\ell-1)!}$ is again dominant for this term (as well as for the first term). The last term is treated in a similar manner and a $\frac{1}{(\ell-2)!}$ decay is found to dominate.

The analysis of $c(o\overset{\ell}{\text{---}}o)$ is analogous to that outlined for $c(oo\overset{\ell}{\text{---}}o)$ and the same general decay behavior is found. All of these correlations, therefore, have a dominant $\frac{1}{(\ell-1)!}$ decay behavior which, as shown in the next subsection, is very different from the equilibrium decay.

An expression for $f(oo\overset{\ell}{---}oo)$ can also be obtained by a recursive method using the following definitions:

$$\chi(\ell) = e^{-A_{22}(t)} f(oo\overset{\ell}{---}oo)$$

$$\eta = 1-\rho_{ox}$$

$$p = 1-q \ .$$

In terms of this notation $f(2)=\exp[-2(\tau_{ox}t+\eta p)]$, $f(4)=f(2)q^2=\exp[-2\tau_{ox}-\delta p-\tau_{oo}t)]$ and

$$\chi(0) = (1-p)^{2\eta} = \sum_{k=0}^{\infty} \frac{(2\eta)!p^k(-1)^k}{(2\eta-k)!k!} \ . \tag{3.33}$$

Starting from the equation for $d/dt\ f(oo\overset{\ell}{---}oo)$ it is found that

$$d/dp\ \chi(\ell) = -2\eta\chi(\ell-1) \ . \tag{3.34}$$

Equation 3.34 can be solved for $\ell=1$ using Equation 3.33. The same equation for $\ell=2$ can then be solved using the $\ell=1$ result. A general formula for $\chi(\ell)$, obtained by iteratively solving Equation 3.34, is

$$\chi(\ell) = e^{-2\eta p}_{\ell-1} + (-2\eta p)^{\ell} \sum_{k=0}^{\infty} \frac{(2\eta)!(-p)^k}{(2\eta-k)!(k+\ell)!} \ . \tag{3.35}$$

By comparison, Equation 3.29 for $f(oo\overset{\ell}{---}oo)$ has the form

$$\chi(\ell) = e^{-2\eta p}_{\ell-1} + \frac{(-2\eta)^{\ell}(-1)^{2\eta}}{(\ell-1)!} \int_{p'=0}^{p} [p-p']^{\ell-1}\, dp' \ . \tag{3.36}$$

The integral of Equation 3.36 is found in Reference 50 and corresponds to the sum in 3.35.

3.3.2. Correlation functions for 1-D, R=1 equilibrium processes

The first order Markovian behavior of equilibrium conditional probabilities (any site, empty or full, will shield cooperative effects) for 1-D, R=1 processes will now be shown.

Define $\gamma_i=\frac{1}{2}[1+(-1)^{\sigma_i}]=0,1$ for each site of a lattice having N total sites. If n is the number of occupied sites, then

$$\sum_{i=1}^{N} \gamma_i = n \ . \tag{3.37}$$

The grand partition function, in terms of the activity $\lambda=e^{\beta\mu}$ (μ is the chemical potential) and the interaction between n.n. occupied pairs, ω, is

$$\Xi = \sum_{n=0}^{\infty} \lambda^n \exp(-\beta\omega \sum_{n.n.} \gamma_i\gamma_j) \ . \tag{3.38}$$

Substituting Equation 3.37 into Equation 3.38 gives

$$\Xi = \sum_{\{\underset{\sim}{\sigma}\}} \exp(\beta\mu \sum_{i=1}^{N} \gamma_i - \beta\omega \sum_{n.n.} \gamma_i\gamma_j) \ . \tag{3.39}$$

The probability of finding the lattice of N sites in configuration $\underset{\sim}{\Sigma}=\{\sigma_i\}$ is

$$f(\underset{\sim}{\Sigma}) = \exp[\beta\mu \sum_{i=0}^{N} \gamma_i - \beta\omega \sum_{n.n.} \gamma_i\gamma_j]/\Xi$$

$$= \exp[\beta\mu \sum_{i\varepsilon\underset{\sim}{\sigma}} \gamma_i - \beta\omega \sum_{n.n.\varepsilon\underset{\sim}{\sigma}} \gamma_i\gamma_j]\exp[\beta\mu \sum_{i\varepsilon\underset{\sim}{\Sigma}-\underset{\sim}{\sigma}} \gamma_i - \beta\omega \sum_{n.n.\varepsilon\underset{\sim}{\Sigma}-\underset{\sim}{\sigma}+\underset{\sim}{\sigma}_{n.n.}} \gamma_i\gamma_j]/\Xi \tag{3.40}$$

where $\underset{\sim}{\sigma}$ is a subconfiguration of $\underset{\sim}{\Sigma}$ and $\underset{\sim}{\sigma}_{n.n.}$ are the sites in $\underset{\sim}{\sigma}$ that are n.n. to $\underset{\sim}{\Sigma}-\underset{\sim}{\sigma}$. Also, n.n.$\varepsilon\underset{\sim}{\sigma}$ means to take all n.n. pairs completely within $\underset{\sim}{\sigma}$. The probability $f(\underset{\sim}{\sigma})$ is given by

$$f(\underset{\sim}{\sigma}) = \sum_{\{\underset{\sim}{\Sigma}-\underset{\sim}{\sigma}\}} f(\underset{\sim}{\Sigma})$$

$$= \exp[\beta\mu \sum_{i\varepsilon\underset{\sim}{\sigma}} \gamma_i - \beta\omega \sum_{n.n.\varepsilon\underset{\sim}{\sigma}} \gamma_i\gamma_j] \sum_{\{\underset{\sim}{\Sigma}-\underset{\sim}{\sigma}\}} \exp[\beta\mu \sum_{i\varepsilon\{\underset{\sim}{\Sigma}-\underset{\sim}{\sigma}\}} \gamma_i$$

$$-\beta\omega \sum_{n.n.\varepsilon\{\underset{\sim}{\Sigma}-\underset{\sim}{\sigma}\}+\underset{\sim}{\sigma}_{n.n.}} \gamma_i\gamma_j]/\Xi \ . \tag{3.41}$$

A general conditional probability for the total lattice is

$$Q(\underset{\sim}{\Sigma}-\underset{\sim}{\sigma})[\underset{\sim}{\sigma}] = \frac{f(\underset{\sim}{\Sigma})}{f(\underset{\sim}{\sigma})} = \frac{\exp[\beta\mu \sum_{i\varepsilon\underset{\sim}{\Sigma}-\underset{\sim}{\sigma}} \gamma_i - \beta\omega \sum_{n.n.\varepsilon\underset{\sim}{\Sigma}-\underset{\sim}{\sigma}+\underset{\sim}{\sigma}_{n.n.}} \gamma_i\gamma_j]}{\sum_{\{\underset{\sim}{\Sigma}-\underset{\sim}{\sigma}\}} \exp[\beta\mu \sum_{i\varepsilon\{\underset{\sim}{\Sigma}-\underset{\sim}{\sigma}\}} \gamma_i - \beta\omega \sum_{n.n.\varepsilon\{\underset{\sim}{\Sigma}-\underset{\sim}{\sigma}\}+\underset{\sim}{\sigma}_{n.n.}} \gamma_i\gamma_j]} \tag{3.42}$$

which is independent of $\underset{\sim}{\sigma}$ (conditioning sites) except for those sites n.n. to $\underset{\sim}{\Sigma}-\underset{\sim}{\sigma}$ (conditioned sites). The previously defined subconfiguration conditional probabilities (q) are trivially obtained from the total lattice conditional probabilities (Q). Furthermore, the result just obtained allows truncation of subconfiguration equilibrium conditional probabilities to single conditioning sites (e.g. qo[xoo]= qo[x]), thus establishing the first order Markovian behavior.

The Markovian nature just discussed allows for a particularly simple evaluation of $f(\sigma_1 \overset{\ell}{\text{---}} \sigma_2)$ as follows:

$$f(\sigma_f \xrightarrow{\ell} \sigma_g) = \sum_{\{\sigma_i\}} f(\sigma_f\sigma_1\sigma_2\cdots\sigma_\ell\sigma_g)$$

$$= \sum_{\{\sigma_i\}} f(\sigma_f) q\sigma_f[\sigma_1] q\sigma_1[\sigma_2]\cdots q\sigma_\ell[\sigma_g]$$

$$= f(\sigma_f)\ (\underset{\sim}{Q}^{\ell+1})_{\sigma_f\sigma_g}\ , \tag{3.43}$$

where the matrix $\underset{\sim}{Q}$ is

$$\underset{\sim}{Q} = \begin{pmatrix} qo[o] & qo[x] \\ qx[o] & qx[x] \end{pmatrix} = \begin{pmatrix} f(2)/(1-\theta) & [1-\theta-f(2)]/(1-\theta) \\ [1-\theta-f(2)]/\theta & [f(2)+2\theta-1]/\theta \end{pmatrix} . \tag{3.44}$$

The eigenvalues and eigenvectors of $\underset{\sim}{Q}$ are

$$\begin{aligned} \lambda_1 &= 1 \\ \lambda_2 &= 1 - \frac{1-f(2)-\theta}{\theta(1-\theta)} \\ \underset{\sim}{\chi}_1 &= \begin{pmatrix} 1 \\ 1 \end{pmatrix} \\ \underset{\sim}{\chi}_2 &= \begin{pmatrix} -\theta/(1-\theta) \\ 1 \end{pmatrix} . \end{aligned} \tag{3.45}$$

Since the probabilities of $\underset{\sim}{Q}$ are bounded by zero and one, the trace of $\underset{\sim}{Q}$ is between zero and two. This, and the fact that $\lambda_1=1$, shows that $|\lambda_2|<1$.

Working through the matrix algebra for the case at hand reveals that

$$\underset{\sim}{Q}^N = \begin{pmatrix} \lambda_1^N(1-\theta)+\lambda_2^N\theta & \lambda_1^N\theta\ \lambda_2^N\theta \\ \lambda_1^N(1-\theta)-\lambda_2^N(1-\theta) & \lambda_1^N\theta+\lambda_2^N(1-\theta) \end{pmatrix} . \qquad (3.46)$$

The correlation functions, obtained from Equations 3.43 and 3.46, are $c(o\overset{\ell}{\text{—}}o)=f(1)\lambda_2^{\ell+1}\theta$, $c(oo\overset{\ell}{\text{—}}o)=\frac{f(2)}{1-\theta}\,c(o\overset{\ell}{\text{—}}o)$ and $c(oo\overset{\ell}{\text{—}}oo)=\frac{f(2)}{(1-\theta)^2}$ $c(o\overset{\ell}{\text{—}}o)$ and $f(2)$ can be obtained from Reference 51.

3.3.3. Comparison of irreversible and equilibrium correlations

It is now possible to compare the irreversible and lattice gas (Ising) correlations. Here the irreversible rates are assumed to be given by an Arrhenius form with pairwise activation energies which are chosen as the interaction energies in the equilibrium case. Figures 3.13-3.15 show corresponding irreversible and equilibrium plots for $c(o\overset{\ell}{\text{—}}o)$, $c(oo\overset{\ell}{\text{—}}o)$ and $c(oo\overset{\ell}{\text{—}}oo)$ at $\theta\cong 0.5$. Figure 3.16 plots $c(o\overset{\ell}{\text{—}}o)$ (irreversible)/$c(o\overset{\ell}{\text{—}}o)$ (equilibrium) against ℓ.

The dominant irreversible $\frac{1}{(\ell-1)!}$ decay is much faster than the equilibrium $\lambda_2^{\ell+1}$ decay. It should also be noted when comparing the irreversible and lattice gas models, that the irreversible process is not fully Markovian to <u>any</u> order. Further, a Markovian type truncation of irreversible equations (keeping a finite, arbitrarily high, number of conditioning sites) will <u>never</u> produce the correct asymptotic fast correlation decay.

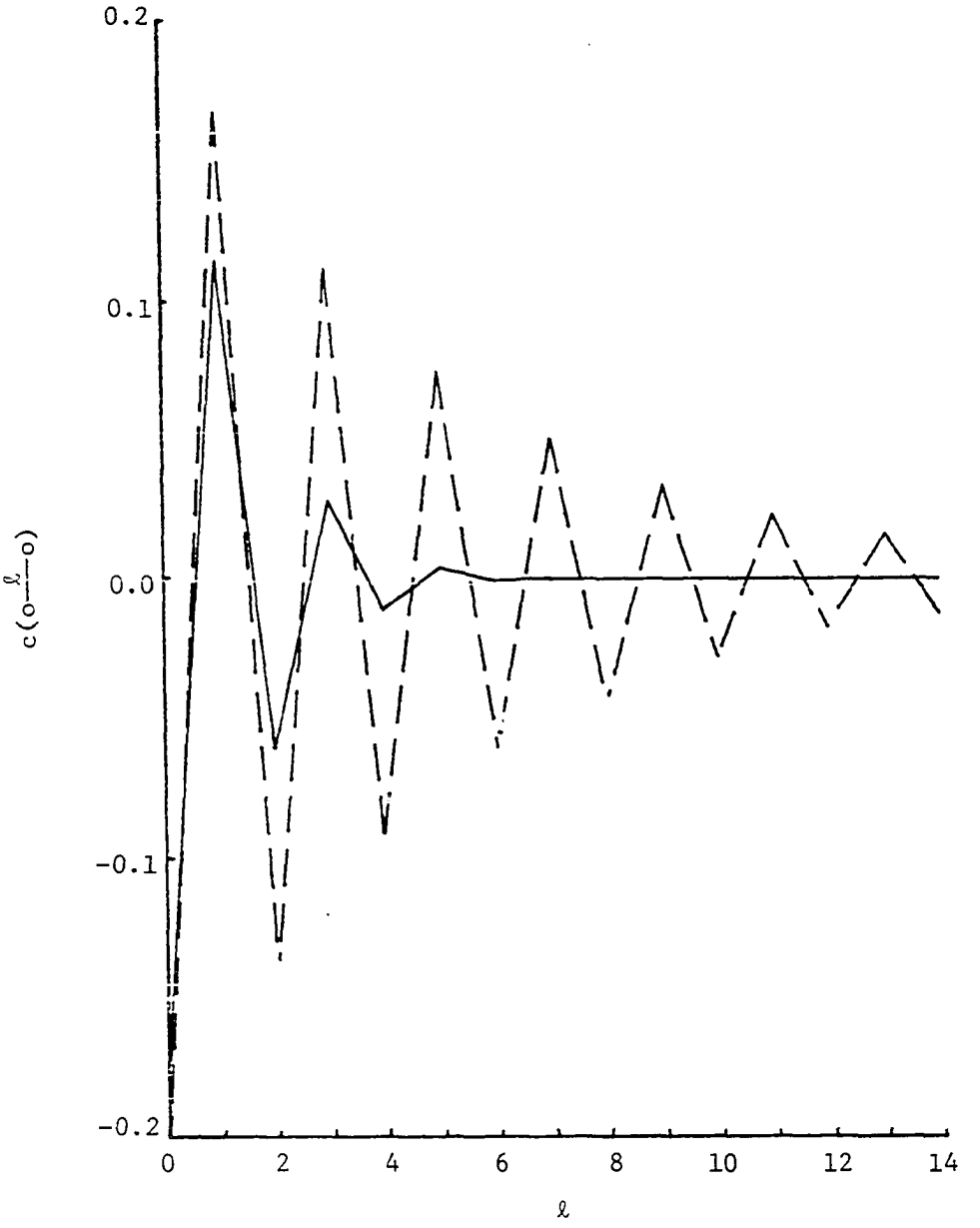

Figure 3.13. Irreversible (——) and equilibrium (- - - -) plots of c(o—ℓ—o) as a function of ℓ at θ≅0.5

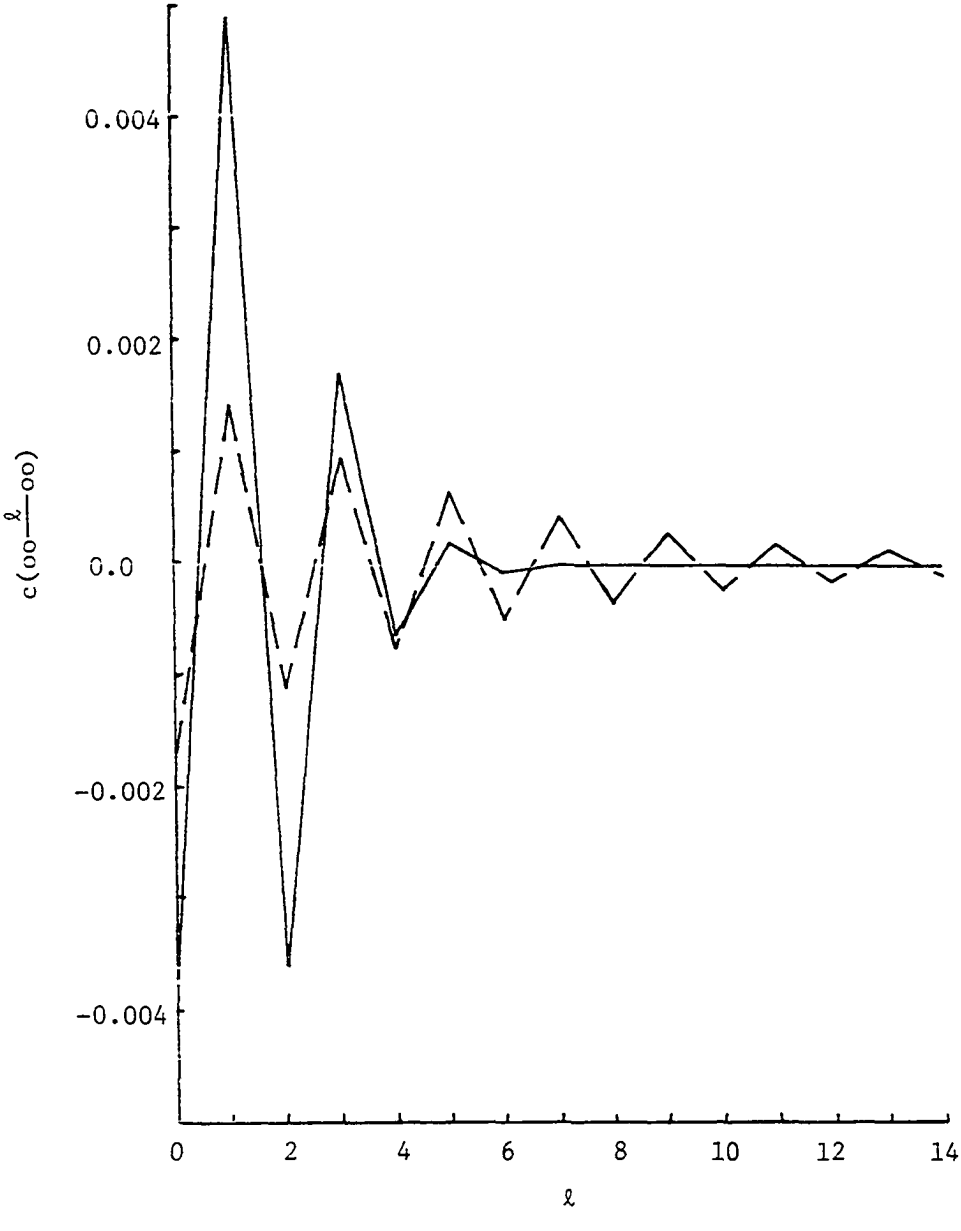

Figure 3.14. Irreversible (——) and equilibrium (- - - -) plots of $c(oo\overset{\ell}{---}oo)$ as a function of ℓ at $\theta \cong 0.5$

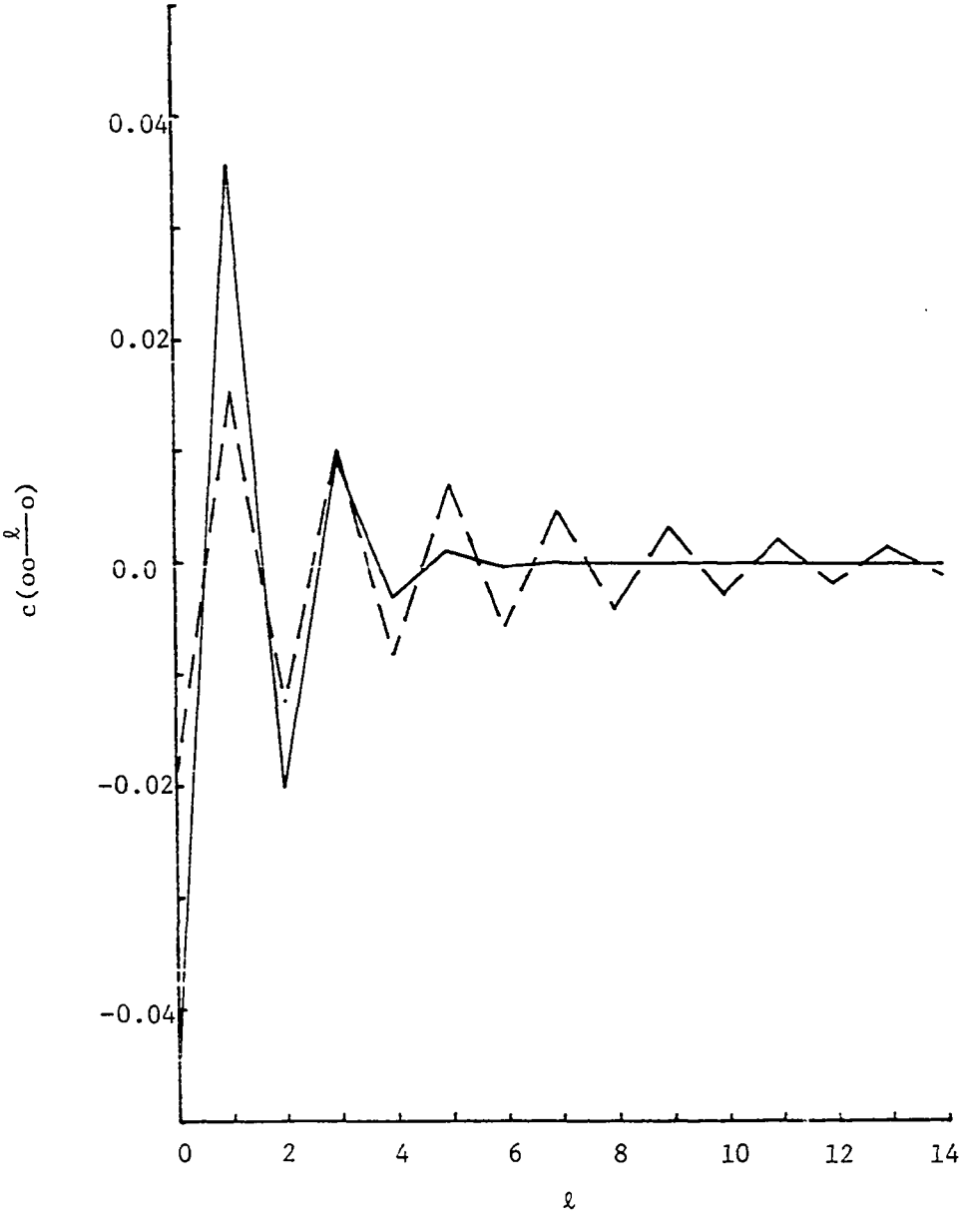

Figure 3.15. Irreversible (——) and equilibrium (- - - -) plots of $c(oo\overset{\ell}{---}o)$ as a function of ℓ at $\theta \cong 0.5$

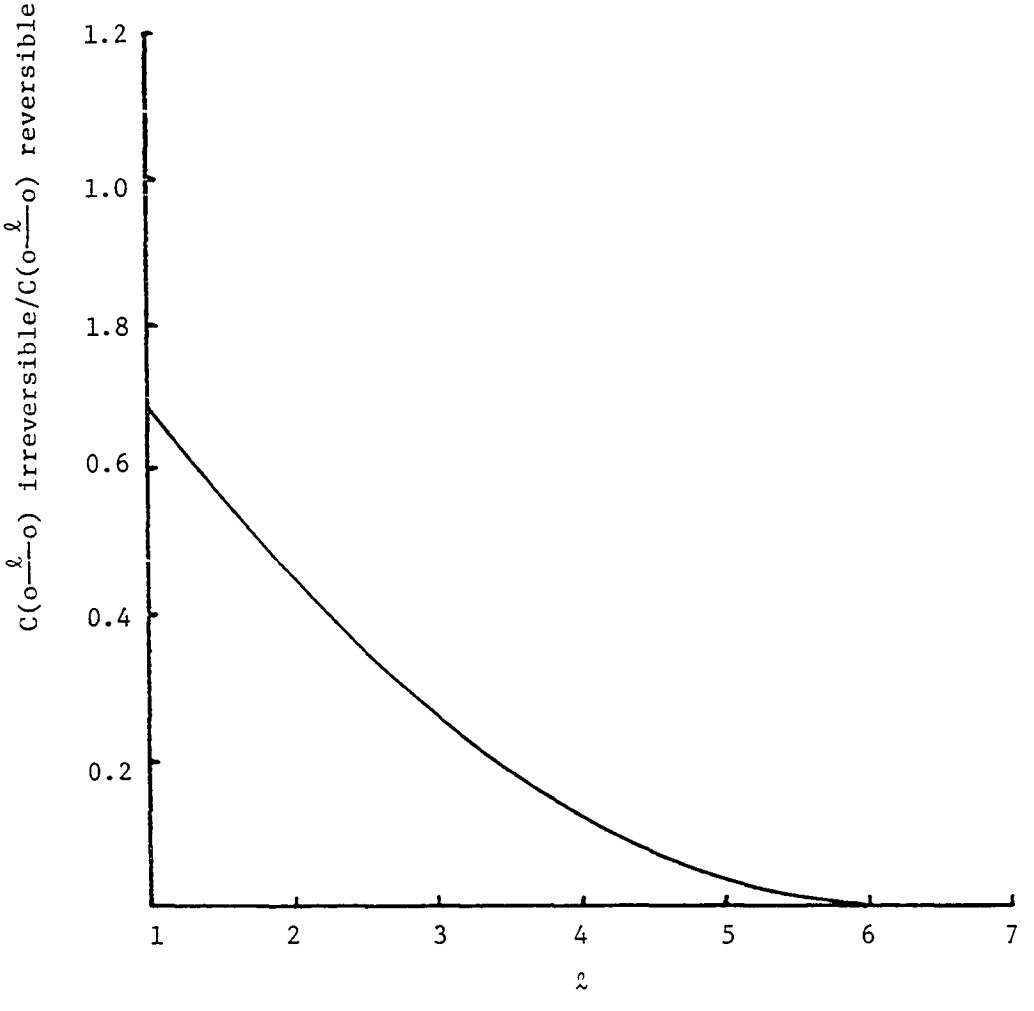

Figure 3.16. Ratio of C(o—ℓ—o) irreversible and C(o—ℓ—o) reversible as a function of ℓ

3.4. Configurational Entropy of Ring Lattices

The configurational entropy of a process on a finite lattice with only one kind of event is given by the grand canonical expression (47)

$$S_{con} = -K \sum_{n=0}^{N} \sum_{\{n\}} f(\{n\}) \ln f(\{n\}) , \tag{3.47}$$

where $f(\{n\})$ is a total lattice probability with n occupied sites, $\{n\}$, and the rest of the lattice empty (N is the total number of sites). In this section, the configurational entropy for irreversible/equilibrium adatom distributions on five and six site ring lattices with n.n. cooperative effects/interactions will be treated.

The equilibrium distribution is described by the lattice gas formalism previously introduced in Section 3.3.2 (cf., Equation 3.40). When there are no cooperative effects (w=o), the familiar Langmuir result,

$$S_{con}(\text{Langmuir}) = -NK[\theta \ln \theta + (1-\theta) \ln (1-\theta)] , \tag{3.48}$$

is obtained.

The irreversible kinetic equations for probabilities of configurations of the whole finite lattice are obtained from Equation 1.1 as

$$d/dt\, f(\{n\}) = \sum_{\substack{j\varepsilon\{n\} \\ \sigma_j=x}} \tau_{\underset{\sim}{\sigma} j}\, f(\{n\}-j) - \left[\sum_{\substack{j=\{n\} \\ \sigma_j=0}} \tau_{\underset{\sim}{\sigma} j} \right] f(\{n\}) \tag{3.49}$$

where $\{n\}-j$ indicates that occupied site j is removed from the set $\{n\}$.

For five/six site ring systems, there are eight/thirteen independent equations respectively.

The five site ring lattice is now discussed. For this system, the equilibrium and irreversible entropy equations are the same in the repulsive limit (see Reference 47 for equilibrium equations cast in a similar form to Equation 3.49). This is due to the limited number of configurations in the five site ring system. Away from the repulsive limit, however, the equations differ. Figure 3.17 shows S/K verses θ both in the limit and slightly off of the limit (ρ_{ox}=0.01). The interesting structure can be explained by considering the process as occurring in stages. Initially, only the empty lattice exists and the entropy is zero. During the first stage, eleven configurations contribute to the entropy (one empty, five with one full site and five with two separated full sites). At the first peak, the ensemble weight is most randomly distributed between these eleven possibilities. Toward the end of the stage, those configurations with two separated full sites are dominant and only those configurations are left at the end of the stage. The entropy is nonzero at the end of the first stage since five possible configurations still exist. During the second stage, ten configurations exist (five with two separated full sites and five with three nonconsecutive full sites). The ensemble weight is most randomly distributed at the second peak of Figure 3.17 and at the end of this stage only the five configurations with three full sites exist. During the last stage, eleven configurations are possible (five with three nonconsecutive full sites, five with four full sites and one with five full sites). As in

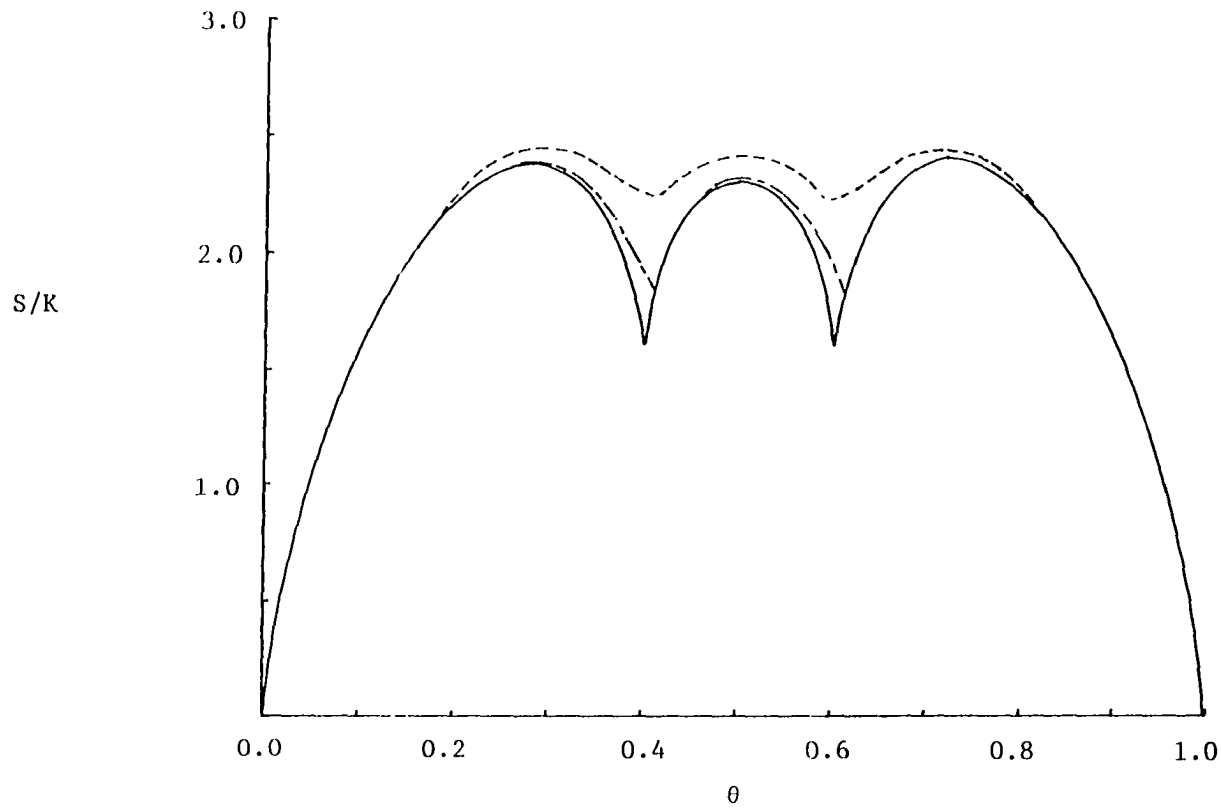

Figure 3.17. Irreversible (—— - ——) and equilibrium (- - - -) configurational entropy for a five site ring lattice when ρ_{ox}=0.01. The solid curve is for both the irreversible and equilibrium entropy in the n.n. repulsive limit ($\rho_{ox}\rightarrow$o)

the other stages a maximum occurs when the configurations are most random, but at the end of this stage only the configuration with five full sites remains and the entropy is zero.

The entropy for a five site lattice away from the repulsive limit, as well as the Langmuir case, is shown in Figure 3.18. The trajectories going from the equilibrium curve to the irreversible curve are obtained by using the equilibrium values at the indicated θ as initial values in the irreversible equations.

The filling in stages of a six site ring lattice is now treated. For the irreversible process, on this lattice there are eighteen possible configurations during the first stage with five of them remaining at the end of the stage (see Table 3.3). During the second stage, twenty configurations are possible with eleven remaining at the end of the stage. Note that more configurations are possible at the end of this stage than at the beginning of this stage. During the last stage, eighteen configurations are possible with only one (all sites full) remaining at the end of the stage. For an equilibrium process, only one minimum entropy occurs for $0<\theta<1$ at $\theta=0.5$ (when every second site is full). Figure 3.19 is a graph of S/K verses θ for a six site ring lattice staged filling process. The low values for S/K during the second stage of the irreversible process are found since relatively few configurations effectively contribute to the ensemble.

The six site ring lattice is a prototype for larger lattices. The irreversible process will occur in three stages (with the minimums in the limiting cases occurring at $\theta \cong \frac{1-e^{-2}}{2}$ and $\theta \cong \frac{1+e^{-2}}{2}$, corresponding to

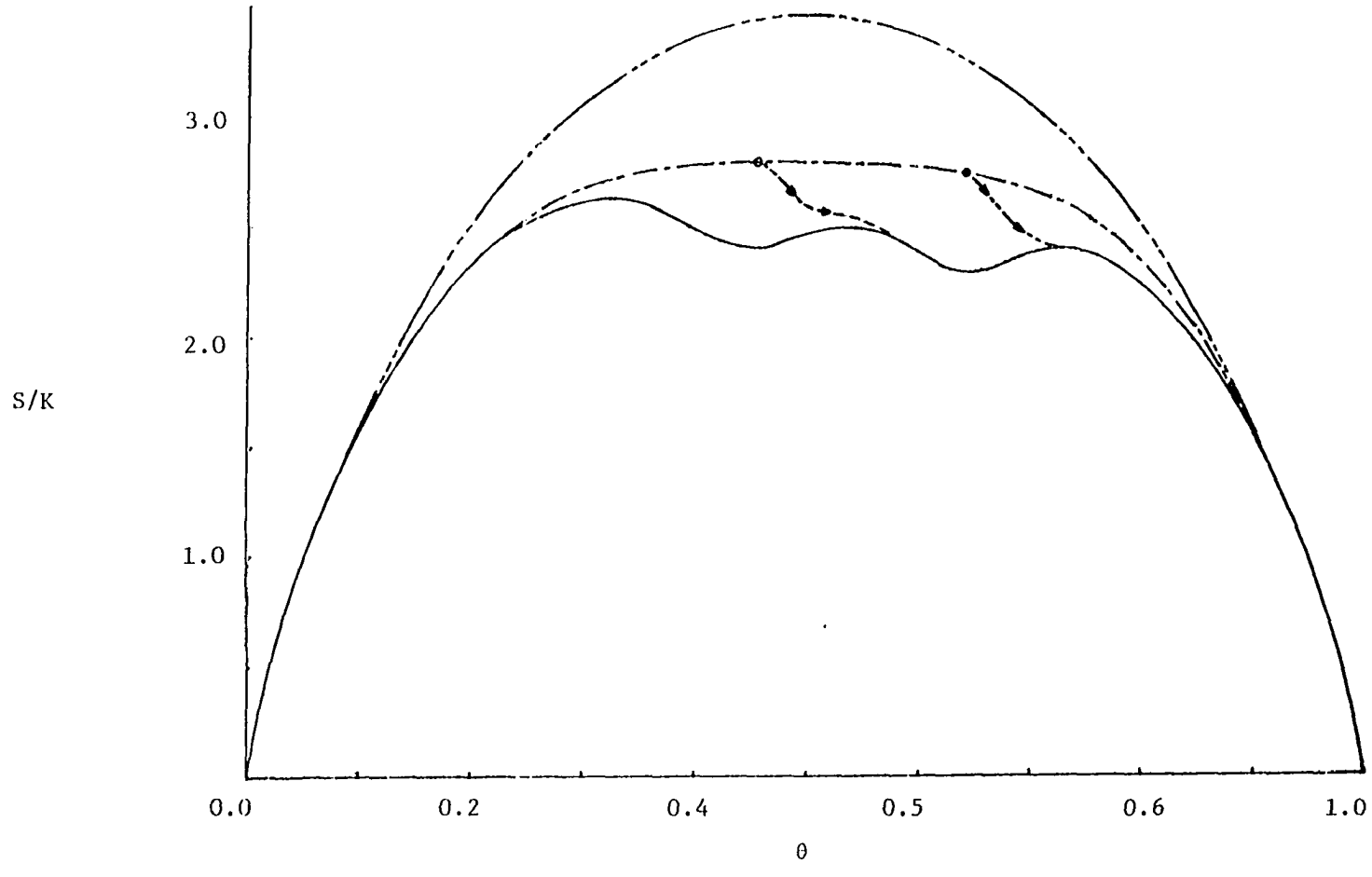

Figure 3.18. Configurational entropy for irreversible (——), equilibrium (— — — — —) and random filling (— · — · —) of a five site ring lattice (ρ_{ox}=0.078). Trajectories going from the equilibrium curve to the irreversible curve (----) are obtained by using the equilibrium values at the indicated θ as initial values in the irreversible equations

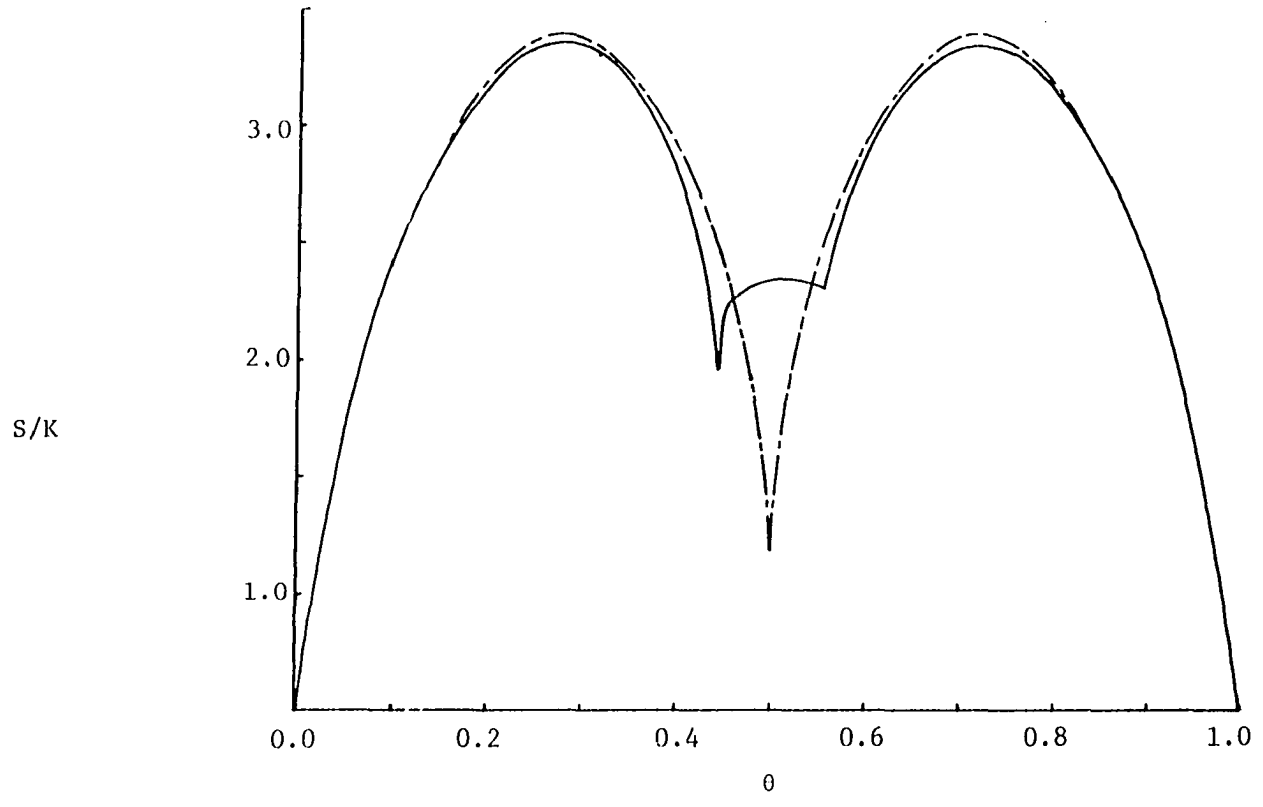

Figure 3.19. Irreversible (——) and equilibrium (— — —) configurational entropy for a six site ring lattice in the n.n. repulsive limit

Table 3.3. Number of configurations for staged filling of a six site ring lattice

First stage:

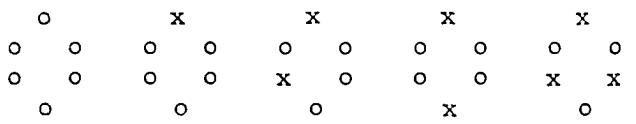

1 + 6 + 6 + 3 + 2 = 18 configurations

Initial/maximum/final number of configurations = 1/18/5

Second stage:

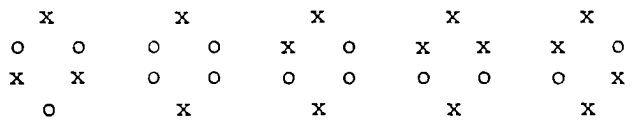

2 + 3 + 12 + 6 + 3 = 26 configurations

Initial/maximum/final number of configurations = 5/26/11

Third stage:

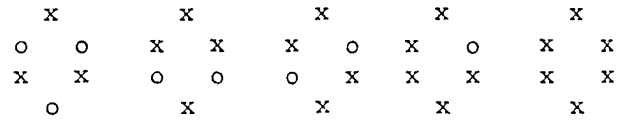

2 + 6 + 3 + 6 + 1 = 18 configurations

Initial/maximum/final number of configurations = 11/18/1

the three stages of filling described for 1-D, R=1 highly repulsive n.n. cooperative effects) with the second stage asymmetric due to the larger number of configurations at the end of the stage than at the beginning of the stage for n.n. inhibitory processes. The equilibrium entropy will have one minimum when every second lattice site is full ($\theta \cong 0.5$).

3.5. Processes with Competing Events

Surface adsorption processes are often complicated by adsorbent impurities that compete for binding sites. Substituents on polymer chains can undergo side reactions which compete with the one of interest. To describe these processes, which have more than one kind of event occurring simultaneously, requires an extension of the kinetic models previously discussed.

For single species adsorption (surface terminology will be used here, but the theory applies to any process with competing events) in 1-D and for R=1 only one conditional probability, $q_o[oo]=\exp[-\tau_{o\cdot o}t]$, is required to truncate the hierarchy of kinetic equations as shown in Section 2.1. For competing events, the situation is more complex.

Suppose, for example, that N species, $i=1,2,\cdots,N$, adsorb. Let τ_{oo}^{i} be the rate of species i landing between two empty sites, τ_{oj}^{i} be the rate of species i landing between an empty site and a site occupied by species j and τ_{kj}^{i} be the rate of species i landing on an empty site flanked by species k on the left and species j on the right. Then,

$$\tau_{kj} = \sum_{i=1}^{N} \tau_{kj}^{i} \tag{3.50}$$

is the rate for any species landing on site flanked by species k on the left and species j on the right. Note that the relative amounts of each species in the source density are incorporated into the rate. After application of the shielding condition, the equations for the minimal set of conditional probabilities are

$$d/dt\ \ell n\ qo[oo] = -\tau_{oo} \tag{3.51}$$

and

$$d/dt\ qi[oo] = \sum_{\ell=0}^{N} (\tau_{o\ell}-\tau_{oi})qi[oo]q\ell[oo] + \sum_{k=0}^{N} \tau_{ko}^{i}\ qk[oo]qo[oo] \ . \tag{3.52}$$

The N independent, closed, coupled differential equations can be simultaneously solved for the conditional probabilities.

As $t\to\infty$, $d/dt\ qi[oo]\to 0$ and $qo[oo]\to 0$. Further, from conservation of probability, $qi[oo]\neq 0$ for at least one i (say i*) which implies

$$0 = \sum_{\ell=0}^{N} (\tau_{o\ell}-\tau_{oi*})qi*[oo]q\ell[oo], \quad t\to\infty \ . \tag{3.53}$$

For example, suppose only two species, a and b, are present and that $qa[oo]\neq 0$. Then, the $t\to\infty$ limit of Equation 3.52 gives

$$0 = (\tau_{ob}-\tau_{oa})qa[oo]qb[oo] \ . \tag{3.54}$$

When $\tau_{ob}\neq\tau_{oa}$, $qb[oo]=0$ and $qa[oo]=1$, since at $t\to\infty$ $qa[oo]+qb[oo]=1$. The conditional probability that goes to one (assumed to be $qa[oo]$ above) is determined by the relative magnitudes of τ_{ob} and τ_{oa}. The rate $d/dt\ qa[oo]$ is strictly positive and hence $qa[oo]\to 1$ if $\tau_{ob}>\tau_{oa}$,

as can be seen from the form of the right hand side of Equation 3.52. Another solution is possible if $\tau_{oa}=\tau_{ob}$. In this case, the conditional probabilities range between zero and one (always summing, of course, to unity). All values in the range are possible and depend on the rates other than $\tau_{oa}=\tau_{ob}$.

The number of rates needed to describe 1-D n.n. cooperative processes (assuming reflection symmetry) is $\frac{1}{2}$ N(N+1)(N+2). Thus, a wide range of choices is possible (e.g., a two-event system requires twelve rates to be specified). Figure 3.20 shows a few selected probabilities as a function of coverage for a two-event system where the rates for landing next to species b are moderately inhibitory and those for landing next to species a are twice as inhibitory. These were obtained by solving the closed set of equations for f(o), f(oo), f(ao), f(aoo), f(aoa), qo[oo] and qa[oo].

The effect of systematically varying the rates of adsorption for species b relative to species a in a two species system is shown in Figure 3.21. The plot labeled ε=1 is obtained by choosing a basis set of rates. The other plots are then obtained by multiplying all of the rates for species b landing a factor ε. When $\varepsilon>1$ the rate of species b landing is enhanced and when $\varepsilon<1$ the rate of species b landing is decreased.

Competitive binding of ligands having various lengths k can also be exactly solved. Epstein (39) has previously discussed the case illustrated in Figure 3.22.

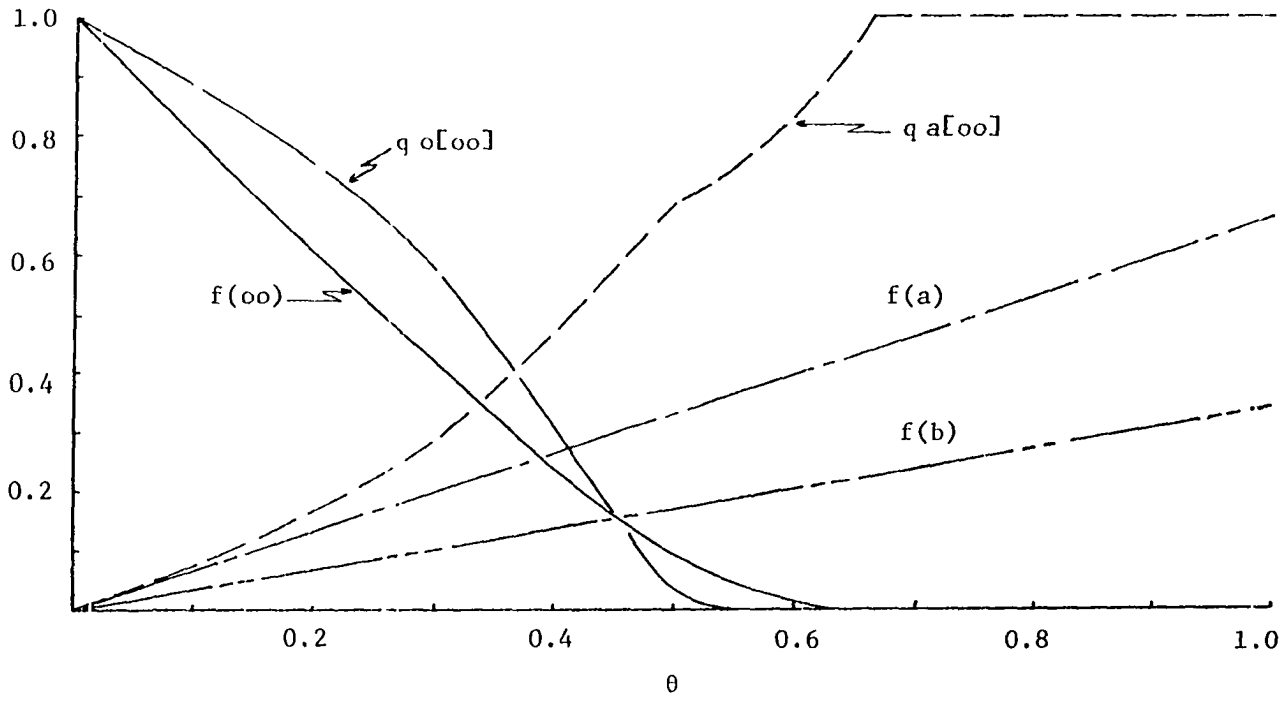

Figure 3.20. Selected probabilities as a function of θ for a two-event system. The rates are: $\tau_{oo}^{a}=1$, $\tau_{ao}^{a}=8\times10^{-2}$, $\tau_{bo}^{a}=1.6\times10^{-1}$, $\tau_{aa}^{a}=6\times10^{-3}$, $\tau_{bb}^{a}=12\times10^{-3}$, $\tau_{oo}^{b}=0.5$, $\tau_{ao}^{b}=4\times10^{-2}$, $\tau_{bo}^{b}=6\times10^{-2}$, $\tau_{aa}^{b}=3\times10^{-3}$, $\tau_{bb}^{b}=2\times10^{-3}$, $\tau_{ab}^{a}=4\times10^{-3}$, $\tau_{ab}^{b}=3\times10^{-3}$

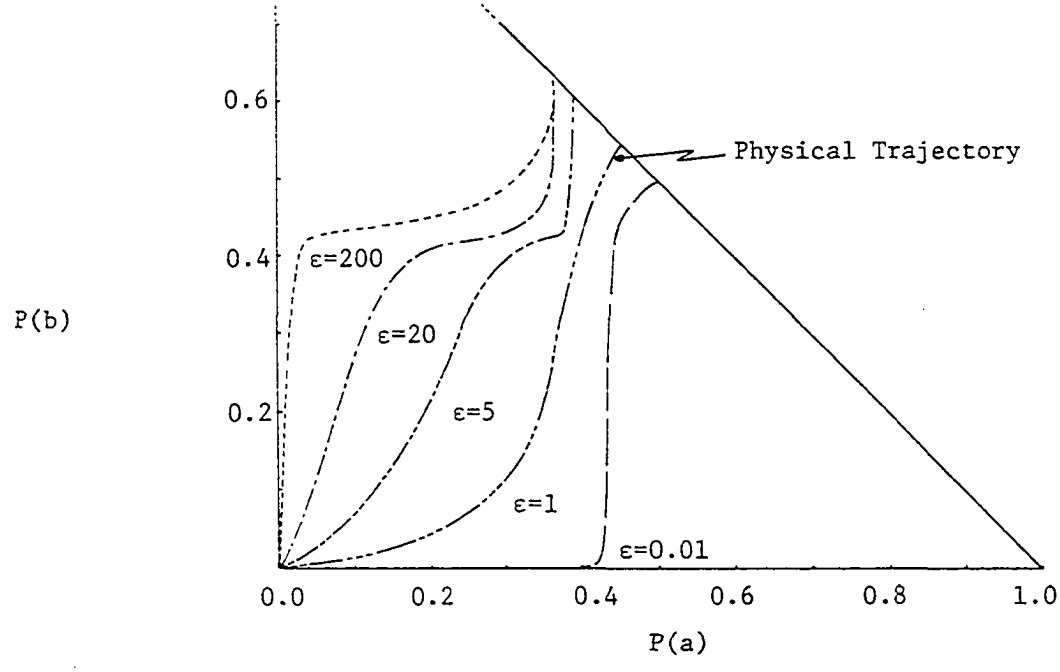

Figure 3.21. Systematic variation of the rates of adsorption for species b relative to species a in a two species system. The rates are: $\tau_{oo}^{a}=1$, $\tau_{ao}^{a}=10^{-4}$, $\tau_{bo}^{a}=0.1$, $\tau_{aa}^{a}=10^{-6}$, $\tau_{bb}^{a}=0.8$, $\tau_{ab}^{a}=10^{-3}$, $\tau_{oo}^{b}=0.1\varepsilon$, $\tau_{ao}^{b}=0.3\varepsilon$, $\tau_{bo}^{b}=10^{-4}\varepsilon$, $\tau_{aa}^{b}=0.8\varepsilon$, $\tau_{bb}^{b}=10^{-6}\varepsilon$, $\tau_{ab}^{b}=10^{-3}\varepsilon$

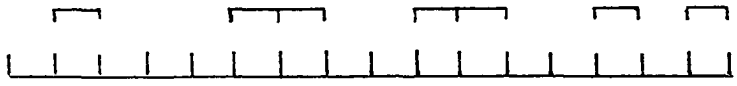

Figure 3.22. Competitive binding of dimer and trimer ligands

In general, $q_o[n_N]=\exp[-t\sum_{k=1}^{N}\tau_{oo}^{k}]$ where n_N is the length of the longest ligand and τ_{oo}^{k} is the rate of an n_k-mer (n_k is the length of the kth ligand) landing between two empty sites. Kinetic equations for $f(\ell)$ in the following blocks of ℓ consecutive empty sites are of generic form: $\ell=1, 1<\ell\leq n_1, n_1<\ell\leq n_2, n_2<\ell\leq n_3, \cdots, n_N<\ell$ where $n_1, n_2, \cdots, n_N$ are in order of increasing ligand lengths. This hierarchy of equations can be closed by using $q_o[n_N]$ to truncate.

3.6. Periodic Lattices

To model copolymer systems (35-38) one must consider lattices with periodic distributions of sites. The kinetic equations for periodic lattices can be written by generalizing Section 2.1 to introduce site dependent rates and probabilities. A similar, but somewhat more complex, treatment could be given for stochastic lattices.

For a system with n.n. cooperative effects on a lattice of alternating sites (A and B) where only one event can occur on each type of site the rates τ_{oo}^{A}, τ_{oo}^{B}, τ_{ox}^{A}, τ_{ox}^{B}, τ_{xx}^{A} and τ_{xx}^{B} are needed (the superscript indicates the kind of site being landed on). If the A and B rates are equal, the process will obviously be identical to that described in Section 2.2. If the B rates all equal zero, the lattice will fill randomly on A sites.

The minimal set of probabilities with closed coupled equations for this case is $f(\overset{A}{o})$, $f(\overset{B}{o})$, f(oo), $q\overset{A}{o}[oo]$ and $q\overset{B}{o}[oo]$. Figure 3.23 is a graph of f(oo) against θ^A, the coverage of type A sites. There the rates for landing on an A site are for highly inhibitory n.n. cooperative effects. Those for landing on a B site are obtained from the above rates by multiplying by a factor ε which ranges from zero (random adsorption on A sites) to five (landing on B sites highly favored). When $\varepsilon=1$, the sites are equivalent and filling in stages is observed as previously (cf., Sections 3.1 and 3.2). For other values of ε, the lattice still fills in stages, but $d/d\theta^A$ f(oo) is shifted according to the relative rates.

Figure 3.24 plots θ^B against θ^A where, for $\varepsilon=1$, a filled B site slightly inhibits occupation of n.n. A sites, but one full n.n. A site greatly inhibits occupation of the B site and two n.n. full sites block occupation of a B site. Other plots are obtained by multiplying the rates of landing on A sites by a factor ε, $0 \leqslant \varepsilon \leqslant 2$.

3.7. Limited Mobility

This section will treat dissociative adsorption of homonuclear diatomic molecules where the dissociated adatoms are allowed limited mobility before they become permanently affixed. In this model, it is assumed that adatoms initially landing on sites i and i+1 immobily occupy sites -m+i and m'+i+1, where $-\ell \leqslant -m < m'+1 \leqslant k+1$. Here ℓ and k are fixed, nonnegative numbers and the sites between -m+i and m'+i+1 are empty before the adsorption event. The maximum number of fixed

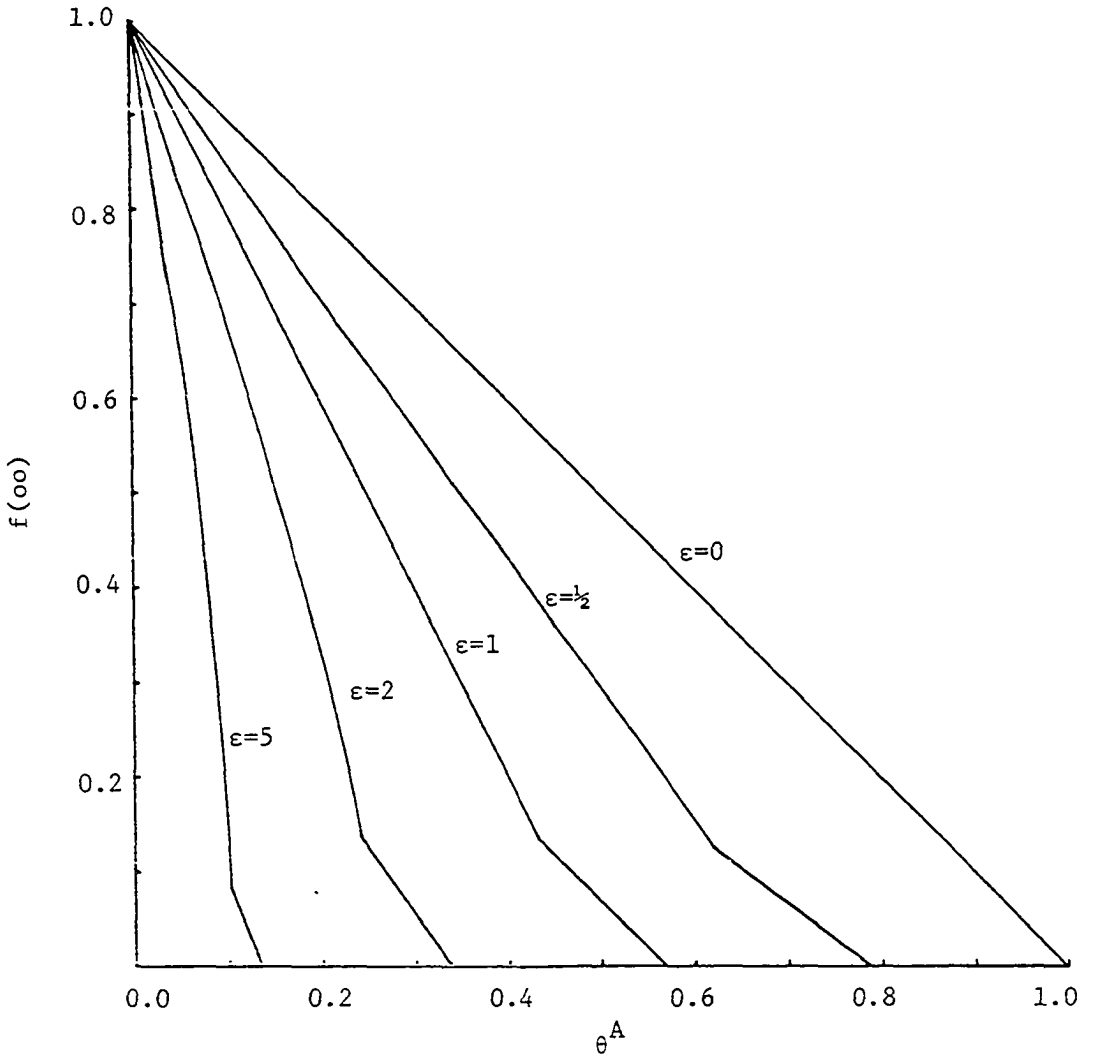

Figure 3.23. f(oo) as a function of θ^A for $\tau_{oo}^A=1$, $\tau_{oo}^B=\varepsilon$, $\tau_{ox}^A=0.01$, $\tau_{ox}^B=0.01\varepsilon$, $\tau_{xx}^A=0.0001$ and $\tau_{xx}^B=0.0001\varepsilon$

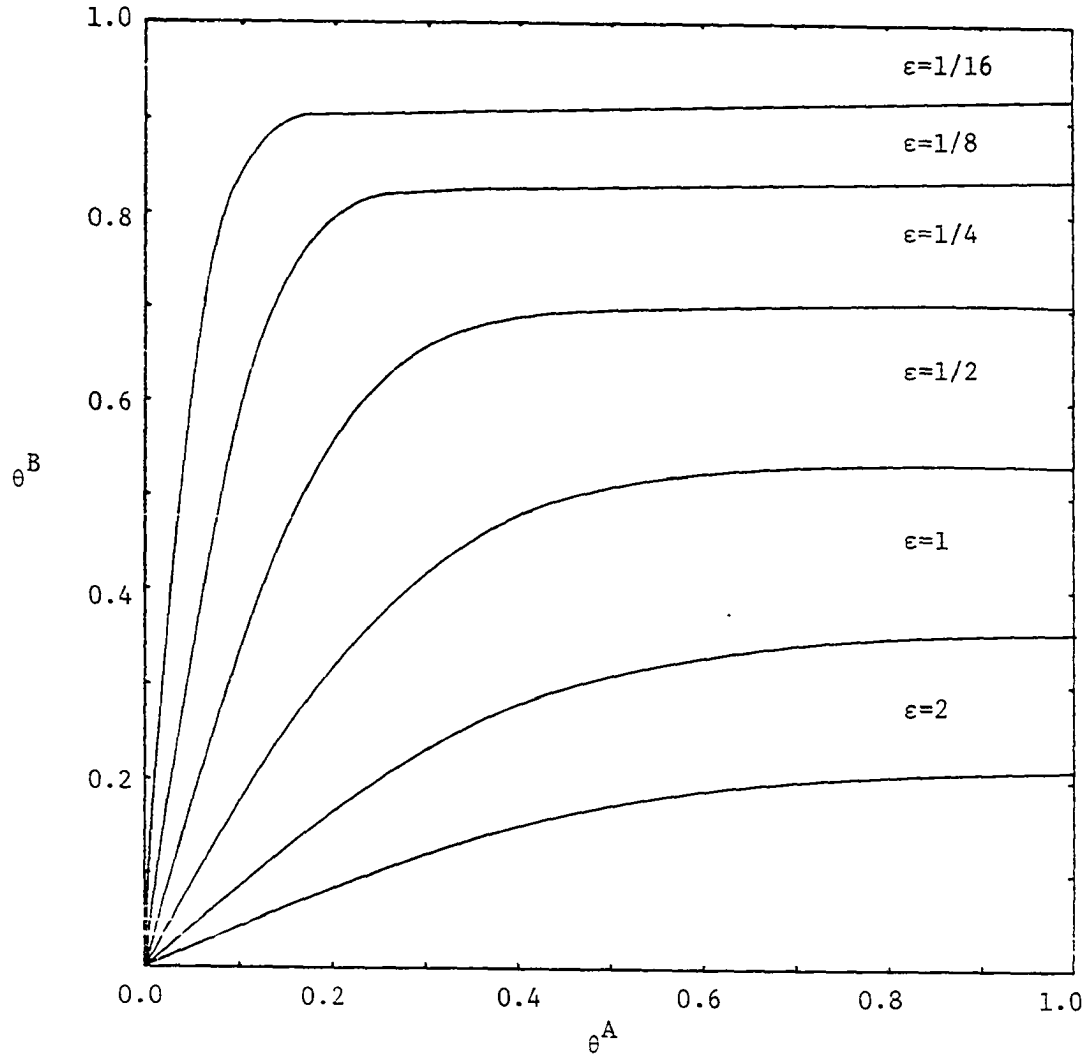

Figure 3.24. Coverage of B sites, θ^B, as a function of the coverage of A sites, θ^A. The rates are: $\tau_{oo}^B=1.0$, $\tau_{oo}^A=\varepsilon$, $\tau_{xo}^B=0.01$, $\tau_{xo}^A=0.7\varepsilon$, $\tau_{xx}^B=0.0$, $\tau_{xx}^A=0.4\varepsilon$

lattice spacing between the immobile adatoms is, therefore, d=ℓ+k+1. More complicated processes are possible, but will not be treated here. In general, the conditions on the cooperativity for exact solvability are the same as for the 1-D monomer problem (the max separation, d, allowed between adatoms is arbitrary). The present treatment will describe in detail the case where r=0, R=1 and d=2, with the extra restriction that m,m'=0 or 1. An initially empty lattice is also assumed.

The kinetic equations for this process are written in the usual way. For example, letting h denote the states of sites i-2 and i-1 as $\alpha = -x$, β=xo or γ=oo and h' denote the sites i+2 and i+3 as α'=x-, β'=ox or γ'=oo yields

$$-d/dt\ f(n) = \tau^{(\gamma,\gamma')}_{(1,0)} f(o\overbrace{\overset{xx}{o\cdots o}}^{n}) + \tau^{(\beta,\gamma')}_{(1,0)} f(x\overbrace{\overset{xx}{o\cdots o}}^{n})$$

$$+ \tau^{(\alpha,\gamma')}_{(0,0)} f(x\overbrace{\overset{xx}{o\cdots o}}^{n}) + \cdots + \tau^{(\gamma,\gamma')}_{(1,0)} f(\overbrace{o\cdots\overset{xx}{o\cdots o}}^{n})$$

$$+ \tau^{(\gamma,\gamma')}_{(0,1)} f(\overbrace{o\cdots\overset{xx}{o\cdots o}}^{n}) + \cdots \qquad (3.55)$$

$$= \sum_{h,h'} \sum_{m,m'} \tau^{(h,h')}_{(m,m')}\, g^{(h,h')}_{(m,m')}(n), \quad 1 \leqslant n \leqslant 4 \qquad (3.56)$$

where m,m'=0,1 is the number of lattice spaces moved to the left (m) and to the right (m') and the functions $g^{(h,h')}_{(m,m')}(n)$ as well as the rates, $\tau^{(h,h')}_{(m,m')}$ are given in Table 3.4. As an example of the rates for this problem, $\tau^{(\gamma,\gamma')}_{(0,1)} = \tau(oo\overset{xx}{o}oo)$ is the rate of a dimer landing in the center of six empty sites and ending in the configuration ooxoxo. A generic

Table 3.4. Equations for limited mobility when d=1 (see text). The notation for probabilities of n consecutive empty sites is $f_n \equiv f(n)$

Rate	Configuration	$g^{(h,h')}_{(m,m')}(1)$	$g^{(h,h')}_{(m,m')}(2)$	$g^{(h,h')}_{(m,m')}(3)$	$g^{(h,h')}_{(m,m')}(4)$
$\tau^{(\gamma,\gamma')}_{(0,1)}$	$o\overset{xx}{o}ooooo$	$2f_6$	$4f_6$	$4f_6+f_7$	$3f_6+f_8+2f_7$
$\tau^{(\gamma,\gamma')}_{(0,0)}$	$oo\overset{xx}{o}ooo$	$2f_6$	$3f_6$	$4f_6$	$3f_6+2f_7$
$\tau^{(\beta,\gamma')}_{(0,1)}$	$xo\overset{xx}{o}ooo$	$2(f_5-f_6)$	$4(f_5-f_6)$	$3f_5-2f_6-f_7$	$2f_5-f_6-f_8$
$\tau^{(\beta,\gamma')}_{(0,0)}$	$xo\overset{xx}{o}ooo$	$2(f_5-f_6)$	$3(f_5-f_6)$	$3(f_5-f_6)$	$2f_5-f_6-f_7$
$\tau^{(\beta,\gamma')}_{(1,0)}$	$x\overset{xx}{o}ooo$	$2(f_5-f_6)$	$3(f_5-f_6)$	$3(f_5-f_6)$	$2f_5-f_6-f_7$
$\tau^{(\beta,\beta')}_{(0,1)}$	$xo\overset{xx}{o}oox$	$2(f_4-2f_5+f_6)$	$3(f_4-2f_5+f_6)$	$2(f_4-2f_5+f_6)$	$f_4-2f_5+f_6$
$\tau^{(\beta,\beta')}_{(0,0)}$	$xo\overset{xx}{o}oox$	$2(f_4-2f_5+f_6)$	$3(f_4-2f_5+f_6)$	$2(f_4-2f_5+f_6)$	$f_4-2f_5+f_6$
$\tau^{(\alpha,\gamma')}_{(0,1)}$	$x\overset{xx}{o}ooo$	$2(f_4-f_5)$	$3(f_4-f_5)$	$2f_4-f_5-f_6$	f_4-f_7
$\tau^{(\alpha,\beta')}_{(0,1)}$	$x\overset{xx}{o}ooo$	$2(f_4-f_5)$	$3(f_4-f_5)$	$2(f_4-f_5)$	f_4-f_6

Table 3.4. (Continued)

Rate	Configuration	$g^{(h,h')(1)}_{(m,m')}$	$g^{(h,h')(2)}_{(m,m')}$	$g^{(h,h')(3)}_{(m,m')}$	$g^{(h,h')(4)}_{(m,m')}$
$\tau^{(\alpha,\beta')}_{(0,1)}$	$x\overset{xx}{o}\overset{\diagdown}{o}ox$	$2(f_3-2f_4+f_5)$	$2(f_3-2f_4+f_5)$	$f_3-2f_4+f_5$	0
$\tau^{(\alpha,\beta')}_{(0,0)}$	$x\overset{xx}{o}oox$	$2(f_3-2f_4+f_5)$	$2(f_3-2f_4+f_5)$	$f_3-2f_4+f_5$	0
$\tau^{(\alpha,\alpha')}_{(0,0)}$	$x\overset{xx}{o}ox$	$2(f_2-2f_3+f_4)$	$f_2-2f_3+f_4$	0	0

equation can be written for $n \geq 4$ which establishes a shielding condition, giving $q_o[n]=q_o[5] \equiv q=\exp\{-[\tau_{(0,0)}^{(\gamma,\gamma')}+\tau_{(0,1)}^{(\gamma,\gamma')}]t\}$ and a closed set of equations using $f(n)=q^{n-5}f(5)$, $n \geq 5$.

A highly repulsive interaction between dissociated adatoms, which causes filling in stages, is of particular interest and will now be treated.

During the first stage of filling ($0 \leq \theta \leq \theta^*(1)$), no n.n. pairs are formed. Only the terms multiplied by $\tau_{(0,1)}^{(\gamma,\gamma')}$ and $\tau_{(0,1)}^{(\beta,\gamma')}$ contribute to the kinetic equations. At $\theta=0$ ($t=0$)

$$d/d\theta\ f(n) = -\frac{n+2}{2}\ ,\quad n \geq 2 \tag{3.57}$$

and at the end of this stage $f(n)=0$, $n \geq 5$. The equation for $f(5)$ is

$$f(5) = q^{\rho_o} \exp\left[-(1-\rho_o)\ \frac{1-q^4}{4} - 2 \sum_{r=1}^{3} \frac{1-q^r}{r}\right] \tag{3.58}$$

where $\rho_o=\tau_{(0,1)}^{(\beta,\gamma')} / \tau_{(0,1)}^{(\gamma,\gamma')}$.

For the special case when $\rho_o=1$, the result $q \equiv q_o[4]$ is also obtained and

$$d/dq\ \theta = -2f(4)\ . \tag{3.59}$$

Using Equation 3.58 in this special case, one obtains

$$f(4) = f(5)/q = \exp\left[-2 \sum_{r=1}^{3} \frac{1-q^r}{r}\right]\ . \tag{3.60}$$

Equation 3.59 can now be integrated using $q(\theta=0)=1$ and $q \to 0$ as $\theta \to \theta^*(1)$ to give

$$\theta^*(1) = 2 \int_{q=0}^{1} \exp[-2 \sum_{r=1}^{3} \frac{1-q^r}{r}]dq \cong 0.402 \qquad (3.61)$$

which is two-thirds of the saturation value for a nondissociative trimer with n.n. blocking (or, equivalently, one-half the saturation value for a nondissociative 4-mer adsorption process).

During the second stage of filling ($\theta^*(1) \leqslant \theta \leqslant \theta^*(2)$), one n.n. pair is formed. The relevant terms are those multiplied by $\tau_{(0,0)}^{(\gamma,\gamma')}$, $\tau_{(1,0)}^{(\beta,\gamma')}$, $\tau_{(0,0)}^{(\beta,\gamma')}$, $\tau_{(0,1)}^{(\beta,\beta')}$, $\tau_{(0,0)}^{(\beta,\beta')}$ and $\tau_{(0,1)}^{(\alpha,\gamma')}$ (and symmetry related rates). The terms with larger rates are multiplied by probabilities that have gone to zero. The equations for this stage are

$$\begin{aligned} d/d\theta\ f(2) &= -3/2 \\ d/d\theta\ f(3) &= -1 \\ d/d\theta\ f(4) &= -1/2 \\ d/d\theta\ f(n) &= 0\ , \quad n \geqslant 5\ . \end{aligned} \qquad (3.62)$$

At the end of this stage, $f(n)=0$, $n \geqslant 4$. The second break can be determined since $f(4) \to 0$ as $\theta \to \theta^*(2)$ and is

$$\theta^*(2) = \theta^*(1) + 2\, f(4)\big|_{\theta^*(1)} \cong 0.453\ . \qquad (3.63)$$

During the third stage of filling ($\theta^*(2) \leqslant \theta \leqslant \theta^*(3)$), two n.n. pairs are formed. The relevant rates are $\tau_{(0,0)}^{(\alpha,\gamma')}$, $\tau_{(0,1)}^{(\alpha,\beta')}$ and $\tau_{(0,0)}^{(\alpha,\beta')}$ (and symmetry related rates). The equations become

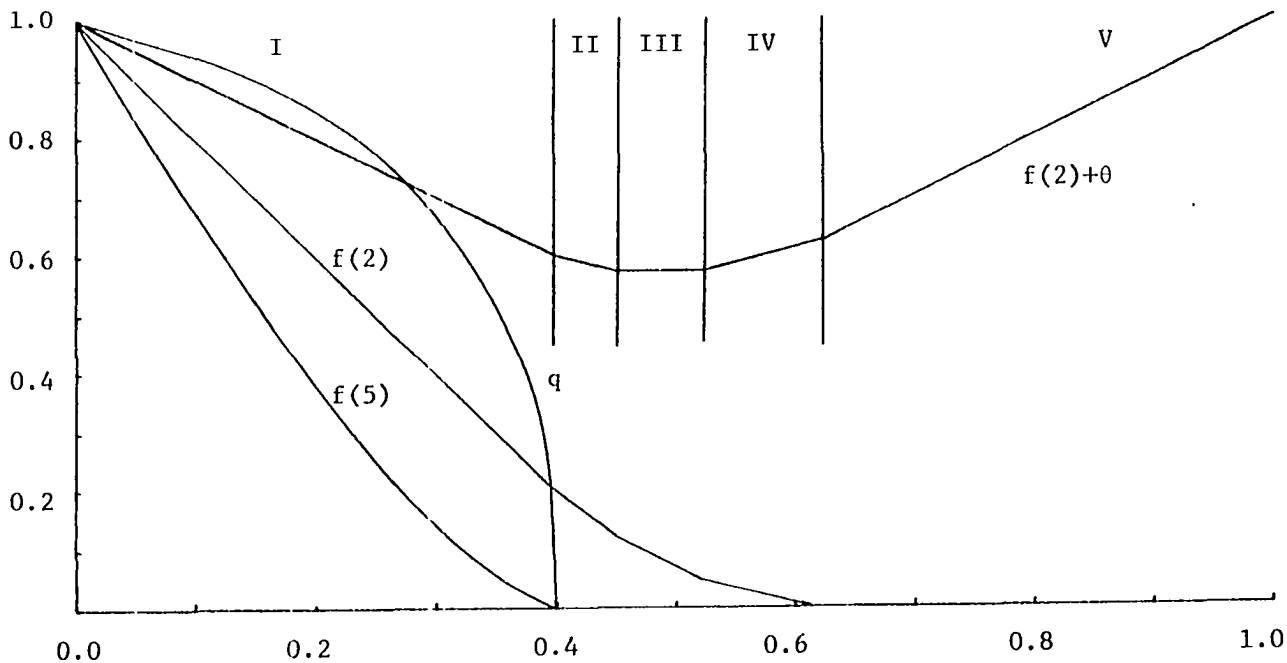

Figure 3.25. Selected functions for a dissociative dimer with limited mobility in the staged filling limit

$$d/d\theta\ f(2) = -1$$
$$d/d\theta\ f(3) = -1/2 \qquad (3.64)$$
$$d/d\theta\ f(n) = 0\ ,\quad n \geqslant 4$$

and $f(3) \to 0$ as $\theta \to \theta^*(3)$. The third break is given by

$$\theta^*(3) = \theta^*(2) + 2\, f(3)\big|_{\theta^*(2)} = \theta^*(2) + 2\left[f(3)\big|_{\theta^*(1)} - 2\, f(4)\big|_{\theta^*(1)}\right]$$
$$\cong 0.523\ . \qquad (3.65)$$

During the fourth or last stage ($\theta^*(3) \leqslant \theta \leqslant \theta^*(4)$), every event creates three n.n. pairs and only $\tau_{(0,0)}^{(\alpha,\alpha')}$ terms are significant. At the end of this stage, the lattice will have only single empty sites remaining. The equations are

$$d/d\theta\ f(2) = -1/2$$
$$d/d\theta\ f(n) = 0\ ,\quad n \geqslant 3 \qquad (3.66)$$

and $f(2) \to 0$ as $\theta \to \theta^*(4)$. The break is found at

$$\theta^*(4) = \theta^*(3) + 2\, f(2)\big|_{\theta^*(3)} \cong 0.623\ . \qquad (3.67)$$

Figure 3.25 shows the behavior of some functions in the staged filling process. Notice the inherent asymmetry of $f(2)+\theta$.

3.8. Approximate Solutions for R=2

In this section, we will discuss the equations for general second n.n. cooperative effects as an example of a hierarchy of equations that

is not exactly soluble. The treatment yields approximate subconfiguration probabilities which can be compared, in certain limits, with exact results. Thus, an estimate of the effectiveness of the approximations can be gauged.

Assuming reflection symmetry, ten rates are needed to describe a general process where first and second n.n. cooperative effects exist. They are $\tau_{\sigma\cdot\sigma'}$, where $\underset{\sim}{\sigma},\underset{\sim}{\sigma}'$=xx,xo,ox,oo.

The corresponding rate equations are quite complex and will not be written explicitly. For example, Equation 2.8 for f(o) includes the probabilities f(oo), f(o_o), f(ooo), f(o_oo), f(o_o_o), f(oooo), f(o_ooo) and f(ooooo). The appearance of unspecified gaps means that exact truncation is not possible.

The following method is used to obtain a closed set of equations:

(1) Enumerate a core set of probabilities. These should include all those appearing in the f(o) equation. Here we choose all possible configurations of empty and unspecified states along five consecutive sites.

(2) Write kinetic equations for the core set of probabilities.

(3) Factor new probabilities. Probabilities not contained in the core set appear in these kinetic equations. These new probabilities are factored into products of the original probabilities and conditional probabilities with a single conditioning site at one end using the following rules:

(a) If possible create a product of one of the original probabilities and a single conditional probability (of the type described above).

(b) If rule (a) cannot be implemented or is ambiguous, factor out the conditional probability with the most consecutive empty sites adjacent to the conditioned site. Then return to rule (a) to factorize the remaining probability (e.g., f(o_oo_o)=f(o_oo)qo[_oo_o] and f(ooo_oo)=f(oo_oo) qo[oo_oo]).

(4) Truncate to nth order. An nth order Markovian truncation is performed on the conditional probabilities. (This section will treat the 3rd, 4th and 5th order cases.)

(5) Write kinetic equations for the conditional probabilities. Kinetic equations are written in the form

$$d/dt\ qo[\underset{\sim}{o}] = [d/dt\ f(o\underset{\sim}{o})-qo[\underset{\sim}{o}]\ d/dt\ f(\underset{\sim}{o})]/f(\underset{\sim}{o}) \ . \qquad (3.68)$$

New probabilities are factorized according to the rules in (3). New conditional probabilities are truncated and have equations written in the same manner.

It should be noted that this choice of approximate equations is only one of many. Another approach that could be used here deals directly with the q-hierarchy. (This approach is demonstrated in the next chapter for a 2-D example.)

It can be shown that for $n \geq 4$, in the n.n. blocking limit, the exact results are recovered for f(o), f(oo), f(ooo), f(oooo), f(ooooo)=q f(oooo) (where $q \equiv qo[oooo]$ and the exact shielding result for this process has been employed) and f(o_o) (and thus, f(x), f(xx) and f(x_x) also). Some specific examples will now be considered:

(1) No n.n. cooperative effect, attractive second n.n. Figures 3.26-3.29 show the results for f(xx) and f(x_x) when nearest neighbors have no cooperative effects, but the second n.n. ranges from slightly attractive to very attractive, thus enhancing the propensity for ooxoxoxoxoo type clustering (island formation). The rates are chosen so that each reacted first/second n.n. changes $\tau_{oo \cdot oo}$ by a factor of α/β, respectively (e.g., $\tau_{xo \cdot xx} = \alpha\beta^2 \tau_{oo \cdot oo}$).

(2) Repulsive n.n., attractive second n.n. Figures 3.30-3.33 show the results for f(xx) and f(x_x) when $\alpha = \frac{1}{2}$ and $1 < \rho < 800$. As expected, when the second n.n. attraction increases the value of f(xx) remains relatively small until $\theta > 0.5$. The three-lattice vector truncation increasingly deviates from the four and five-lattice vector truncations as the second n.n. attractiveness increases.

Figure 3.34 shows the variation of f(x_x) going from a slightly repulsive n.n. to blocking n.n. ($0 \leq \alpha \leq 1$) when $\beta = 2$ in the four site truncation. The n.n. blocking problem has previously been exactly solved (cf., Section 3.1). This figure illustrates convergence of the four site truncation approximate equations to the exact result as the n.n. repulsiveness goes to infinity.

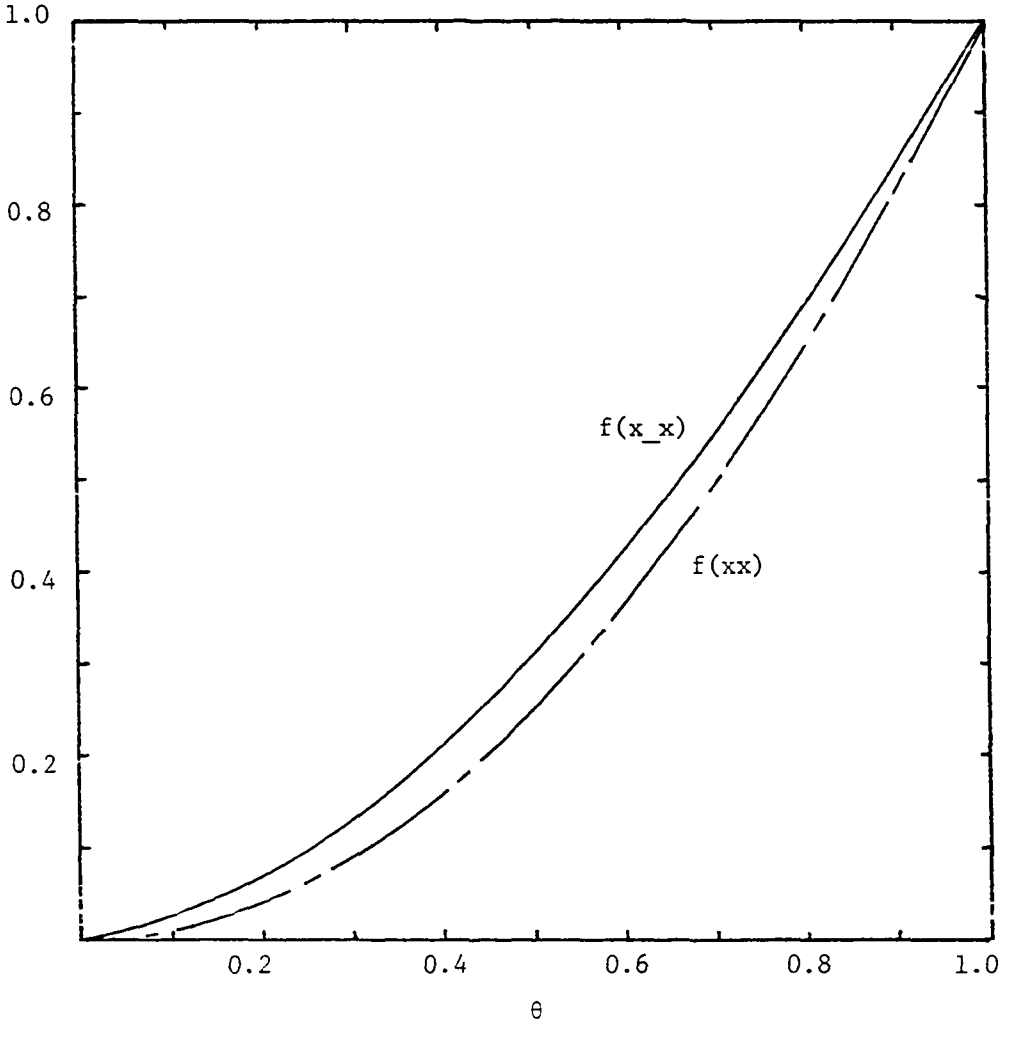

Figure 3.26. The probabilities f(x_x) (——) and f(xx) (—— - ——) as a function of θ for α=1 and β=2 in the three, four and five site truncations

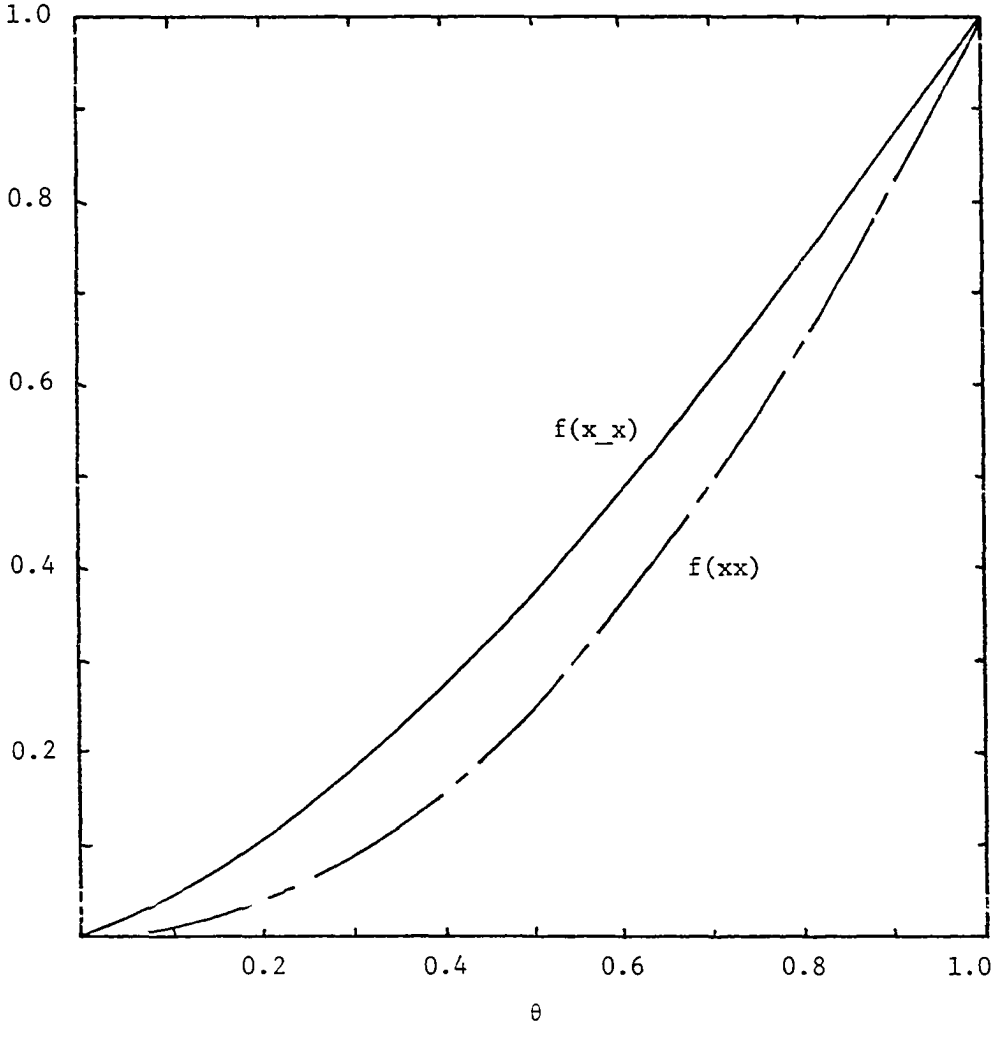

Figure 3.27. The probabilities f(x_x) (——) and f(xx) (—— - ——) as a function of θ for α=1 and β=5 in the three, four and five site truncations

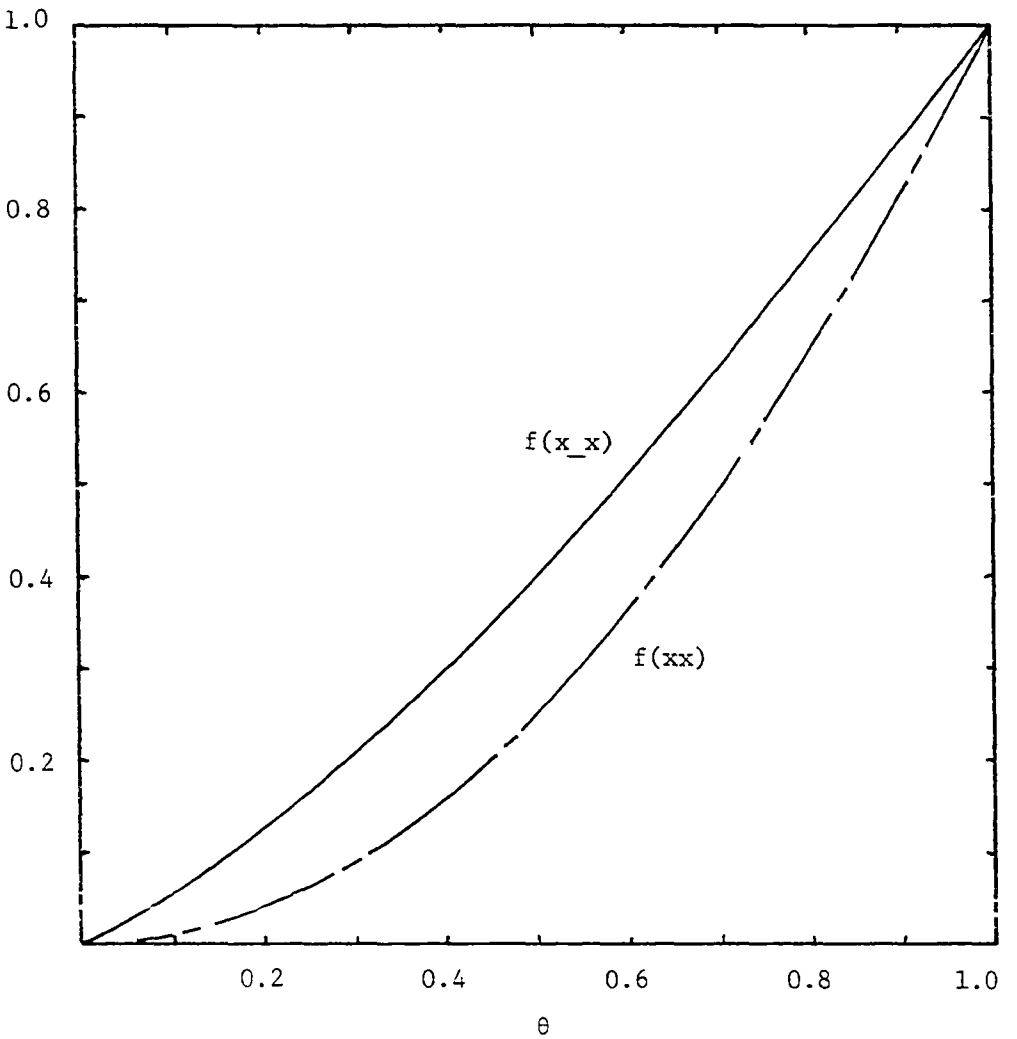

Figure 3.28. The probabilities f(x_x) (——) and f(xx) (—— - ——) as a function of θ for α=1 and β=10 in the three, four and five site truncations

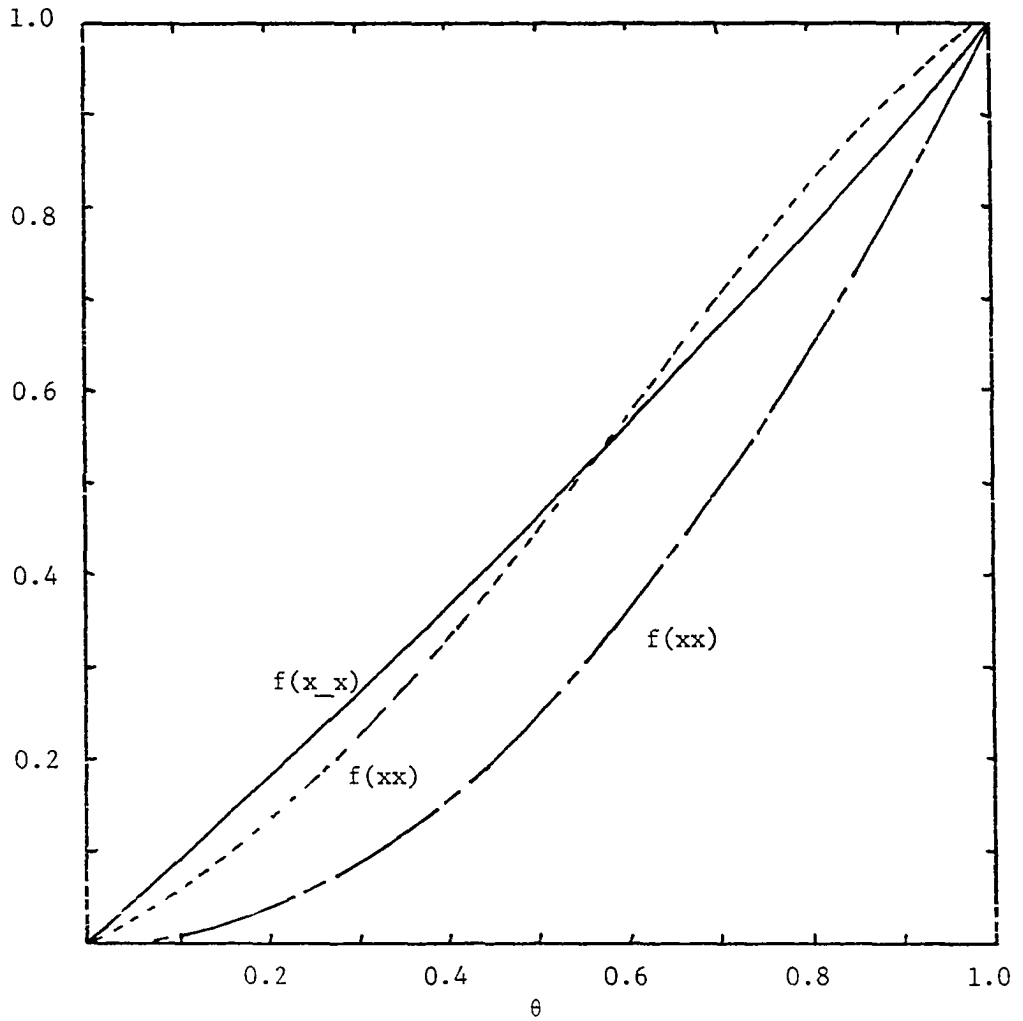

Figure 3.29. The probabilities f(x_x) (——) and f(xx) (—— - ——) as a function of θ for α=1 and β=100 in the four and five site truncations. The dashed line (----) is f(xx) in the three site truncation

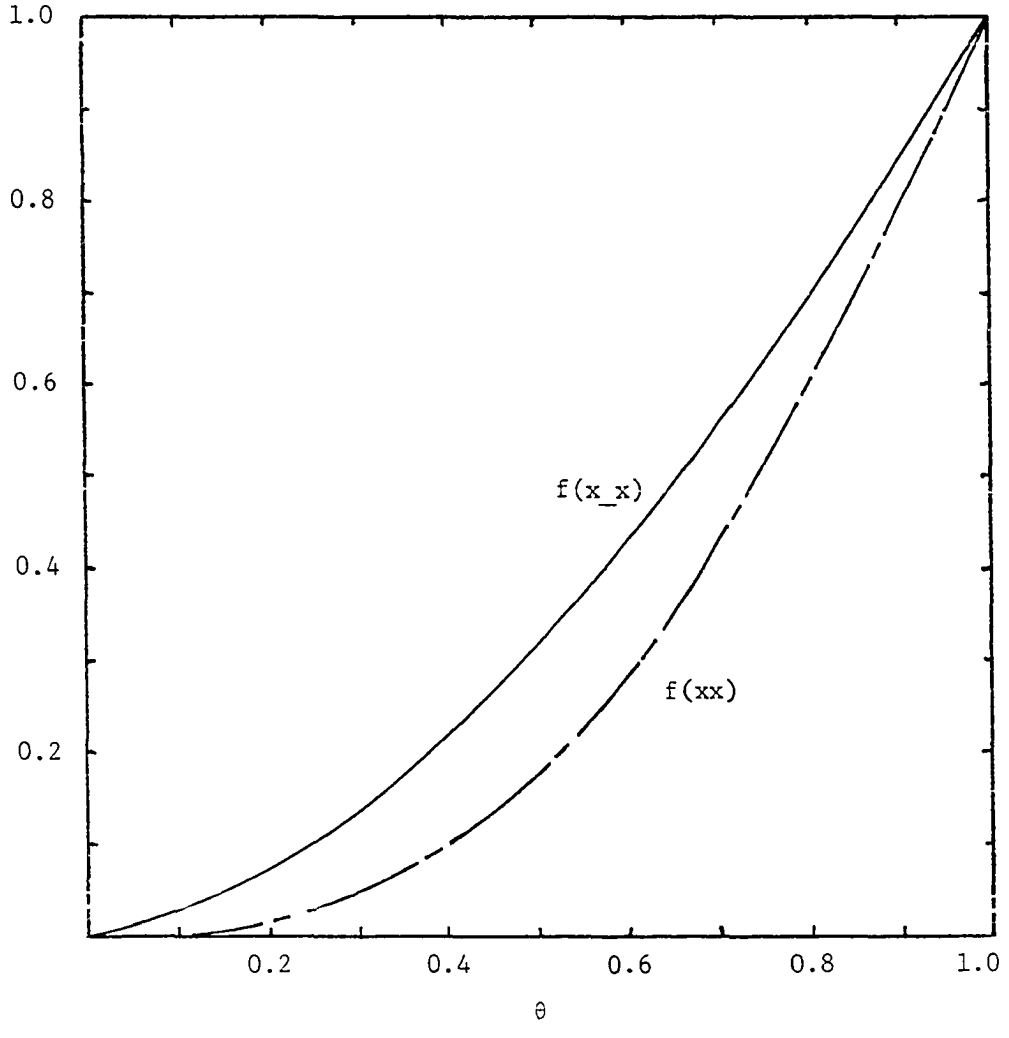

Figure 3.30. The probabilities f(x_x) (——) and f(xx) (—— - ——) as a function of θ for $\alpha=\frac{1}{2}$ and $\beta=2$ in the three, four and five site truncations

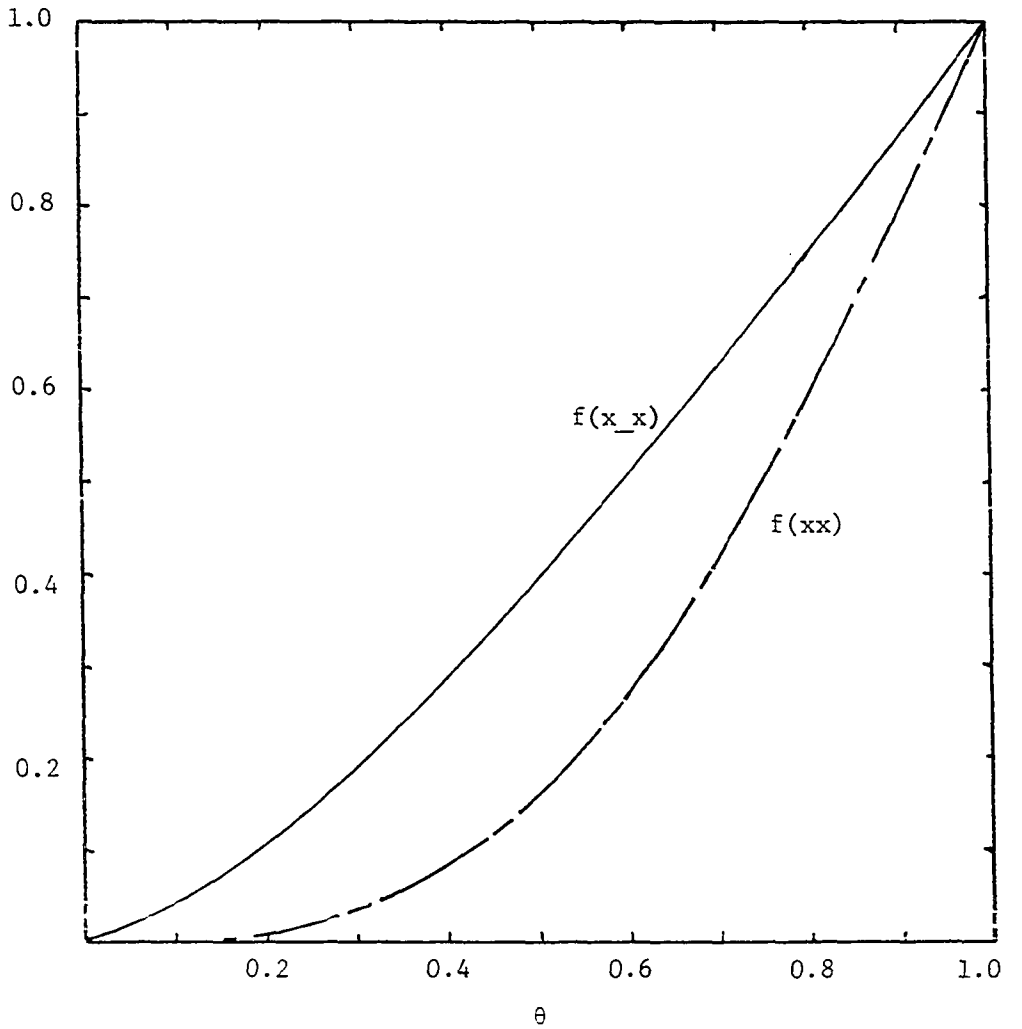

Figure 3.31. The probabilities f(x_x) (——) and f(xx) (—— - ——) as a function of θ for $\alpha=\frac{1}{2}$ and $\beta=5$ in the three, four and five site truncations

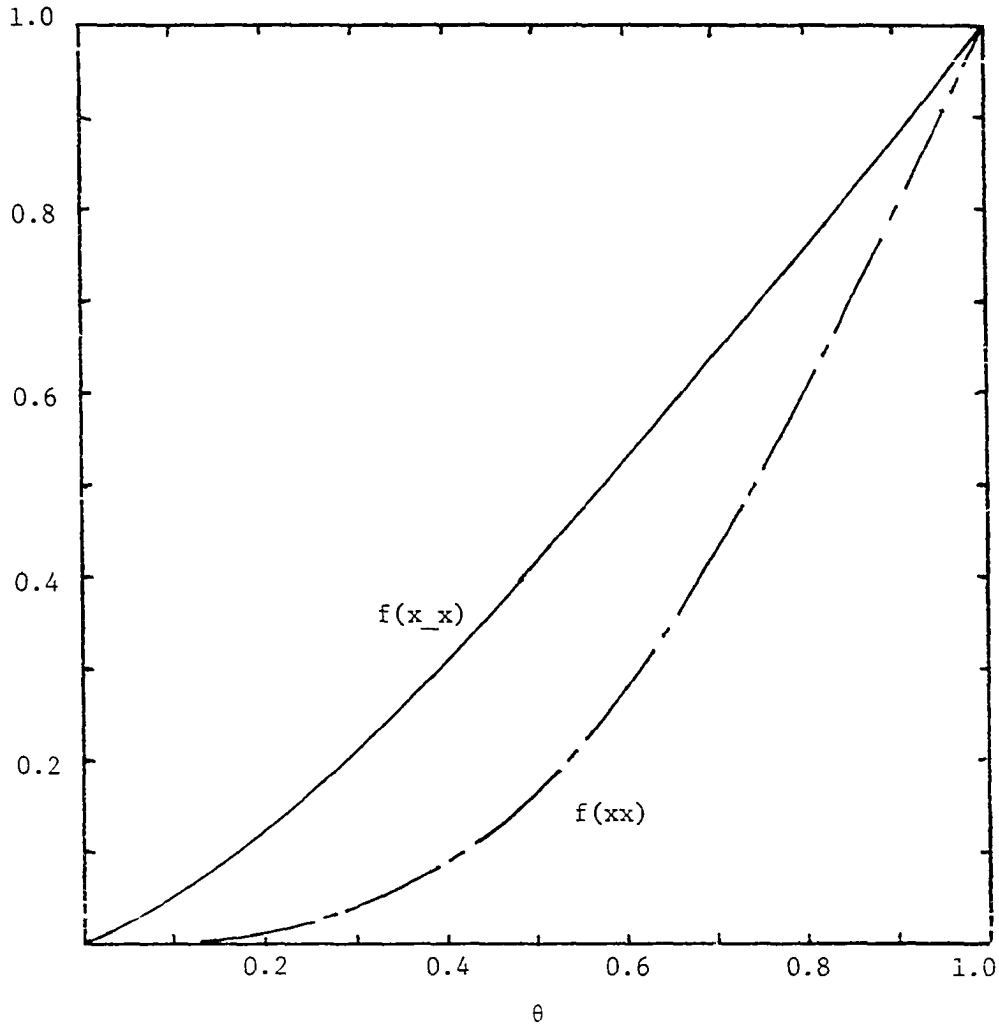

Figure 3.32. The probabilities f(x_x) (——) and f(xx) (—— - ——) as a function of θ for $\alpha=\frac{1}{2}$ and $\beta=10$ in the three, four and five site truncations

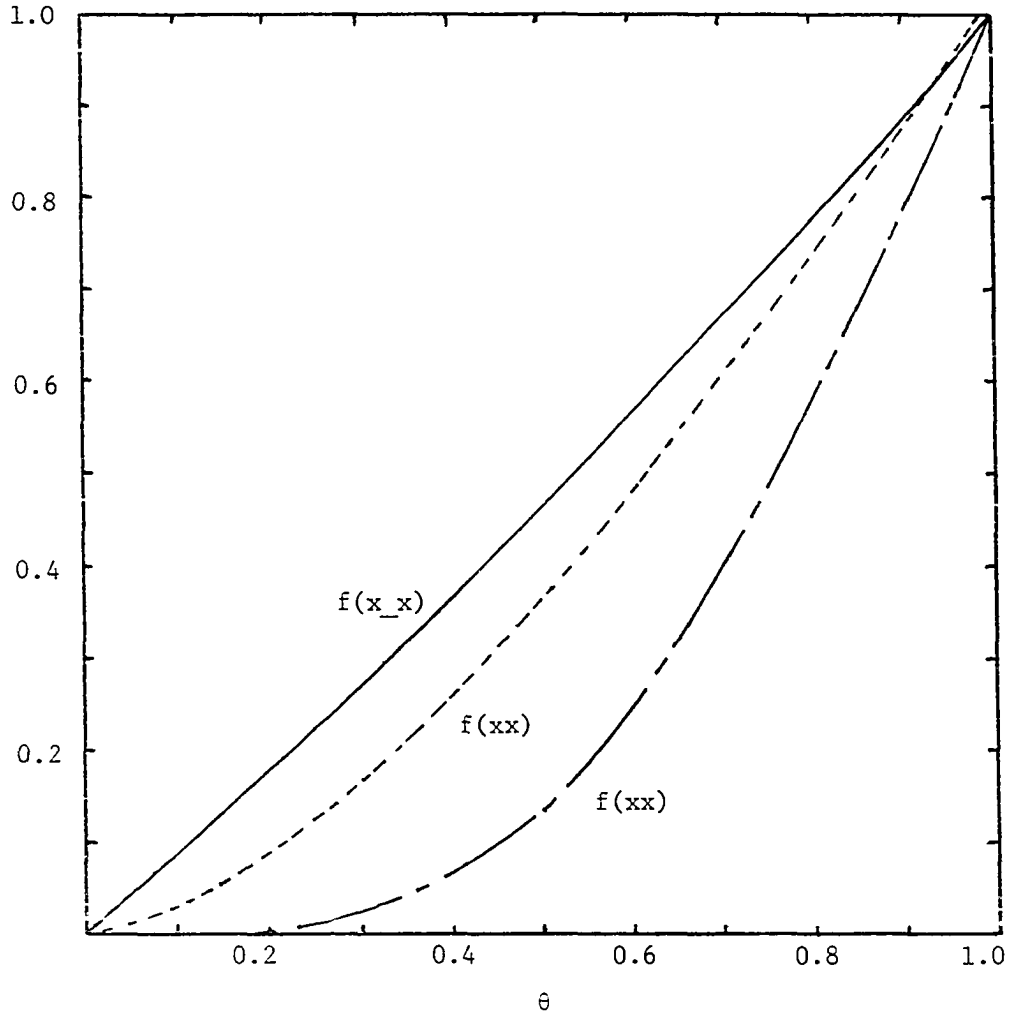

Figure 3.33. The probabilities f(x_x) (——) and f(xx) (—— - ——) as a function of θ for $\alpha=\frac{1}{2}$ and $\beta=100$ in the four and five site truncations. The dashed line (----) is f(xx) in the three site truncation

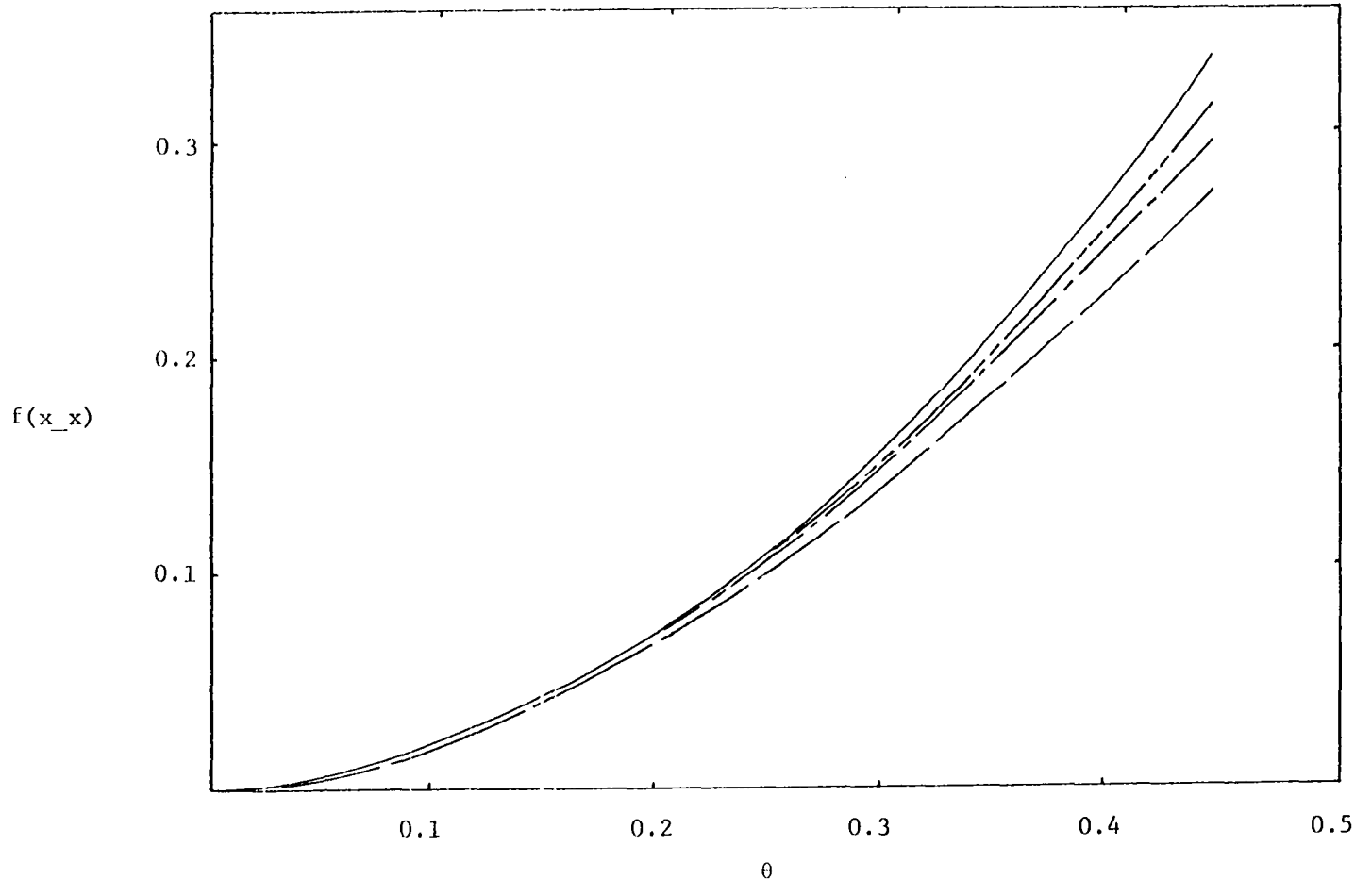

Figure 3.34. Variation of f(x_x) with α in the four site truncation. In the figure α=1/2(— —), 1/5(— - —), 1/10(— - - —) and 1/100(——). The solid curve is also the exact plot for n.n. blocking

(3) Repulsive n.n., repulsive second n.n. For this example, consider a process where $\tau_{\underset{\sim}{\sigma}o\cdot x\underset{\sim}{\sigma}'}=\tau_{\underset{\sim}{\sigma}o\cdot x}$, $\tau_{\underset{\sim}{\sigma}x\cdot x\underset{\sim}{\sigma}'}=\tau_{x\cdot x}$ for all σ,σ' and $\tau_{oo\cdot oo} \gg \tau_{oo\cdot ox} \gg \tau_{xo\cdot ox} \gg \tau_{x\cdot o} \gg \tau_{x\cdot x}$. This choice of rates causes filling in stages (cf., Section 3.2). For illustration purposes, the behavior of qo[_ooo] with respect to θ will be examined. This conditional probability changes dramatically with θ and is thus a good test of the approximate equations.

From previous analysis of filling in stages, it was found that qo[-ooo] has a complicated θ dependence during the first two slopes, is equal to one during the third stage, and is piecewise linear during the last two stages. The plot is given in Figure 3.29. The four and five site approximations when the rates are close to the limit and when the rates are separated by one order of magnitude ($\tau_{oo\cdot oo}=1$, $\tau_{oo\cdot ox}=0.1$, etc.) are also shown. The rates close to the limit only allow integration through the first two stages, where the five site approximation lies along the exact curve (not shown) and the four site approximation deviates during the second stage. (This conditional probability is not in the set that reduces to the exact result in the limit.) The four site approximation also predicts qo[_ooo]>1 during the third stage. When the repulsiveness is relaxed to an order of magnitude difference, the plots retain the same general form.

One deficiency of these approximate equations is their inability to integrate to $\theta=1$. This is in part due to the form of Equation 3.68 incorporating division by probabilities. If the denominator of Equation 3.68 goes to zero faster than the numerator, the derivative

will become very large. There is, however, a more fundamental potential cause of bad behavior. This is shown by the fifth stage equation for qo[_o_o], which is

$$d/d\theta \ \ell n \ qo[\_o\_o] = - \frac{1-2 \ qo[\_o\_o\_o]}{p(1)} \ . \qquad (3.69)$$

If the approximate equations give qo[_o_o_o] greater than 0.5 at the end of the fourth stage, the value of qo[_o_o] will increase (see Equation 3.69) rather than go to zero. This last difficulty manifests itself in the 2-D approximate equations.

4. THE 2-D SQUARE LATTICE

Hierarchy equations for 2-D square lattice probabilities are obtained from Equation 2.12. For the purposes of this chapter, it is desirable to extract from these a closed subset of equations for conditional probabilities with only one unoccupied conditioned site (i.e., $q_o[\underset{\sim}{\sigma}]$). This can be accomplished, nonuniquely, by factorizing the conditional probabilities appearing on the right hand side of the $d/dt\ \ell n\ q_o[\underset{\sim}{\sigma}]$ equation that have more than one conditioned site into products of conditional probabilities with only one conditioned site. For example,

$$q\left(\begin{smallmatrix} o & \phi \\ \phi & \phi \end{smallmatrix}\right) = q\left(\begin{smallmatrix} o & \phi \\ \phi & \end{smallmatrix}\right) q\left(\begin{smallmatrix} \phi & \\ \phi & \end{smallmatrix}\right) = q\left(\begin{smallmatrix} \phi & \phi \\ \phi & \end{smallmatrix}\right) q\left(\begin{smallmatrix} o & \phi \\ & \end{smallmatrix}\right) , \tag{4.1}$$

where o indicates a conditioned site and ϕ indicates a conditioning site. The order of factorization is important because it influences the number of equations needed to close the set upon truncation. The least number of equations will be generated by consistently choosing the conditioned site with the smallest number of surrounding conditioning sites as the first (single) conditioned site. If more than one conditioned site has the same number of surrounding conditioning sites, a consistent ordering is chosen and has been coded into the computer program used to derive the equations of this chapter (see Section 4.1).

In order to get a closed set of equations it is necessary to truncate the conditional probabilities. Two methods of truncation

have been developed. Method A first factorizes and then truncates conditioning sites more than a specified distance (calculated along the lattice) from the (single) conditioned site. Method B truncates conditioning sites beyond a specified distance from any conditioned site before factorizing. For example, using method A

$$q\left(\begin{smallmatrix} & \phi & \\ o & \phi & \phi \\ & \phi & \end{smallmatrix}\right) = q\left(\begin{smallmatrix} & \phi & \\ o & \phi & \phi \\ & \phi & \end{smallmatrix}\right) q\left(\begin{smallmatrix} & \phi & \\ & \phi & \phi \\ & \phi & \end{smallmatrix}\right) \rightarrow q\left(\begin{smallmatrix} & \phi & \\ o & \phi & \phi \\ & \phi & \end{smallmatrix}\right) q\left(\begin{smallmatrix} & \phi & \\ & \phi & \phi \\ & \phi & \end{smallmatrix}\right) \tag{4.2}$$

where a two lattice vector truncation has been employed. Applying method B to the same conditional probability gives

$$q\left(\begin{smallmatrix} & \phi & \\ o & \phi & \phi \\ & \phi & \end{smallmatrix}\right) \rightarrow q\left(\begin{smallmatrix} & \phi & \\ o & \phi & \phi \\ & o & \end{smallmatrix}\right) = q\left(\begin{smallmatrix} & \phi & \\ \phi & \phi & \phi \\ & o & \end{smallmatrix}\right) q\left(\begin{smallmatrix} & \phi & \\ o & \phi & \phi \\ & & \end{smallmatrix}\right) , \tag{4.3}$$

again for a two lattice vector truncation. It is clear that method B is a more severe truncation.

As a shorthand notation, let C (for cross) represent $R^1=R^2=1$ cooperative effects and D (for diagonal) represent $R^2=\sqrt{2}$ cooperative effects (having six and 51 rates, respectively, when reflection and rotation symmetry is assumed). See Figure 1.7 for a diagram of these cooperative ranges. The approximations to be considered in this chapter are CA2, CB2, CB3 and DB2 where the last integer represents the order of the truncation.

It is a relatively easy task to write the closed coupled set of conditional probability equations for the CB2/CA2 cases by hand. There are eight/nine conditional probabilities generated. They are

$q\left[\circ\right]=f(1)$, $q\left[\circ\phi\right]$, $q\left[\begin{smallmatrix}\circ\\ \phi\end{smallmatrix}\right]$, $q\left[\begin{smallmatrix}\circ\phi\\ \phi\end{smallmatrix}\right]$, $q\left[\begin{smallmatrix}\circ\\ \phi\\ \phi\end{smallmatrix}\right]$, $q\left[\circ\phi\phi\right]$, $q\left[\begin{smallmatrix}\circ\\ \phi\\ \phi\end{smallmatrix}\right]$, (and $q\left[\begin{smallmatrix}\circ\phi\\ \phi\phi\end{smallmatrix}\right]$ for CA2 only). For the CB3 case, however, there are 128 conditional probabilities generated. These are listed in Appendix A. It is, therefore, useful to explore alternatives to writing these equations by hand. The next section will describe a way to generate these sets of equations using the computer. The last section of this chapter will present some results from integration of the approximate equations.

4.1. Computer Generation of Kinetic Equations

For any given conditional probability, the general procedure for obtaining approximate 2-D equations from

$$d/dt\ \ln q_o[\underset{\sim}{\sigma}] = -\sum_{j\in o\underset{\sim}{\sigma}} \sum_{\underset{\sim}{\sigma}^j_*} \tau_{\underset{\sim}{\sigma}j}\, q\,\underset{\sim}{\sigma}^j_*[o\underset{\sim}{\sigma}] + \sum_{j\in\underset{\sim}{\sigma}} \sum_{\underset{\sim}{\sigma}^j_*} \tau_{\underset{\sim}{\sigma}j}\, q\,\underset{\sim}{\sigma}^j_*[\underset{\sim}{\sigma}] \quad (4.4)$$

(see Equation 2.12) is to choose a site of interest (j), sum over all possible configurations $\underset{\sim}{\sigma}^j_*$ within the cooperative range of j, and then convert to conditional probabilities with a single empty conditioned site.

This procedure is amenable to computer techniques. The major tasks the computer must perform are:

(1) Uniquely label each $q_o[\underset{\sim}{\sigma}]$ and $\tau_{\underset{\sim}{\sigma}j}$. A square grid is used to individually label each $q_o(\underset{\sim}{\sigma})$ and $\tau_{\underset{\sim}{\sigma}j}$ (see below).

(2) Identify specified sites. Each site of the configuration is given two coordinates to identify its position on a square grid. This facilitates truncation and identification of the condition of surrounding lattice sites.

(3) Identify unspecified sites. Unspecified sites within the cooperative range of the site of interest must be identified and then various empty/full configurations of these sites must be generated.

(4) Transform to empty configurations and factorize/truncate. It is necessary to transform conditional probabilities with full conditioned sites to have only empty conditioned sites and then employ the desired truncation/factorization procedure.

(5) Write equations. Rates and conditional probabilities must be combined and written as the desired kinetic equation.

A program has been written to perform these tasks. It is currently operational for generating equations in the CA2, CA3, CB2, CB3, DA2, DA3, and DB3 cases, but may be extended to other cases with relatively slight modification.

As an example of the novel methods used in this program, we illustrate the numerical representation of conditional probabilities and the factorization procedure. One way to uniquely identify a conditional probability is to define a seven by seven square grid with each row of the grid identifying a number 2^i, i=1,2,3,..., going from bottom to top and each column representing (from right to left) tens, hundreds, ten thousands, etc. See Figure 4.1.

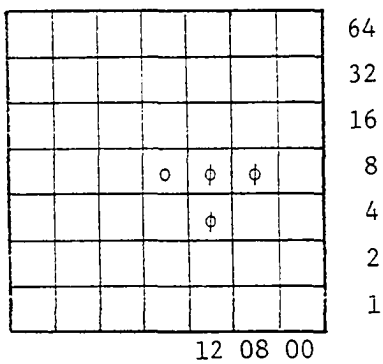

Figure 4.1. Numerical representation of conditional probabilities

One first places the configuration $o[\underset{\sim}{g}]$ on the grid so the site o is at the center position. Then each conditioning site (ϕ) is given a value corresponding to the row where it resides. A number labeling $qo[\underset{\sim}{g}]$ is obtained by summing the columns and treating the resultant string of numbers along the bottom as one number. The configuration in Figure 4.1 is $q\begin{pmatrix} o\phi\phi \\ \phi \end{pmatrix}$=120800. Since reflection and rotation symmetry are assumed in this work, other numbers could be given for the same conditional probability (e.g., $q\begin{pmatrix} \phi \\ o\phi\phi \end{pmatrix}$=240800). A consistent representation is obtained if the smallest possible number is always chosen.

Factorization of conditional probabilities with more than one conditioned site into products of conditional probabilities with single conditioned sites can often be accomplished in more than one way as previously discussed. The computer program consistently orders which conditioned site is taken first for factorization. These are grouped according to the number of surrounding conditioning sites and those with the least chosen first. To determine the somewhat arbitrary order within each group, the following procedure is implemented. The configuration is placed on a square grid with the site of interest at the center. Each orientation is labeled using conditioning sites exactly as above. The one with the minimum label is chosen. Then the conditioned sites (with the same number of surrounding conditioning sites) are chosen beginning with the site in the rightmost column closest to the bottom of the grid. Conditioned sites are then taken in order going up that column. Conditioned sites (if any) in the

next column to the left are then taken in order from bottom to top. This is continued until all conditioned sites have been used. For example, $q\left(\begin{smallmatrix} & \circ & \\ \circ & \bullet & \bullet \\ & \circ & \end{smallmatrix}\right)$ is oriented and factored as follows:

$$q\left(\begin{smallmatrix} & \circ & \\ \circ & \bullet & \bullet \\ & \bullet & \end{smallmatrix}\right) = q\left(\begin{smallmatrix} & \circ & \\ \bullet & \bullet & \bullet \\ & \bullet & \end{smallmatrix}\right) q\left(\begin{smallmatrix} & \bullet & \\ \circ & \bullet & \bullet \\ & \bullet & \end{smallmatrix}\right) q\left(\begin{smallmatrix} & \bullet & \\ \bullet & \bullet & \bullet \\ & \bullet & \end{smallmatrix}\right) . \qquad (4.5)$$

The other tasks have also been accomplished in one or more of the 17 different program procedures (subroutines) that have been written. Table 4.1 is the computer generated equation for d/dt $q\left(\begin{smallmatrix} \circ & \bullet \\ \bullet & \end{smallmatrix}\right)$ in the CA2 case.

4.2. Results

Closed sets of equations have been generated for the CA2, CB2, CB3 and DB2 cases. The sets contain nine, eight, 128 and 14 equations respectively. As mentioned previously, the number of equations depends on the factorization scheme employed. For example, the CA2 case was factorized, beginning with the conditioned site having the most surrounding conditioning sites, and over 70 equations (with more to be derived) resulted. This section will now consider several choices of rates for the CA2 and CB3 approximations which illustrate different processes that can occur on a 2-D square lattice.

(1) $\tau\left(\begin{smallmatrix} & \circ & \\ \circ & \bullet & \circ \\ & \circ & \end{smallmatrix}\right)=1,\ \tau\left(\begin{smallmatrix} & \circ & \\ \circ & \bullet & x \\ & \circ & \end{smallmatrix}\right)=\alpha,\ \tau\left(\begin{smallmatrix} & x & \\ \circ & \bullet & x \\ & \circ & \end{smallmatrix}\right)=\tau\left(\begin{smallmatrix} & \circ & \\ x & \bullet & x \\ & \circ & \end{smallmatrix}\right)=\alpha^2,\ \tau\left(\begin{smallmatrix} & x & \\ x & \bullet & x \\ & \circ & \end{smallmatrix}\right)=\alpha^3,\ \tau\left(\begin{smallmatrix} & x & \\ x & \bullet & x \\ & x & \end{smallmatrix}\right)=\alpha^4.$

A natural way to choose the rates is in a pairwise additive Arrhenius form. Truncated equations recover exact results for the random case when $\alpha=1$. Figure 4.2 shows f(oo) as a function of θ for $0.2 \leqslant \alpha \leqslant 6.0$.

Table 4.1. Computer generated equation for d/dt q$\begin{pmatrix} o\phi \\ \phi \end{pmatrix}$ (YDOT(3)) in the CA2 approximation. The conditional probabilities and rates are kept in the arrays Q(I), $1 \leq I \leq 9$, and R(J), $1 \leq J \leq 6$, respectively. The intermediate arrays AA(k), BB(k) and CC(k) are individually summed and then combined to give the final equation

```
    AA(1) = RE*Q(4)*Q(5)-R(2)*(Q(4)*Q(5)-Q(4))*2 + R(3)*(Q(4)*Q(5)-Q(4
   C)*2 + 1)
    AA(2) = -R(4)*(Q(3)*Q(4)-Q(6)-Q(8)*Q(4)*Q(5) + Q(8)*Q(4)) + R(5)*(
   CQ(3)*Q(4)-Q(3)-Q(6)-Q(8)*Q(4)*Q(5) + Q(8)*Q(4)*2-Q(8) + 1) + Q(8)*
   CRE*Q(4)*Q(5) + R(2)*(Q(3)*Q(4)-Q(8)*Q(4)*Q(5))-R(2)*(Q(8)*Q(4)*Q(5
   C)-Q(8)*Q(4))*2-R(3)*(Q(3)*Q(4)-Q(3)-Q(8)*Q(4)*Q(5) + Q(8)*Q(4)) +
   CR(3)*(Q(8)*Q(4)*Q(5)-Q(8)*Q(4)*2 + Q(8))
    I1 = 2
       A=0.D0
       DO 8 I=1,I1
       A=A+AA(I)
 8     CONTINUE
    BB(1) = Q(3)*RE*Q(4)*Q(5) + R(4)*(Q(3)*Q(4)*Q(5)-Q(3)*Q(4)*2 + Q(6
   C))-R(5)*(Q(3)*Q(4)*Q(5)-Q(3)*Q(4)*3 + Q(3)*2 + Q(6)-1)-R(2)*(Q(3)*
   CQ(4)*Q(5)-Q(3)*Q(4))*3 + R(3)*(Q(3)*Q(4)*Q(5)-Q(3)*Q(4)*2 + Q(3))*
   C2
    I2 = 1
       B=0.D0
       DO 9 I=1,I2
       B=B+BB(I)
 9     CONTINUE
    CC(1) = -R(4)*(Q(3)*Q(4)-Q(6)-Q(8)*Q(4)*Q(5) + Q(8)*Q(4)) + R(5)*(
   CQ(3)*Q(4)-Q(3)-Q(6)-Q(8)*Q(4)*Q(5) + Q(8)*Q(4)*2-Q(8) + 1) + Q(8)*
   CRE*Q(4)*Q(5) + R(2)*(Q(3)*Q(4)-Q(8)*Q(4)*Q(5))-R(2)*(Q(8)*Q(4)*Q(5
   C)-Q(8)*Q(4))*2-R(3)*(Q(3)*Q(4)-Q(3)-Q(8)*Q(4)*Q(5) + Q(8)*Q(4)) +
   CR(3)*(Q(8)*Q(4)*Q(5)-Q(8)*Q(4)*2 + Q(8))
    CC(2) = -Q(3)*RE*Q(4)*Q(5)-R(4)*(Q(3)*Q(4)*Q(5)-Q(3)*Q(4)*2 + Q(6)
   C) + R(5)*(Q(3)*Q(4)*Q(5)-Q(3)*Q(4)*3 + Q(3)*2 + Q(6)-1) + R(2)*(Q(
   C3)*Q(4)*Q(5)-Q(3)*Q(4))*3-R(3)*(Q(3)*Q(4)*Q(5)-Q(3)*Q(4)*2 + Q(3))
   C*2
    I3 = 2
       C=0.D0
       DO 10 I=1,I3
       C=C+CC(I)
10     CONTINUE
    YDOT(3) = -Q(3)*(A-B + C)
```

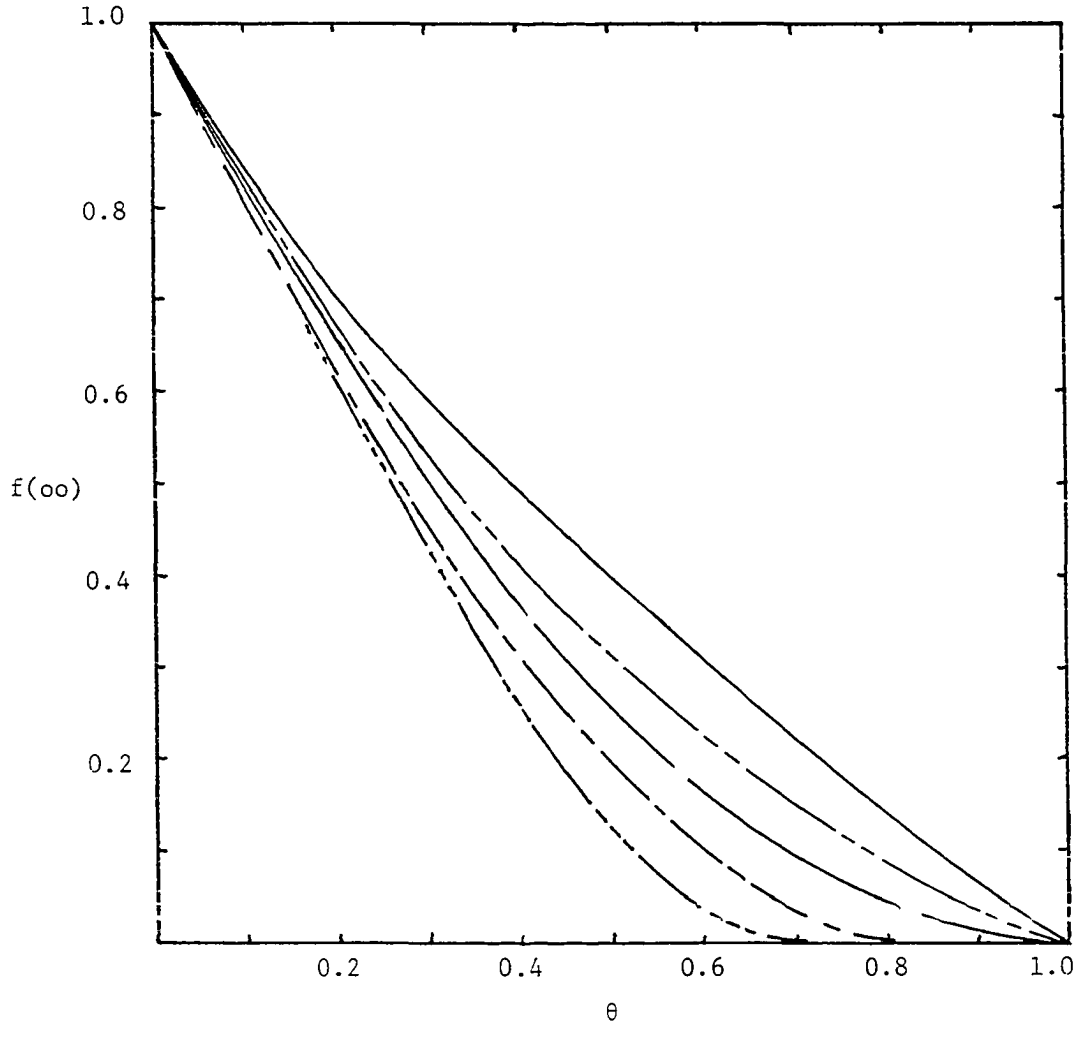

Figure 4.2a. f(oo) as a function of θ for α=0.2 (———), 0.5 (—— - ——), 1.0 (—— ——), 2.0 (———) and 5 (——) using CA2 and CB3 approximations

Below α=0.2/0.3 and above α=6.0/3.0 the CA2/CB3 approximate equations do not integrate to θ=1. One explanation of this behavior for small α is discussed in the next subsection. When α is large it appears that the very large rates dominate in the approximate equations to the extent of forcing an unphysical solution. The limiting behavior of f(oo) as $\alpha \to 0$ or $\alpha \to \infty$ can be discussed from simple arguments.

For α very small filling in stages, similar to that described in Section 3.2 will occur. There are five stages for this case corresponding to addition at sites with zero, one, two, three and then four occupied n.n. with $d/d\theta$ f(oo)=-2, -3/2, -1, -1/2 and zero respectively. These slopes are not readily apparent in Figure 4.2 indicating that α=0.2 is not small enough to demonstrate filling in stages. The values of $d/d\theta$ f(oo) do not rule out the possibility that f(oo)+θ is symmetric in this limit. General full/empty symmetry does not hold, however, since at θ=0.5, $f\left(\begin{smallmatrix} & o & \\ o & & o \\ & o & \end{smallmatrix}\right)=0$ but $f\left(\begin{smallmatrix} & x & \\ x & & x \\ & x & \end{smallmatrix}\right)\neq 0$.

For α approaching infinity the first occupied site will "seed" the process and a single, large rectangular island will form (choice of rates favors a rectangular shape). The slope of f(oo) versus θ will be minus one since addition will proceed by filling along edges of the island where, at finite coverages, almost always two pairs of empty n.n. sites are destroyed each time a lattice site is filled.

(2) $\underline{\tau\left(\begin{smallmatrix} & o & \\ o & \cdot & o \\ & o & \end{smallmatrix}\right)=1,\ \tau\left(\begin{smallmatrix} & o & \\ o & \cdot & x \\ & o & \end{smallmatrix}\right)=\tau\left(\begin{smallmatrix} & x & \\ o & \cdot & x \\ & o & \end{smallmatrix}\right)=\tau\left(\begin{smallmatrix} & o & \\ x & \cdot & x \\ & o & \end{smallmatrix}\right)=\tau\left(\begin{smallmatrix} & x & \\ x & \cdot & x \\ & o & \end{smallmatrix}\right)=\tau\left(\begin{smallmatrix} & x & \\ x & \cdot & x \\ & x & \end{smallmatrix}\right)=0.}$

For the case of n.n. blocking the CB2, CB3 and CA2 approximations predict final coverages of 0.333, 0.365 and 0.371, respectively.

Relative agreement of these approximations is found. The worst deviation is found in $f\left(\begin{smallmatrix}o&o\\o&o\end{smallmatrix}\right)$. This is shown in Figure 4.2a. Various probabilities are shown in Figure 4.3 for this choice of rates. Table 4.2 also shows the values of these probabilities at saturation.

The CB2 approximation assigns $f(ooo)=f\left(\begin{smallmatrix}o&o\\&o\end{smallmatrix}\right)$. This is caused from the severe truncation of this approximation since for the exact hierarchy (using $\tau_c=\tau\left(\begin{smallmatrix}o\\o\cdot o\end{smallmatrix}\right)$)

$$d/dt\ [f(ooo)-f\left(\begin{smallmatrix}o&o\\&o\end{smallmatrix}\right)] = -\tau_c[f\left(\begin{smallmatrix}o&o&\\&o&o\end{smallmatrix}\right)-f\left(\begin{smallmatrix}o&\\o&o\end{smallmatrix}\right)] ,$$

$$d/dt\ [f\left(\begin{smallmatrix}o&o&\\&o&o\end{smallmatrix}\right)-f\left(\begin{smallmatrix}o&\\o&o\end{smallmatrix}\right) = -\tau_c[f\left(\begin{smallmatrix}o&o&\\&o&o\end{smallmatrix}\right)+f\left(\begin{smallmatrix}o&o\\o&o\end{smallmatrix}\right)+2f\left(\begin{smallmatrix}o&o&\\o&o&o\end{smallmatrix}\right)$$

$$+f\left(\begin{smallmatrix}o&o&\\o&o&o\end{smallmatrix}\right)-f\left(\begin{smallmatrix}o&\\o&o\end{smallmatrix}\right)-2f\left(\begin{smallmatrix}o&o\\o&o\end{smallmatrix}\right)$$

$$-f\left(\begin{smallmatrix}o&o\\o&o\end{smallmatrix}\right)-f\left(\begin{smallmatrix}o&o\\o&o\end{smallmatrix}\right)] ,$$

etc., which together imply

$$\begin{aligned} &f(ooo)\big|_{t=0} - f\left(\begin{smallmatrix}o&o\\&o\end{smallmatrix}\right)\big|_{t=0} = 0 \\ &d/dt\ [f(ooo)-f\left(\begin{smallmatrix}o&o\\&o\end{smallmatrix}\right)]_{t=0} = 0 \\ &d^2/dt^2\ [f(ooo)-f\left(\begin{smallmatrix}o&o\\&o\end{smallmatrix}\right)]_{t=0} = 0 \end{aligned} \qquad (4.6)$$

and

$$d^3/dt^3\ [f(ooo)-f\left(\begin{smallmatrix}o&o\\&o\end{smallmatrix}\right)]_{t=0} = -4\tau_c^3 .$$

The deviation of $4\tau_c^3$ is very small when compared to $d^3/dt^3\ f(ooo)\big|_{t=0}$ which is $-136\tau_c^3$.

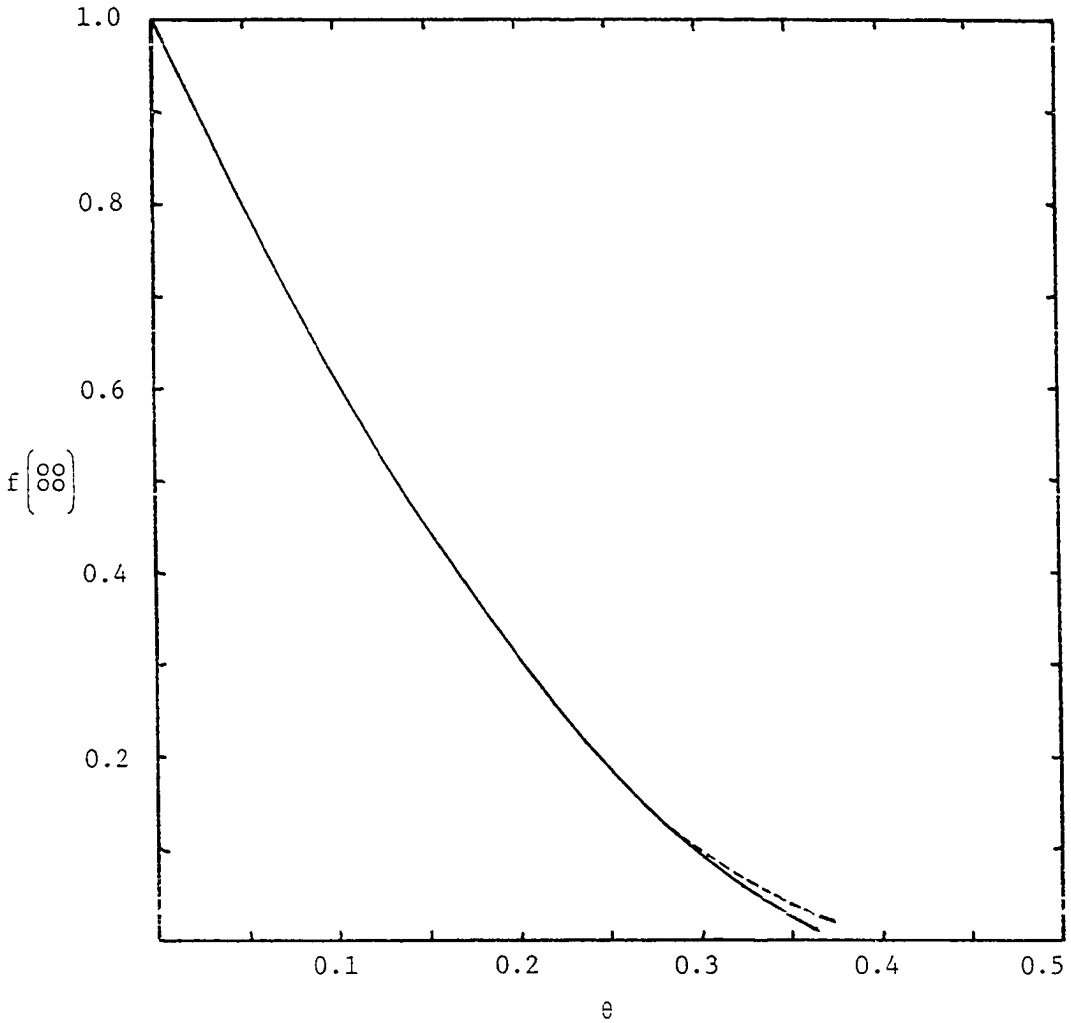

Figure 4.2b. Deviation of the CA2 (----) and CB3 (——) approximations for $f\begin{pmatrix} o & o \\ o & o \end{pmatrix}$ as a function of θ

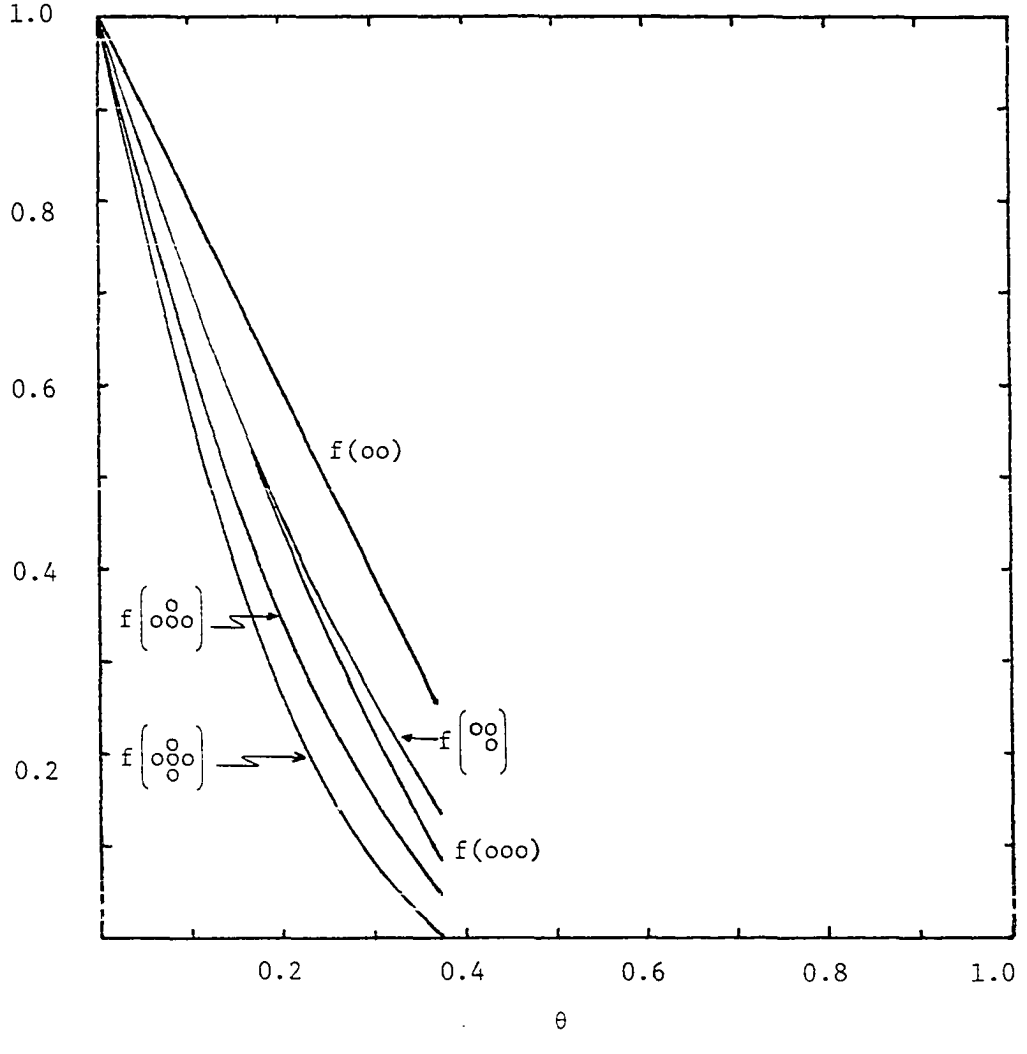

Figure 4.3. Selected probabilities as a function of θ for n.n. blocking in the CA2 and CB3 approximations

Table 4.2. Saturation values for random filling with n.n. blocking

Truncation Scheme	CB2	CB3	CA2
$\theta=1-f(o)$	0.3333	0.3650	0.3711
$f(ooo)$	0.1502	0.0843	0.0856
$f\left(\begin{smallmatrix} o & o \\ o & \end{smallmatrix}\right)$	0.1502	0.1414	0.1401
$f\left(\begin{smallmatrix} o & o \\ o & o \end{smallmatrix}\right)$	0.0412	0.0124	0.0206
$f\left(\begin{smallmatrix} & o & \\ o & & o \end{smallmatrix}\right)$	0.0516	0.0435	0.0479
$f\left(\begin{smallmatrix} & o & \\ o & & o \\ & o & \end{smallmatrix}\right)$	0.000	0.000	0.000

(3) $\tau\left(\begin{smallmatrix} & o & \\ o & \cdot & o \\ & o & \end{smallmatrix}\right)=1,\ \tau\left(\begin{smallmatrix} & o & \\ o & \cdot & x \\ & o & \end{smallmatrix}\right)=\alpha,\ \tau\left(\begin{smallmatrix} & x & \\ o & \cdot & x \\ & o & \end{smallmatrix}\right)=\tau\left(\begin{smallmatrix} & o & \\ x & \cdot & x \\ & o & \end{smallmatrix}\right)=\tau\left(\begin{smallmatrix} & x & \\ x & \cdot & x \\ & o & \end{smallmatrix}\right)=\tau\left(\begin{smallmatrix} & x & \\ x & \cdot & x \\ & x & \end{smallmatrix}\right)=0.$

Figure 4.4 shows some typical lattice configurations for intermediate times during a process where the rate of addition to a site with one n.n. is (a) highly inhibitory, $\alpha << 1$, (b) random, $\alpha=1$, (c) slightly enhanced, $\alpha \geq 1$ and (d) highly enhanced, $\alpha >> 1$ (and the rate of addition to sites with more than one n.n. is zero). A very repulsive n.n. replicating the 1st two stages of staged filling discussed in (1). It is found that $q\left(\begin{smallmatrix} & \phi & \\ \phi & \cdot & \phi \\ & \phi & \end{smallmatrix}\right)$ in the CA2 approximation gets large at the beginning of the second stage when close to the blocking limit. A 1-D analogue of how this bad behavior can be produced was given in Section 3.8. Keeping only the dominant terms during the second stage in the CA2 approximation gives

$$d/d\theta\ \ell n\ q\left(\begin{smallmatrix} & \phi & \\ \phi & \cdot & \phi \\ & \phi & \end{smallmatrix}\right) = -[1-2\ q\left(\begin{smallmatrix} & \phi & \\ \phi & \cdot & \phi \\ & \phi & \end{smallmatrix}\right)] \ . \qquad (4.7)$$

It is clear that $q\left(\begin{smallmatrix} & \phi & \\ \phi & \cdot & \phi \\ & \phi & \end{smallmatrix}\right)$ must be less than 0.5 at the beginning of the second stage or the slope will be positive causing $q\left(\begin{smallmatrix} & \phi & \\ \phi & \cdot & \phi \\ & \phi & \end{smallmatrix}\right)$ to get large. This effect is easily seen for α as large as 0.1 where the minimum observed value for $q\left(\begin{smallmatrix} & \phi & \\ \phi & \cdot & \phi \\ & \phi & \end{smallmatrix}\right)$ is 0.545 at $\theta=0.407$, corresponding to the effective start of the second stage. Figure 4.5 shows $q\left(\begin{smallmatrix} & \phi & \\ \phi & \cdot & \phi \\ & \phi & \end{smallmatrix}\right)$ versus θ for $\alpha=0.01$ in the CA2, CB2 and CB3 approximations.

Figure 4.6 shows some probabilities as functions of θ for $\alpha=1$ corresponding to random filling of sites with zero or one n.n. As α is increased, strings of occupied sites (islands) are formed. When α is large, the islands become larger and fewer boundaries are formed.

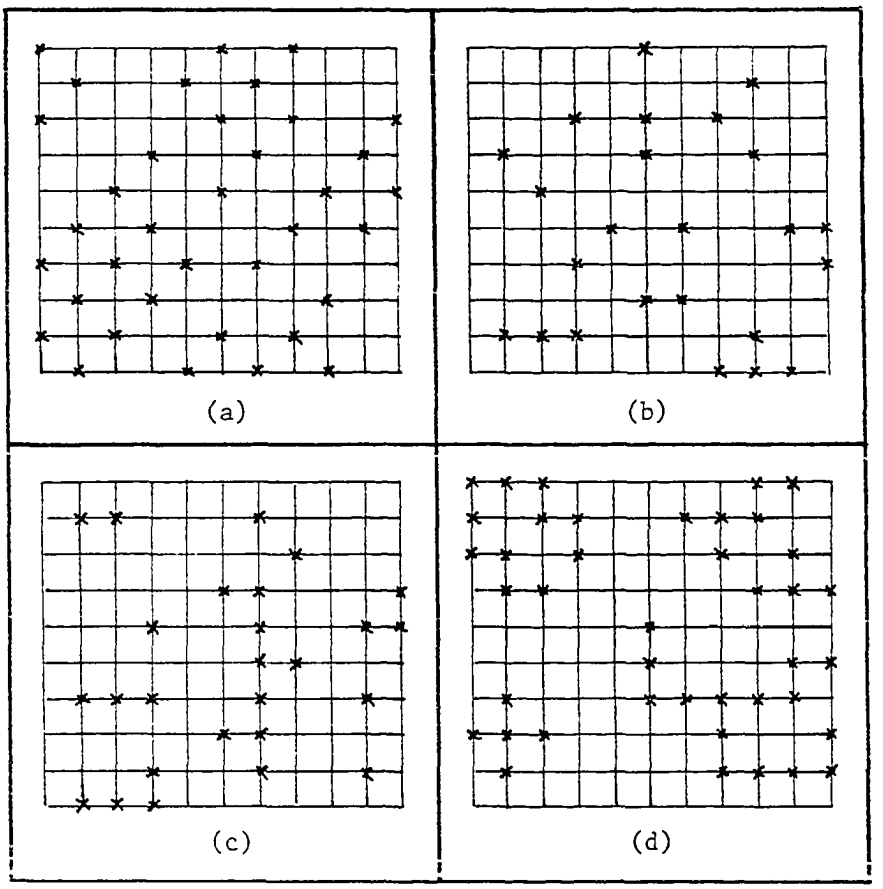

Figure 4.4. Typical lattice configurations for intermediate times during a process where the rate of addition to a site with one n.n. (rate equals α) is (a) highly inhibitory, $\alpha \ll 1$, (b) random, $\alpha=1$, (c) slightly enhanced, $\alpha \geq 1$ and (d) highly enhanced, $\alpha \gg 1$. Rate of addition to sites with two or more occupied n.n. is zero

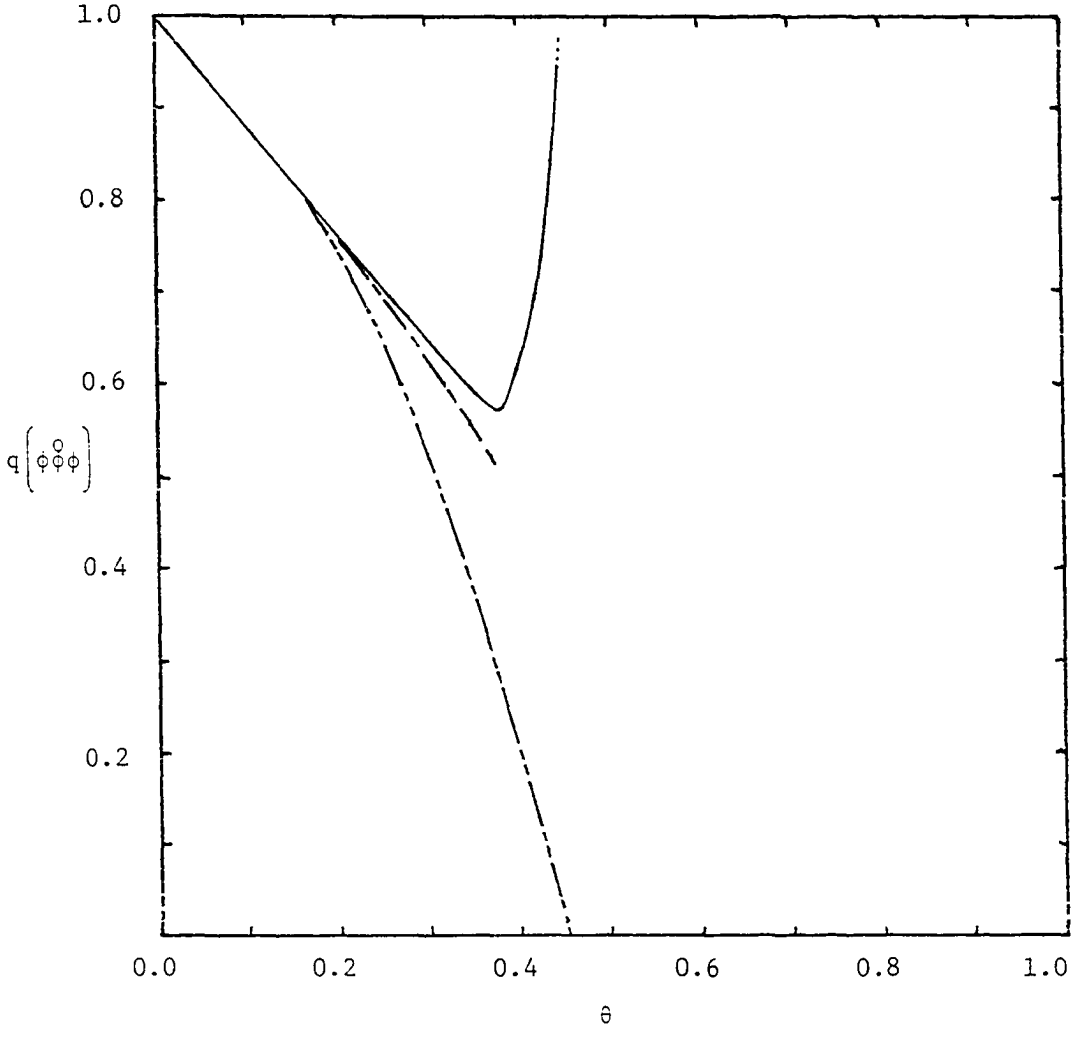

Figure 4.5. $q\left(\phi\overset{\circ}{\phi}\phi\right)$ as a function of θ for α=0.01 and blocking with two, three or four n.n. in the CA2 (——), CB3 (—— - ——) and CB2 (————) approximations

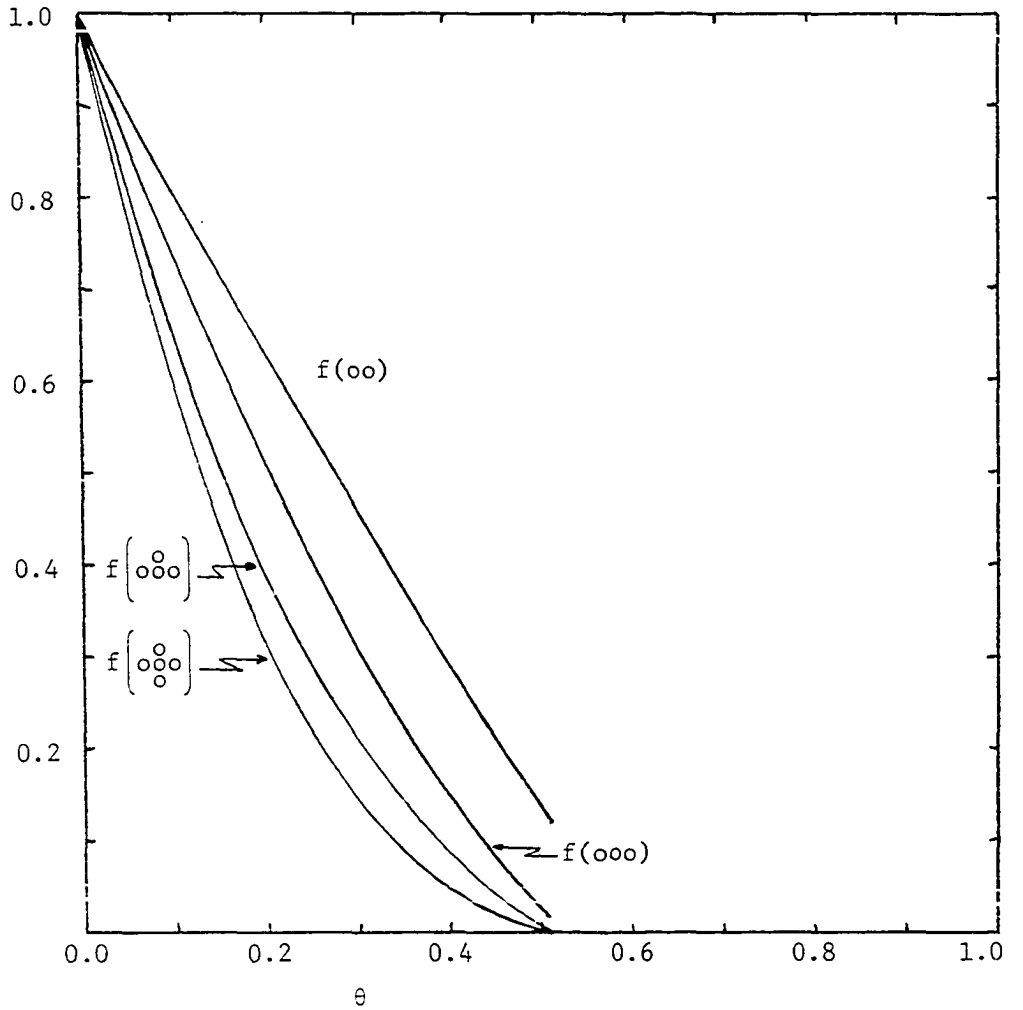

Figure 4.6. Selected probabilities as functions of θ for random filling of sites with zero or one n.n. (two or more occupied n.n. sites blocking) for the CA2 and CB3 approximations

A plot of the saturation coverage, θ_{sat}, as a function of α is given in Figure 4.7 which varies little with θ as might be anticipated.

Figure 4.8 shows the behavior of f(xx) as α goes from highly repulsive to highly attractive. When α is very repulsive, not many occupied pairs are formed causing f(xx) to be small until only sites with one n.n. remain when f(xx) then increases with slope $\frac{1}{2}$ to θ_{sat}. As α gets larger, more occupied pairs are formed and the slope rises to the maximum value of $\frac{1}{2}$.

(4) $\tau\left(\begin{smallmatrix} & o & \\ o & \cdot & o \\ & o & \end{smallmatrix}\right)=1,\ \tau\left(\begin{smallmatrix} & o & \\ o & \cdot & x \\ & o & \end{smallmatrix}\right)=\alpha,\ \tau\left(\begin{smallmatrix} & x & \\ o & \cdot & x \\ & o & \end{smallmatrix}\right)=\tau\left(\begin{smallmatrix} & o & \\ x & \cdot & x \\ & o & \end{smallmatrix}\right)=\beta,\ \tau\left(\begin{smallmatrix} & x & \\ x & \cdot & x \\ & o & \end{smallmatrix}\right)=\tau\left(\begin{smallmatrix} & x & \\ x & \cdot & x \\ & x & \end{smallmatrix}\right)=0.$

Figure 4.9 shows some configurations for processes where events can occur on sites with zero, one (with rate α) or two (with rate β) occupied n.n. when (a) $\alpha=\beta=1$, (b) $\alpha=1$ and $\beta\neq 0$, (c) $\alpha=\beta>1$ and (d) $\beta=\alpha^2>1$.

When $\alpha=\beta=1$, the lattice randomly fills but does not obtain $\theta=1$ since sites with three or four n.n. are created and cannot be filled. Figure 4.10 shows the behavior of some probabilities for this choice of rates.

Some processes, rather than being completely random, may involve steric inhibition for two occupied n.n. Figure 4.11 shows the effect on θ_{sat} of varying β from very small to very large values while maintaining $\alpha=1$.

Figures 4.12a and 4.12b show θ_{sat} as a function of α for $\alpha=\beta$ and $\beta=\alpha^2$ respectively. Figures 4.7 and 4.12a, for $\alpha\neq\beta=0$ and $\alpha=\beta$ saturations, are very similar. When $\beta=\alpha^2$, however, the curve is significantly

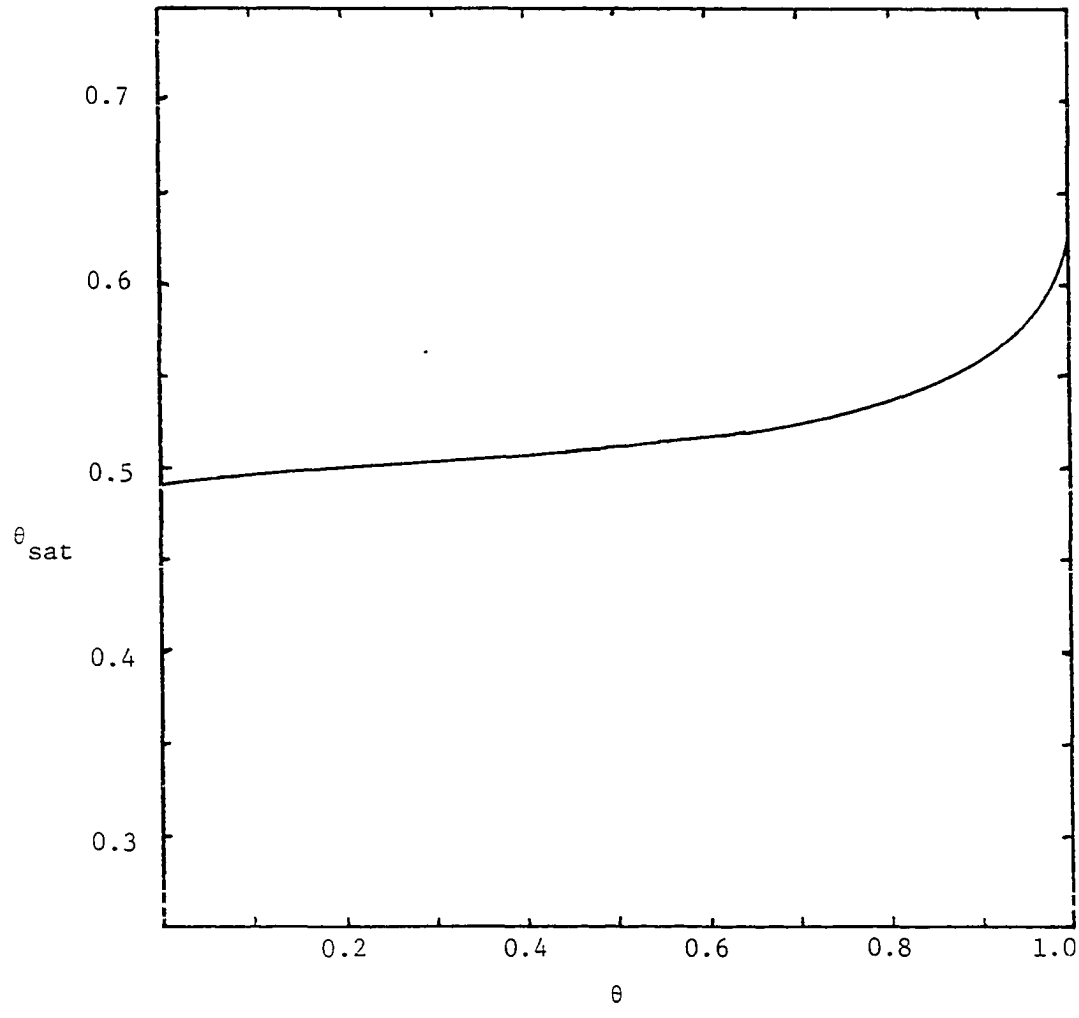

Figure 4.7. Saturation coverage, θ_{sat}, as a function of α (with two or more n.n. occupied sites blocking) in the CA2 approximation

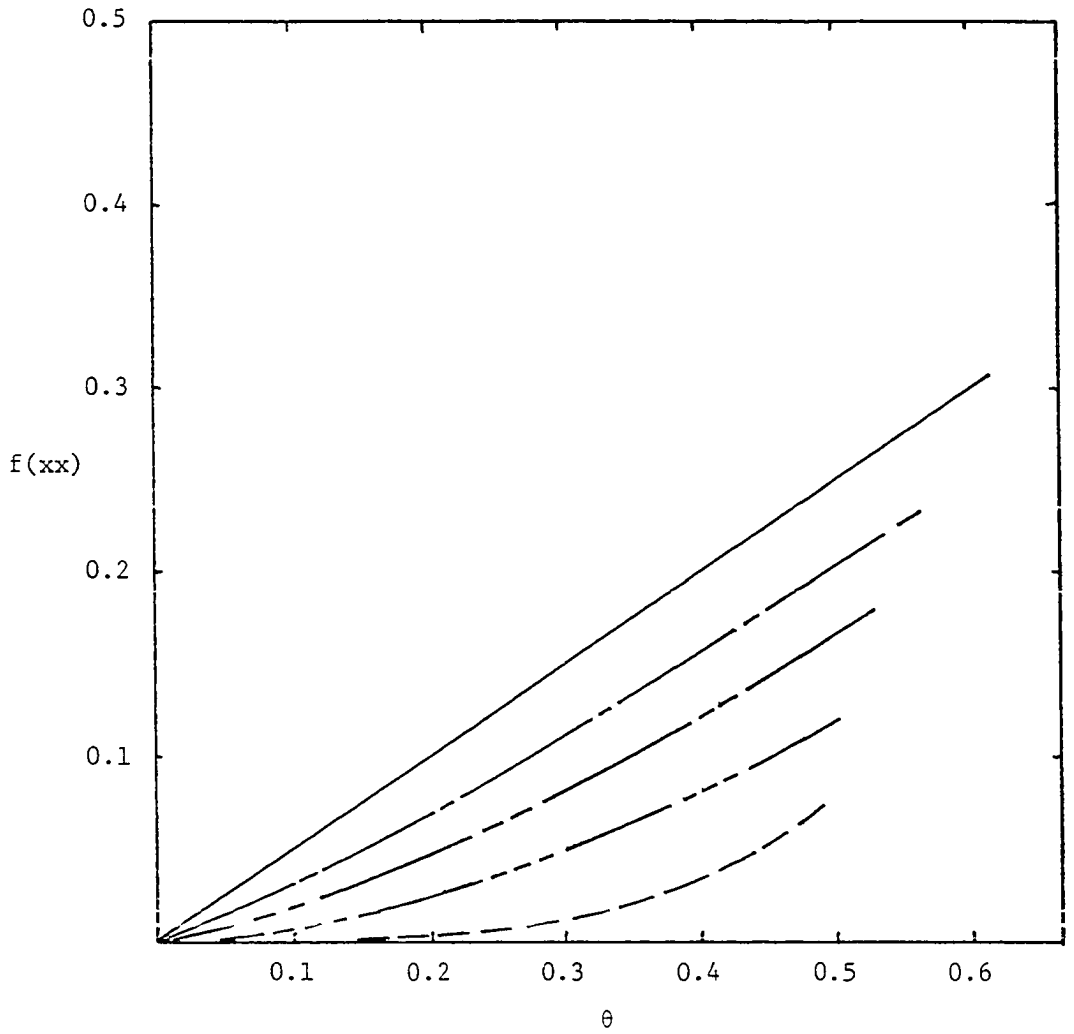

Figure 4.8. f(xx) as a function of θ for α=0.1 (—— ——), 0.7 (————————), 2.5 (————————), 10.0 (—— - ——) and 800 (——) (with two or more n.n. occupied sites blocking) in the CA2 approximation

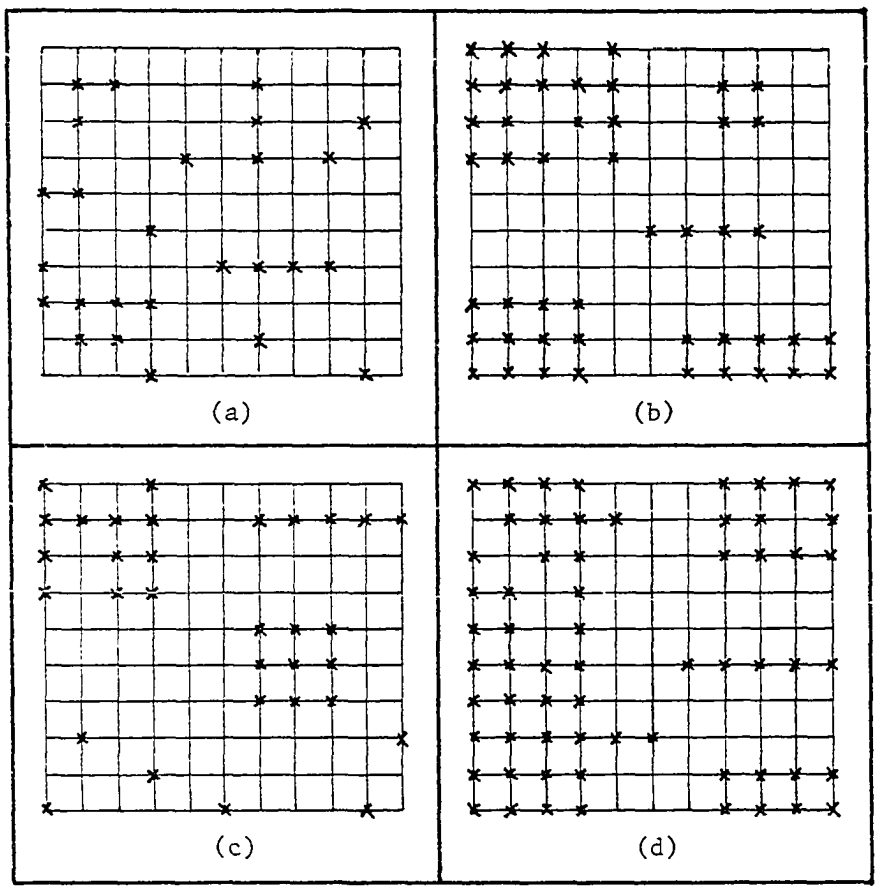

Figure 4.9. Typical lattice configurations for intermediate times during a process where events (x) can occur on sites with zero (rate equals one), one (rate equals α) or two (rate equals β) occupied n.n. when (a) $\alpha=\beta=1$, (b) $\alpha=1$ and $\beta\neq 0$, (c) $\alpha=\beta>1$ and (d) $\beta=\alpha^2>1$. Rate of addition to sites with three or more occupied n.n. is zero

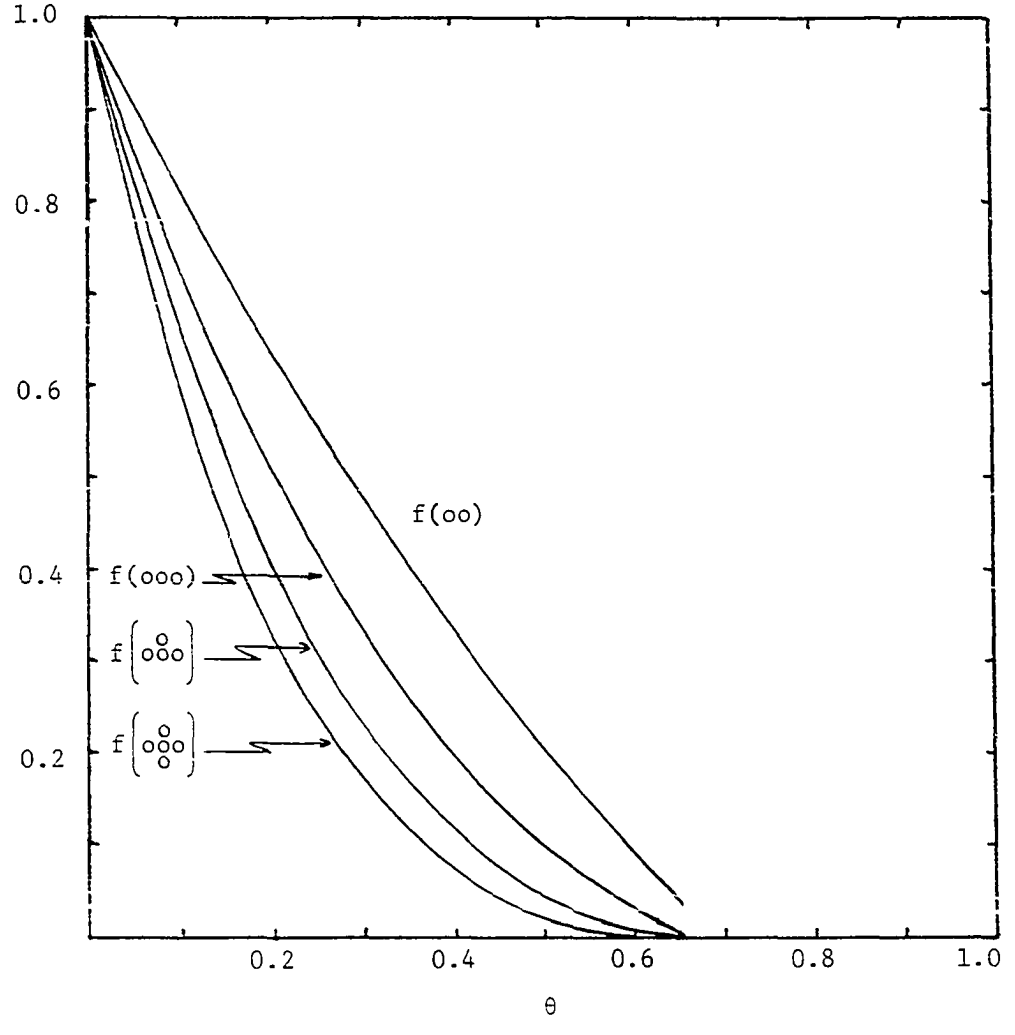

Figure 4.10. Selected probabilities as functions of θ for random filling of sites with zero, one or two occupied n.n. (three or more occupied n.n. blocking) in the CA2 and CB3 approximations

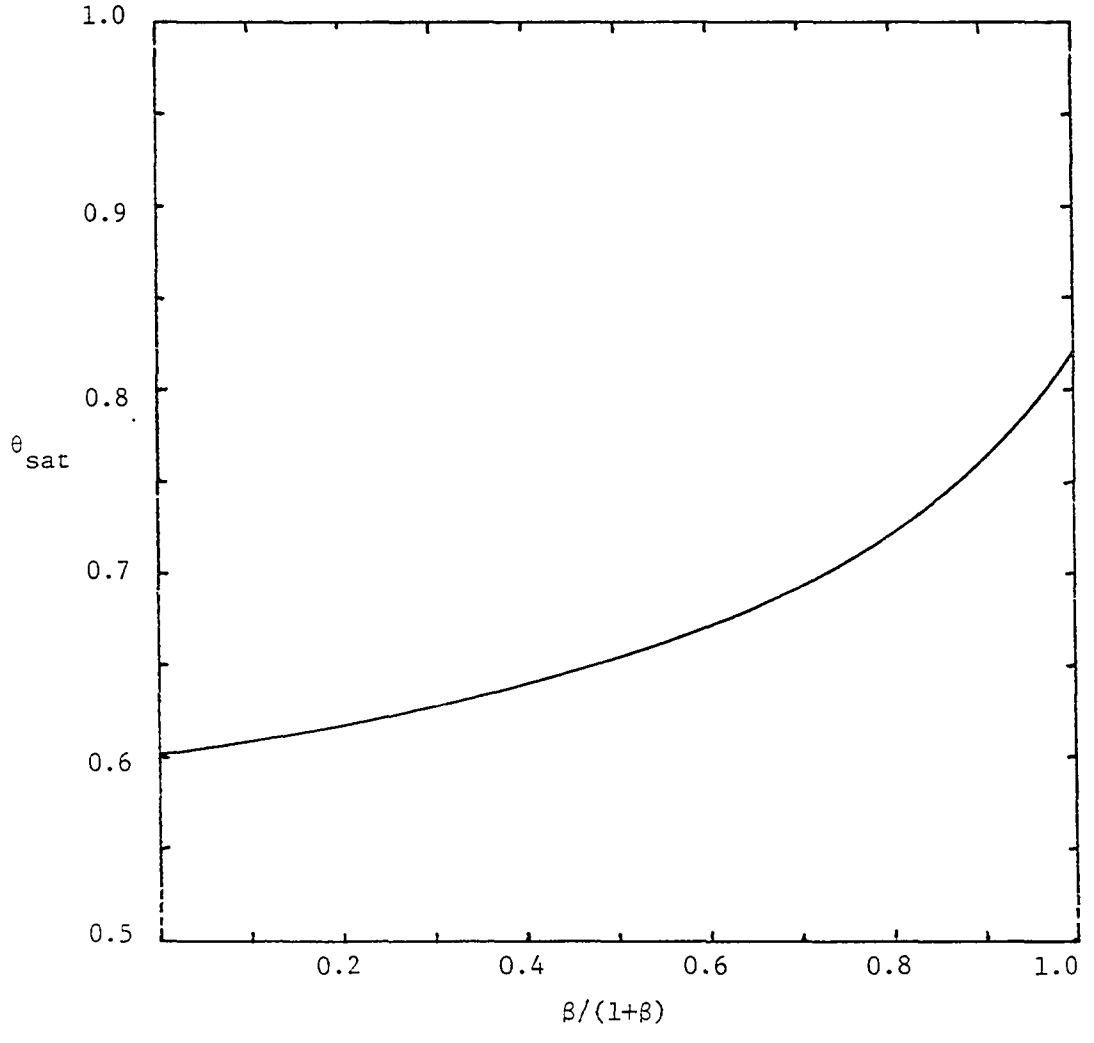

Figure 4.11. Saturation coverage, θ_{sat}, as a function of β while maintaining $\alpha=1$ in the CA2 approximation

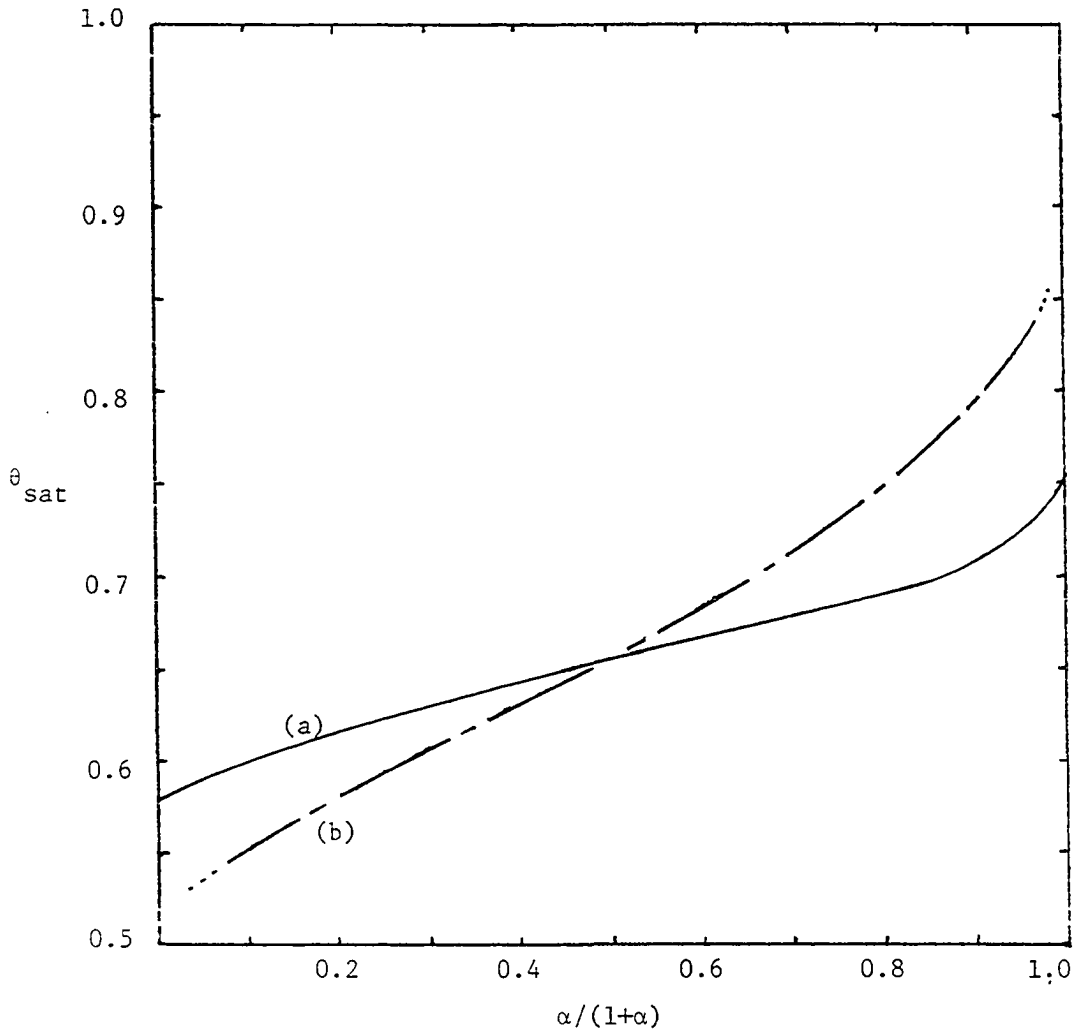

Figure 4.12. Saturation coverage, θ_{sat}, as a function of α for (a) $\alpha=\beta$ (——) and (b) $\alpha=\beta^2$ (—— - ——) (rates for addition with more than two n.n. are zero) in the CA2 approximation

different. The difference between $\alpha=\beta>1$ and $\beta=\alpha^2>1$ is further shown by considering $f\begin{pmatrix}\circ\circ\\ \circ\circ\end{pmatrix}$. When $\alpha=\beta>1$ island growth is favored, but $\alpha=\beta$ results in "sidechains" and open configurations. If $\beta=\alpha^2>1$, on the other hand, the islands will tend to be rectangular with more unoccupied area between larger islands and $f\begin{pmatrix}\circ\circ\\ \circ\circ\end{pmatrix}$ will be larger. Figure 4.13 illustrates this for $\alpha=0.2$, 2 and 10.

(5) $\tau\left(\begin{smallmatrix}&\circ&\\ \circ&\bullet&\circ\\ &\circ&\end{smallmatrix}\right)=1,\ \tau\left(\begin{smallmatrix}&\circ&\\ \circ&\bullet&\times\\ &\circ&\end{smallmatrix}\right)=\alpha,\ \tau\left(\begin{smallmatrix}&\times&\\ \circ&\bullet&\times\\ &\circ&\end{smallmatrix}\right)=\tau\left(\begin{smallmatrix}&\circ&\\ \times&\bullet&\times\\ &\circ&\end{smallmatrix}\right)=\beta,\ \tau\left(\begin{smallmatrix}&\times&\\ \times&\bullet&\times\\ &\circ&\end{smallmatrix}\right)=\gamma,\ \tau\left(\begin{smallmatrix}&\times&\\ \times&\bullet&\times\\ &\times&\end{smallmatrix}\right)=0.$

Many possible choices of rates exist when addition to all sites, except those with four n.n., is possible. The saturation versus α curves are shown in Figures 4.14a and 4.14b for $\alpha=\beta=\gamma$ and $\beta=\alpha^2$ with $\gamma=\alpha^3$, respectively.

Some probabilities, as a function of θ, are shown in Figure 4.15 for the random filling case ($\alpha=\beta=\gamma=1$).

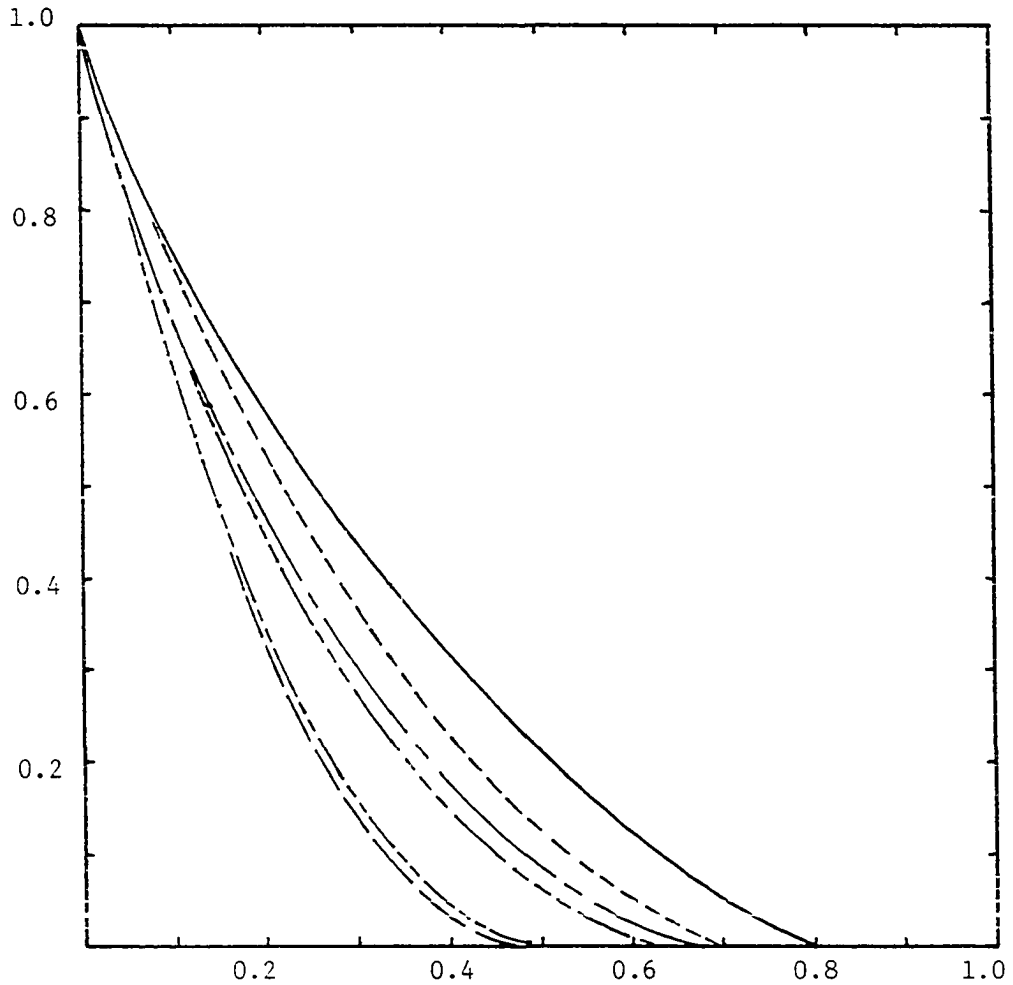

Figure 4.13. $f\begin{pmatrix}\infty\\ \infty\end{pmatrix}$ as a function of θ when
(a) $\alpha=10$, $\beta=100$ (——), (b) $\alpha=\beta=10$ (----),
(c) $\alpha=2$, $\beta=4$ (—— - ——), (d) $\alpha=\beta=2$ (————),
(e) $\alpha=\beta=0.2$ (————) and (f) $\alpha=0.2$, $\beta=0.4$ (—— ——)

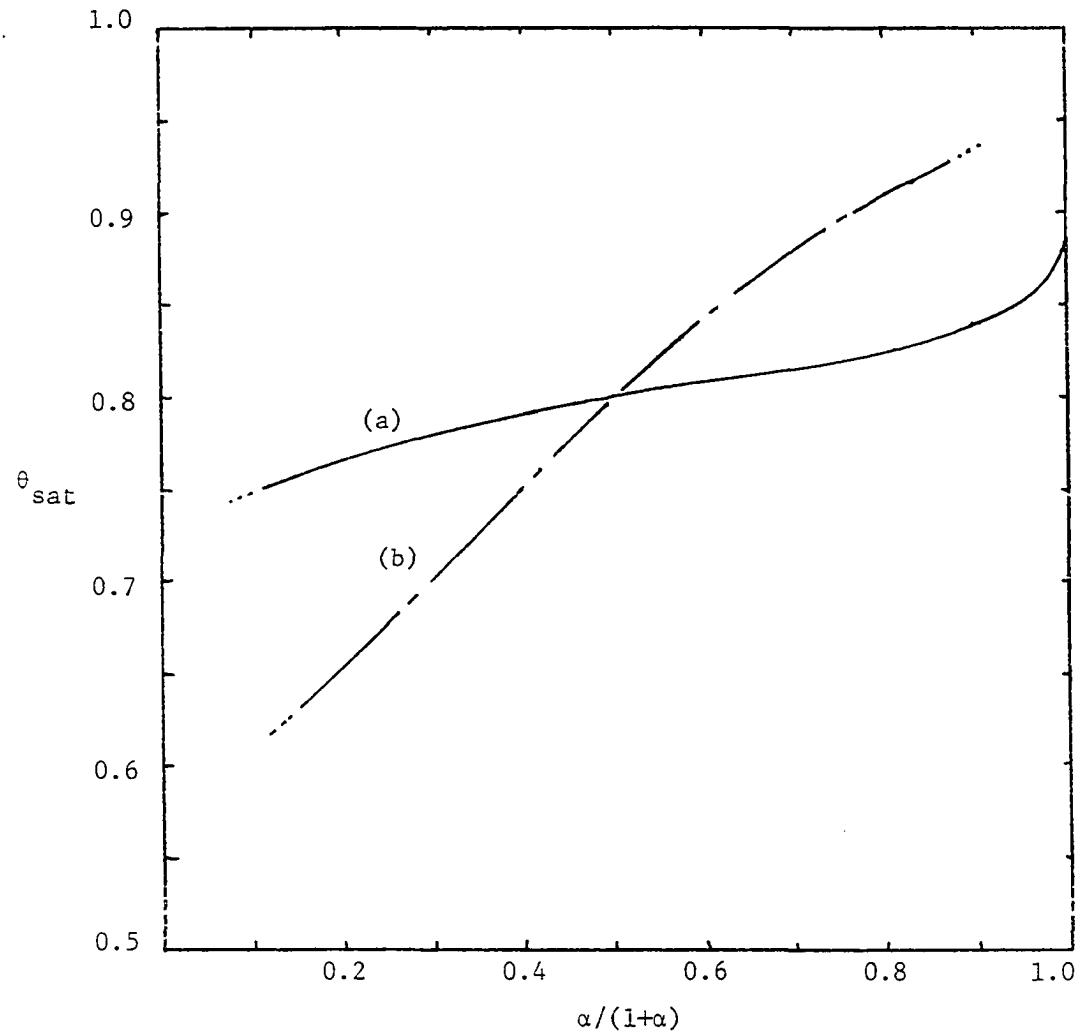

Figure 4.14. Saturation coverage, θ_{sat} as a function of α for (a) $\alpha=\beta=\gamma$ (——) and (b) $\beta=\alpha^2$ and $\gamma=\alpha^3$ (—— - ——) for the CA2 approximation

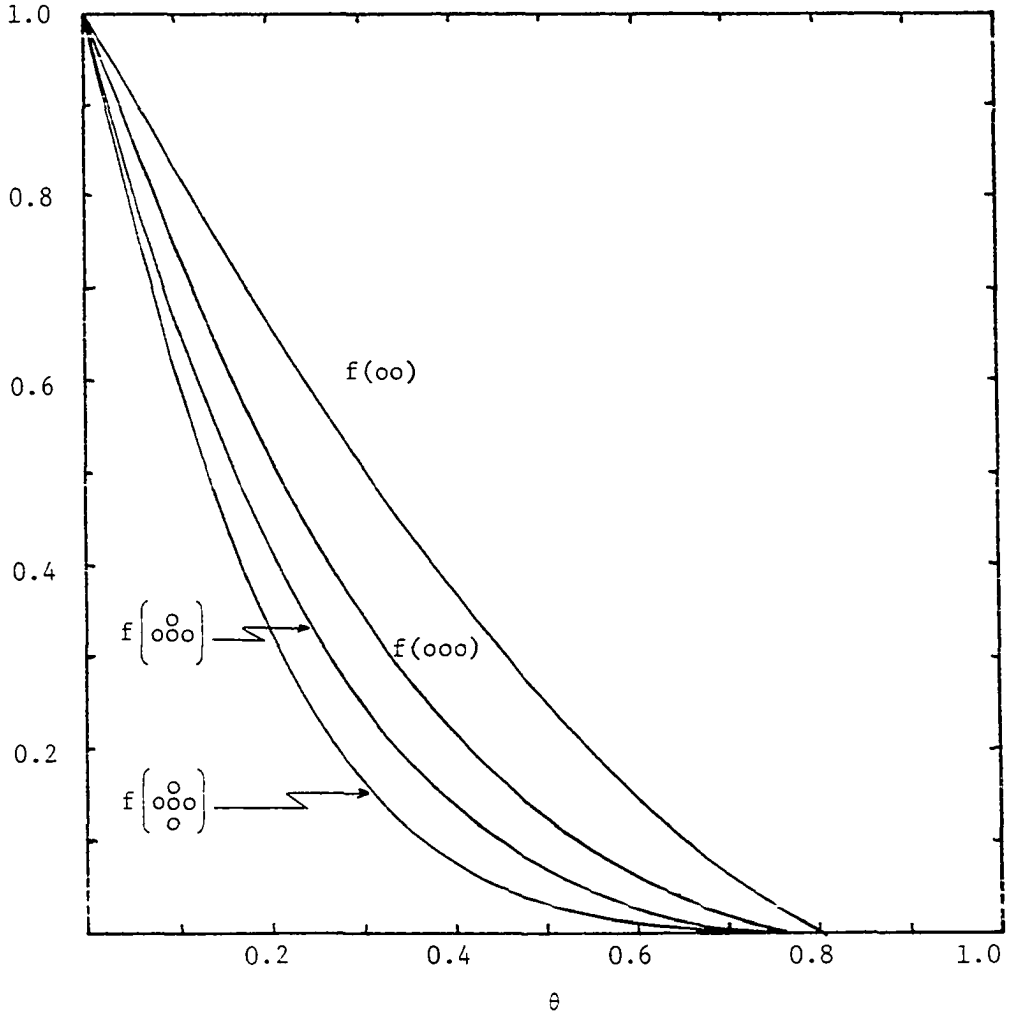

Figure 4.15. Selected probabilities as a function of θ for the random filling case (α=β=γ=1) in the CA2 and CB3 approximations

5. APPLICATION TO POLYMER REACTIONS

Irreversible processes are common in polymer reactions as evidenced, for example, by poly(methyl vinyl)ketone condensation (1) (cf., Figure 1.1). Flory's well-known theoretical model for this reaction can be applied to any reaction that can be modeled as a 1-D random dimer type process. Several groups (52-56) have observed reactions of the random dimer type which come close to his theoretical limiting conversion of 86.4%. For instance, the lactonization of vinylchloride-methyl methacrylate (see Figure 5.1) by Tanaka, et al. (55) obtained a final conversion of 86%. All polymer reactions are, of course, not random dimer type processes. This chapter elucidates

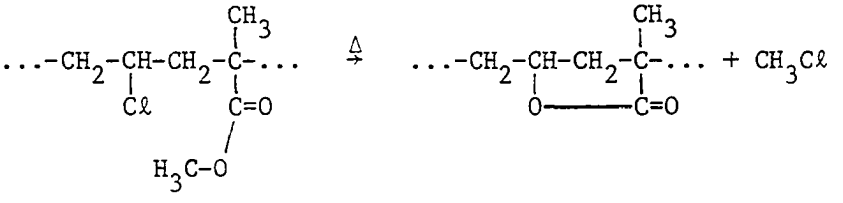

Figure 5.1. Lactonization of vinylchloride-methyl methacrylate

a variety of other polymer reactions which require more general models (e.g., those developed in Chapters two and three).

Several workers have dealt with reactions which are n.n. cooperative (governed by the rates $\tau_{o\cdot o}$, $\tau_{o\cdot x}$ and $\tau_{x\cdot x}$ corresponding to zero, one and two reacted n.n. sites). They are often interested in measuring the limiting conversion of their reaction as well as determining values for the rates. Whereas the limiting conversion can be experimentally obtained, the rates are generally found from a semiempirical model. One

appropriate fitting method, developed to describe the quanterization of poly-4-vinylpyridine, by Fuoss et al. (57) (see Figure 5.2), originates in the idea that the first stage of the process is

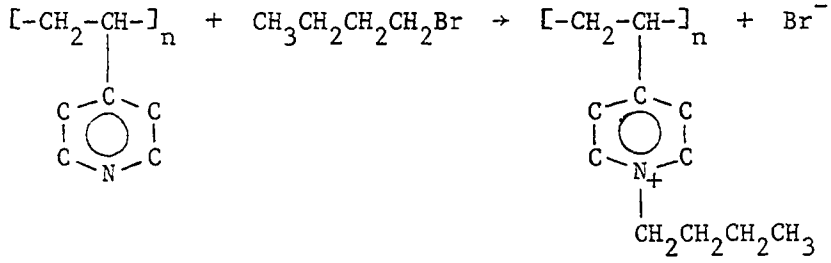

Figure 5.2. Quanterization of poly-4-vinylpyridine

governed by one rate ($\tau_{o\cdot o}$), the last by a difference rate ($\tau_{x\cdot x}$), and that a continuous transition from $\tau_{o\cdot o}$ to $\tau_{x\cdot x}$ occurs during the process. They propose the following semiempirical equation to describe this shift

$$d\theta/dt = [\tau_{o\cdot o}\, e^{-\alpha t} + \tau_{x\cdot x}(-e^{-\alpha t})]\,[A-\theta]\,[1-\theta]\ , \qquad (5.1)$$

where A is the ratio of initial alkyl halide to initial unquaternized nitrogens and θ is the fraction of quaternized nitrogens. Equation 5.1 can be integrated to give

$$1/t \int \frac{d\theta}{[A-\theta][1-\theta]} \equiv g(\theta)/t = \tau_{x\cdot x} + (\tau_{o\cdot o} - \tau_{x\cdot x})(1-e^{-\alpha t})/t\ . \qquad (5.2)$$

The left hand side of Equation 5.2 can be evaluated from experimental data. The rates are determined by graphing $g(\theta)/t$ against $(1-e^{-\alpha t})/t$, choosing trial values for α until a straight line plot is obtained.

The models described in Chapters two and three directly provide upper bounds for limiting conversions as well as eliminate the need for the use of semiempirical methods to determine the rates.

The rates are determined by analyzing θ as a function of t during each stage of filling. During the first stage (q=qo[oo]),

$$d\theta/dt = \tau_{o\cdot o}\, f(ooo) = \tau_{o\cdot o}\, q\, f(oo)$$
$$= \tau_{o\cdot o}\, e^{-\tau_{o\cdot o}t}\, e^{-2(1-q)} \quad . \tag{5.3}$$

Since q stays relatively close to one during much of this stage and then goes to zero quickly at the end of the stage (see Figure 3.4),

$$d\theta/dt \cong \tau_{o\cdot o}\, e^{-\tau_{o\cdot o}t} \quad . \tag{5.4}$$

Integrating Equation 5.4 gives

$$-\ell n[1-\theta] = \tau_{o\cdot o}t \quad . \tag{5.5}$$

A plot of $-\ell n[1-\theta]$ verses t will have slope $\tau_{o\cdot o}$ for small θ, thus determining this rate.

During the second stage,

$$d/dt\ \theta = 2\ \tau_{o\cdot x}\, f(2) = 2\ \tau_{o\cdot x}(1-\theta^*-\theta) \tag{5.6}$$

where $\theta^*=\frac{1}{2}(1-e^{-2})$ and, after integration,

$$-\ell n[1-\theta^*-\theta] = 2\ \tau_{o\cdot x}(t+t_o) \quad . \tag{5.7}$$

The slope of $-\ell n[1-\theta^*-\theta]$ verses $(t+t_o)$ gives $2\ \tau_{o\cdot x}$ in this case.

Finally, during the third stage

$$d/dt\ \theta = \tau_{x\cdot x}\ f(1) = \tau_{x\cdot x}(1-\theta) \tag{5.8}$$

and $$-\ell n[1-\theta] = \tau_{x\cdot x}(t+t_o') \ . \tag{5.9}$$

The rate is again obtained by graphing $-\ell n[1-\theta]$ against $(t+t_o')$. It is seen therefore, that all rates are easily obtained from non-empirical analysis of experimental data.

The above analysis will now be applied to two reactions reported by Rempp (58). Figure 5.3 shows a generic chemical description for the reaction of CH_3SOCH_2Na or $CH_3SO_2CH_2Li$ onto polymethylmethacrylate (PMMA).

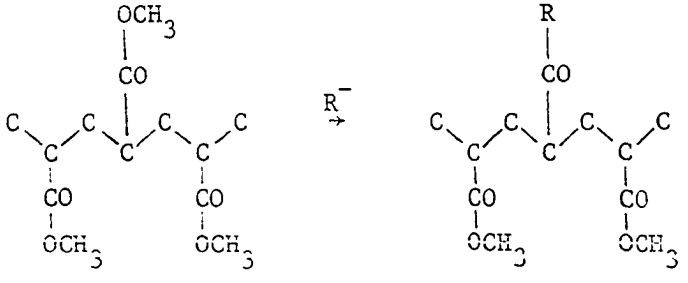

Figure 5.3. Reaction of R^- onto PMMA, $R^-=CH_3SOCH_2^-$ or $CH_3SO_2CH_2^-$

These experiments were performed at 25°C with the degree of substitution (conversion) determined by elemental analysis. Rempp stated that the reactions were n.n. cooperative with $\tau_{o\cdot o} > \tau_{o\cdot x} > \tau_{x\cdot x}$ and that less than 1% cyclization occurred. He also said that the theoretical work of Higuchi and Senju (59) suggested that if the saturation value of θ was less than 2/3 it can be assumed that $\tau_{x\cdot x} \cong 0$. In agreement with

Higushi and Senju, it will be shown later in this chapter that 2/3 is the highest possible conversion for a process where $\tau_{x\cdot x}=0$ and occurs when $\tau_{o\cdot o}=\tau_{o\cdot x}\neq 0$.

The reaction of CH_3SOCH_2Na was onto atactic PMMA (70% of the pendant groups alternate sides along the carbon chain) in DMSO solution. The appropriate graphs are shown in Figure 5.4. The rates (in inverse hours), as obtained from the slopes, are $\tau_{o\cdot o}=2.4$, $\tau_{o\cdot x}=0.14$ and $\tau_{x\cdot x}=0.022$. Rempp, using the method of Fuoss et al. described earlier (replacing $\tau_{x\cdot x}$ by $\tau_{o\cdot x}$), reported 8.33, 0.34 and approximately zero, respectively. The assignment of $\tau_{x\cdot x}\cong 0$ is not consistent with the data since $\theta\cong 0.63$, but for $\tau_{o\cdot o}\gg\tau_{o\cdot x}$ and $\tau_{x\cdot x}=0$ the maximum θ is 0.568 as shown in Chapter three. The breaks occur at $\theta\cong 0.42$ and $\theta\cong 0.56$ which are very close to the theoretically predicted values of 0.432 and 0.568 for n.n. cooperative processes where $\tau_{o\cdot o}\gg\tau_{o\cdot x}\gg\tau_{x\cdot x}$.

The reaction of $CH_3SO_2CH_2Li$ was onto syndiotactic PMMA (virtually all of the pendant groups alternate sides along the carbon chain) in a 5:1 DMSO:benzene solution. The appropriate graphs are shown in Figure 5.5. Three distinct slopes are again observed and the rates are found to be $\tau_{o\cdot o}=1.2$, $\tau_{o\cdot x}=0.20$ and $\tau_{x\cdot x}=0.035$ (compared to Rempp's values of 9.9×10^{-2}, 5.5×10^{-3} and approximately zero). Rempp reported a final θ of 0.52. Bourguignon and Galin (60) found a final θ of 0.665 for this reaction in a homogeneous tetrahydrofuran-DMSO solution. (Unfortunately, they didn't report θ versus t data.) Assuming the ratios of the rates reported above are not affected by

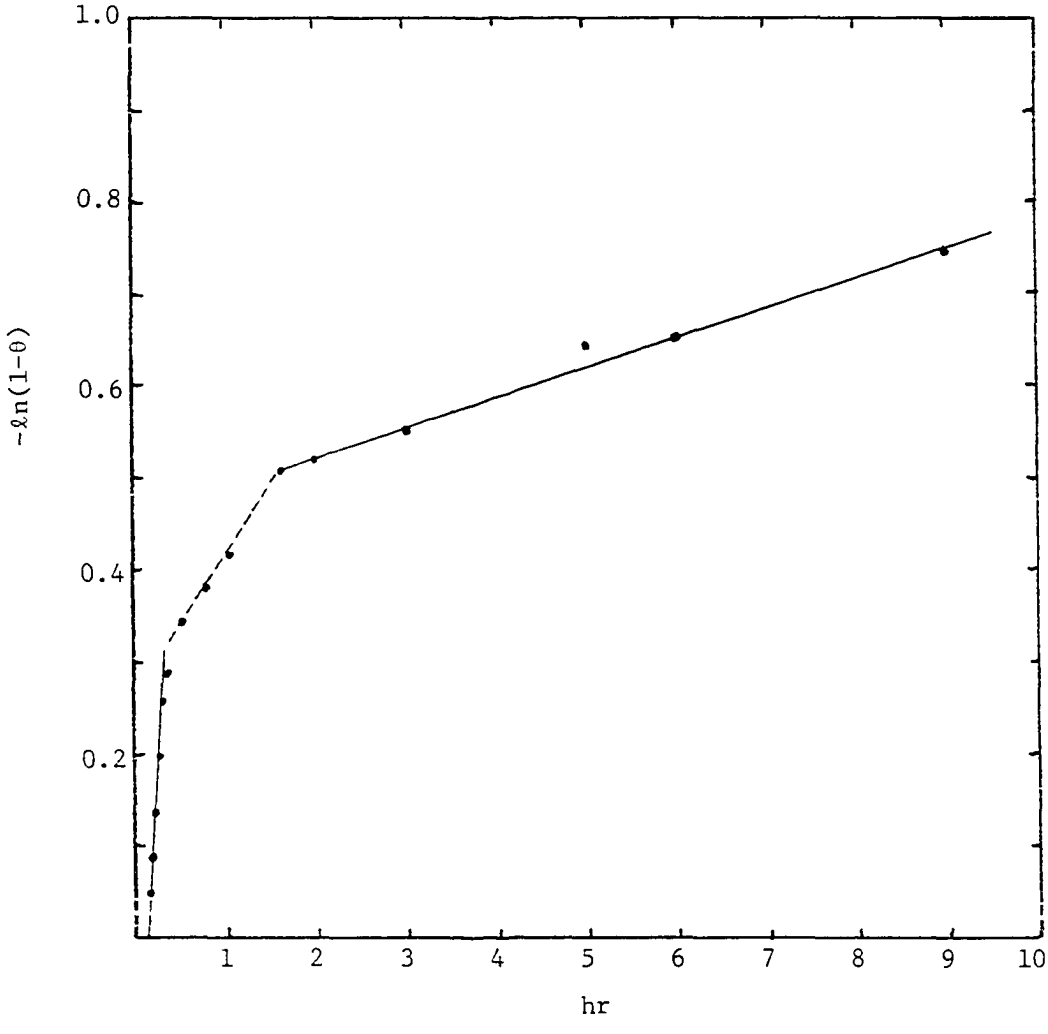

Figure 5.4a. $-\ell n(1-\theta)$ as a function of time for the reaction of $CH_3SO_2CH_2Li$ onto syndiotactic PMMA. The rates for the initial and final stages can be found using this plot. The second stage is analyzed in Figure 5.4b. Data points are taken from Rempp (58)

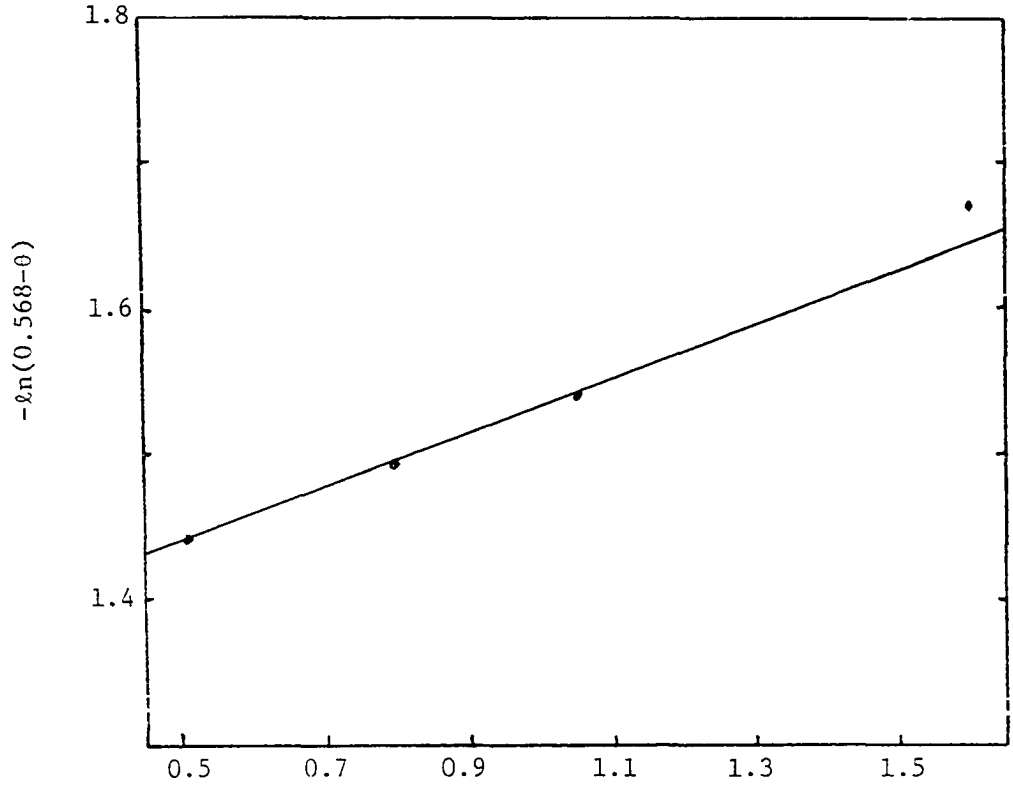

Figure 5.4b. Second stage graph of data for $CH_3SO_2CH_2Li$ onto PMMA (58)

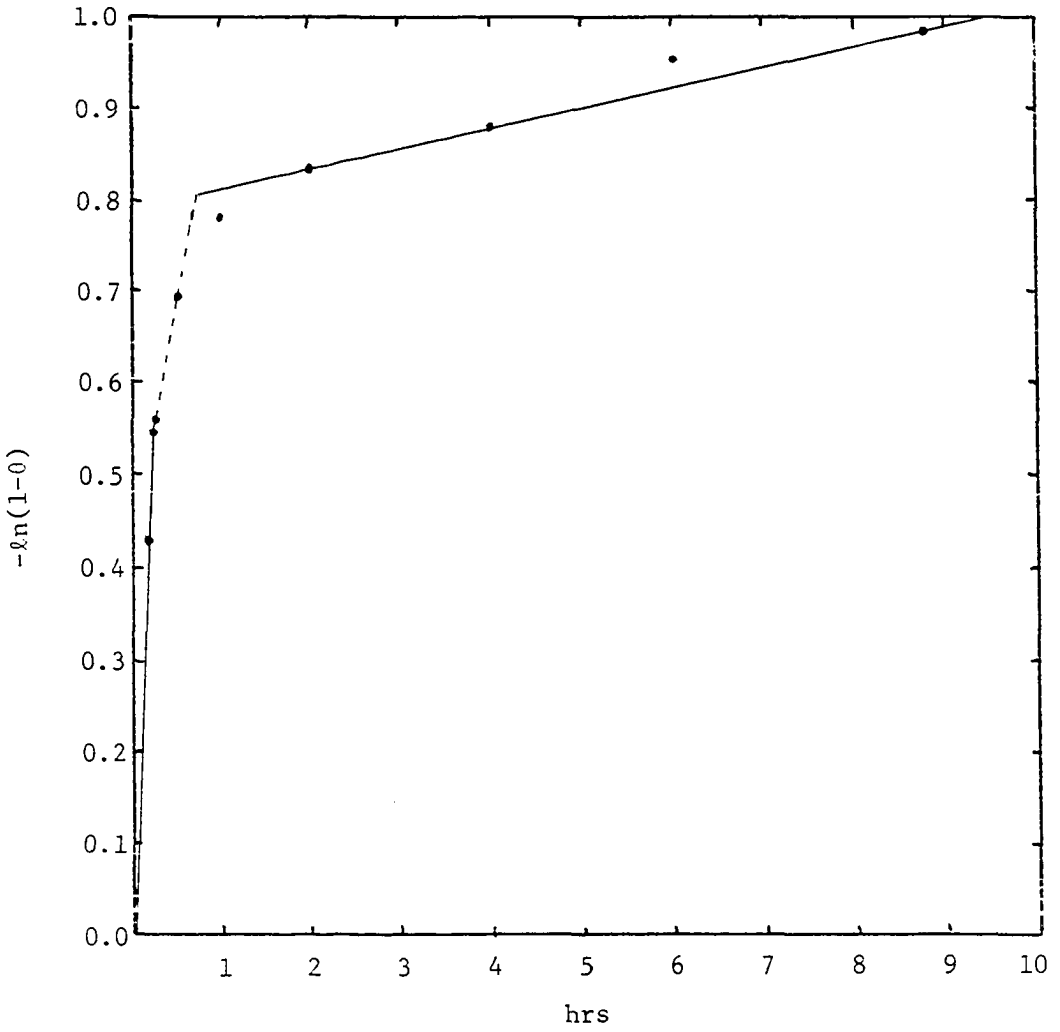

Figure 5.5a. $-\ell n(1-\theta)$ as a function of time for the reaction of CH_3SOCH_2Na onto PMMA as reported by Rempp (58)

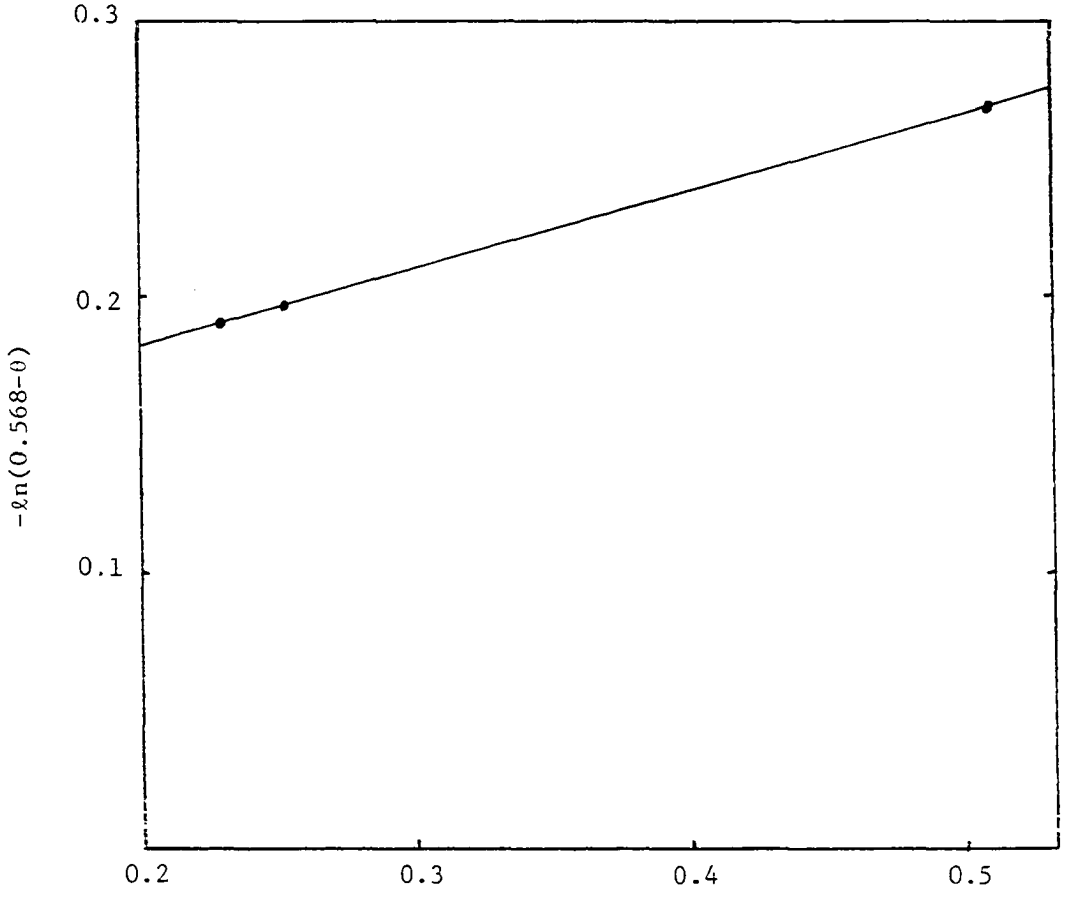

Figure 5.5b. Second stage graph of data for CH_3SOCH_2Na onto PMMA (58)

the change in solvent, a limiting conversion 0.665 is compatible with our model. The first stage data points suggest that Rempp's values for $-\ell n(1-\theta)$ are systematically low, since the line intersects the $-\ell n(1-\theta)$ axis below the origin.

A third reaction reported by Rempp (58) is $CH_3SO_2CH_2Li$ onto isotactic PMMA (all pendant groups are on the same side of the carbon chain) at 25C in 5:1 DEMSO:benzene mixture (see Figure 5.6). The reported rates are $\tau_{o\cdot o}=\tau_{o\cdot x}=4.7\times10^{-1}$ and $\tau_{x\cdot x}=1.4\times10^{-3}$. Processes where $\tau_{o\cdot o}=\tau_{o\cdot x} \gg \tau_{x\cdot x} \neq 0$, of which this is an example (presuming Rempp's rates are correct) have some interesting theoretical aspects.

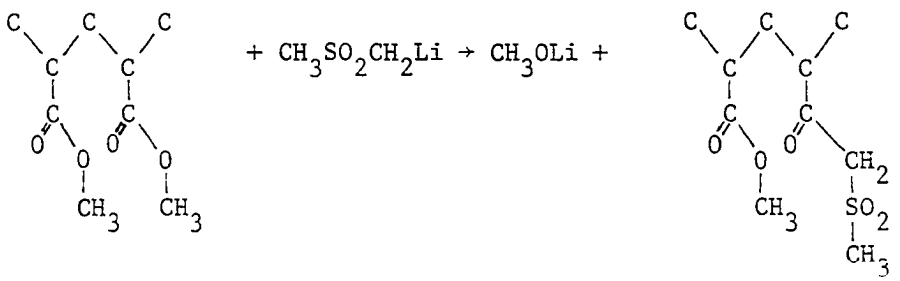

Figure 5.6. Reaction of $CH_3SO_2CH_2Li$ onto isotactic PMMA

The appropriate equations can be written from Equation 1.1. In this case, the resultant equations can be directly integrated to give

$$f(n) = e^{-n\tau_{o\cdot o}t} , \quad n \geq 2 \tag{5.10}$$

and

$$f(1) = 1 - \frac{2(\tau_{o\cdot o}-\tau_{x\cdot x})}{(-2\tau_{o\cdot o}+\tau_{x\cdot x})} e^{-2\tau_{o\cdot o}t} - \frac{\tau_{x\cdot x}-\tau_{o\cdot o}}{(-3\tau_{o\cdot o}+\tau_{x\cdot x})} e^{-3\tau_{o\cdot o}t}$$

$$+ \frac{2(\tau_{o\cdot o}-\tau_{x\cdot x})}{-2\tau_{o\cdot o}+\tau_{x\cdot x}} + \frac{\tau_{x\cdot x}-\tau_{o\cdot o}}{-3\tau_{o\cdot o}+\tau_{x\cdot x}} e^{-\tau_{x\cdot x}t} . \qquad (5.11)$$

In the experiment under discussion, $\tau_{o\cdot o}=\tau_{o\cdot x}$ (as given by Rempp) is two orders of magnitude greater than $\tau_{x\cdot x}$ which implies that the reaction on sites with both n.n. occupied is strongly inhibited. If the limit as $\tau_{x\cdot x}\to 0$ is taken, Equation 5.7 becomes

$$f(1) = e^{-2\tau_{o\cdot o}t} + 1/3\ e^{-3\tau_{o\cdot o}t} + 1/3 . \qquad (5.12)$$

Thus, the limiting conversion is $\theta=2/3$. This result provides an upper conversion limit for processes where $\tau_{o\cdot o}=\tau_{o\cdot x}\neq 0$ and $\tau_{x\cdot x}=0$.

Rempp reported a limiting conversion of $\theta=0.59$. (The time of observation is not given.) This value is low for the proposed rates since the limiting conversion is less than 2/3. Rempp does not give the θ verses t data for this reaction, thus making an analysis of the type previously discussed impossible. If, however, the final covering fraction is assumed correct an adjustment in the rates to $\tau_{o\cdot x}/\tau_{o\cdot o}=1/8$, $\tau_{x\cdot x}=0$ would be needed.

Another polymer reaction which can be better understood using irreversible cooperative kinetic modeling is the coordination of $ZnCl_2$ with poly(propylene oxide) as reported by James et al. (61) (see Figure 5.7).

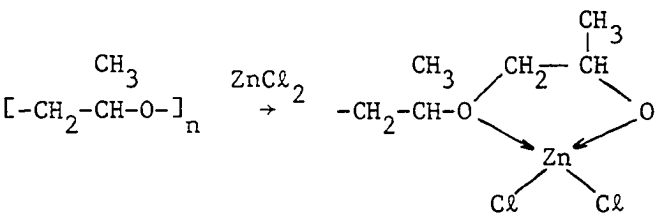

Figure 5.7. Coordination of $ZnCl_2$ with poly(propylene oxide)

The reaction is a dimer type reaction since adjacent oxygens are coordinated during each event. (These workers show that intermolecular coordination is unimportant.)

The coordination of oxygens by $ZnCl_2$ influences Tg, the glass transition temperature. This effect is predicted by the Gordon-Taylor-Wood equation (62) to be

$$Tg = \frac{T_{gA}+(KT_{gB}-T_{gA})W_B}{1-(1-K)W_B} , \qquad (5.13)$$

where T_{gA} and T_{gB} are the glass transition temperatures for completely unreacted and completely reacted polymers respectively. The constant $0 < K < 1$ is specific to the copolymer under consideration and W_B is the weight fraction of coordinated units. For this copolymer $W_B=126\theta/(58+68\theta)$ where θ is the fraction of oxygens coordinated, $T_{gA}=208$, $T_{gB}=400$ and $K=.3$. As shown in Figure 5.8, Equation 5.13 only works to $\theta\cong0.52$. The authors try unsuccessfully to relate this

phenomenon to the Flory model by assuming that this results from no more oxygen pairs being available beyond θ=0.52, thus causing the $ZnC\ell_2$ to coordinate with individual oxygens. However, the authors also point out that the simple Flory model is not adequate since it predicts a deviation at θ=0.864. The observed behavior can be explained by assuming that the process is initially of the dimer filling type with n.n. blocking and Equation 5.13 holds only to saturation. The deviation point thus predicted is θ=0.549 compared to the experimental value of 0.52. From the experimental data of Figure 5.8, $ZnC\ell_2$ continues to be coordinated until θ=1. There appears to be a break at around θ=0.73. This might be explained as follows. First, assume the process initially continues by random monodentate complexation on sites with at least one empty neighbor. This increases θ to 0.708. In the final stage the remaining single sites are complexed. The mechanism proposed beyond the first stage is obviously speculative, but as a general proposition one would expect complexation to occur at regions of greatest flexibility on the chain. Further, the less flexible the chain, the smaller the effect on T_g as a function of θ.

The examples of this chapter point out the importance of appropriately modeling irreversibility in polymer processes. The number of models for polymer processes exploited to date is small. Because of its obvious successes, the Flory model has been used beyond its range of applicability. It is hoped that the theoretical models developed here will serve as guides, much like Flory's result has in the past, to help resolve mechanistic questions in the exciting field of polymer chemistry.

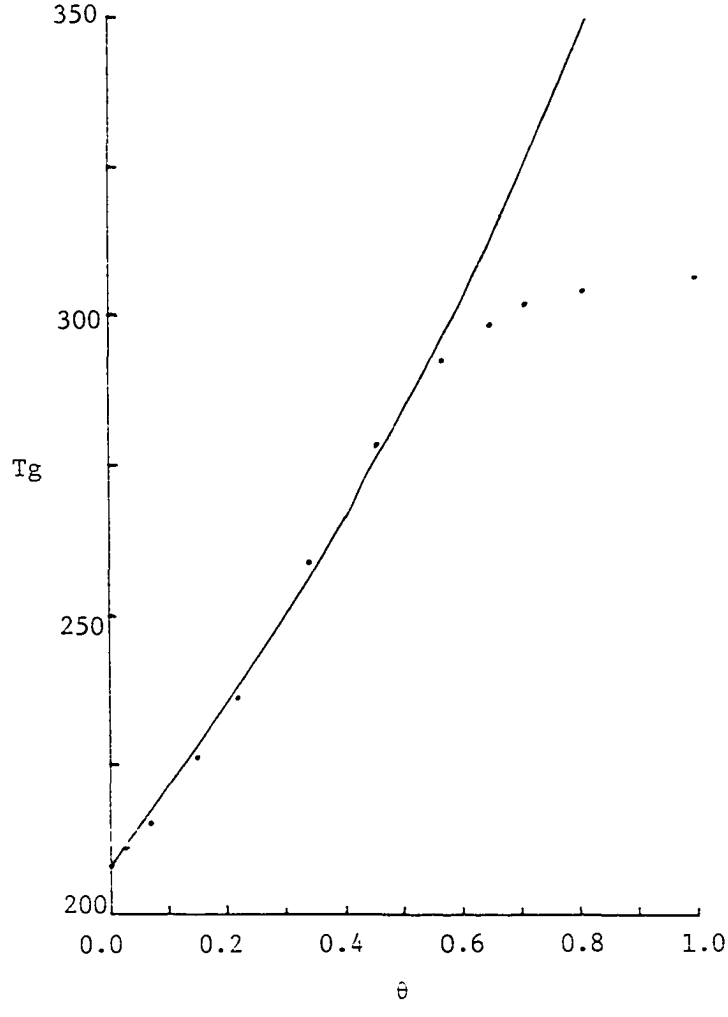

Figure 5.8. Tg as a function of θ. The data points (•) are from the work of James, et al. (61). The theoretical (solid) curve is obtained from Equation 5.13

6. APPLICATION TO SURFACE PROCESSES

Gas adsorption onto a metal is of basic interest since it leads to an understanding of thin film formation, oxidation, corrosion, catalysis and a variety of other interesting processes. Technologically it is important in understanding thin film semi-conductors, passivity of metals, structural stability, catalytic production of industrially important materials, etc. There has been a recent upsurge of interest in this field, mainly due to the advance of experimental techniques which can better characterize the adsorbed layer on surfaces. Some of the steps in adsorption processes may be irreversible and, thus, the models developed in previous chapters are helpful.

Dash (63) has enumerated six idealized categories, of increasing complexity, useful in modern theory for the description of a substrate. They are:

(1) Plane boundary. The plane boundary surface is a flat, structureless, mathematical surface.

(2) Attracting plane. The attracting plane accounts for the surface normal attraction between substrate and absorbate atoms.

(3) Adsorption sites. The structure of the substrate may be approximated by an array of equivalent adsorption sites with pairwise additive single potentials.

(4) Structured substrate. Periodic variations of attractive interactions on the surface may more realistically represent the structure of the substrate.

(5) Deformable substrate. Excitations and deformations of the substrate may occur upon adsorption.

(6) Heterogeneity. Variation of the substrate due to imperfections or differing species.

The models in this thesis basically encompass descriptions three and four when adsorption onto the substrate is irreversible with no, or limited mobility. The microscopic dynamics of the process are incorporated in the rates. An Arrhenius form of the rates is appropriate when the adatom distribution depends primarily on the activation energies. Other rate descriptions are needed when more complex events occur. For example, in the case of irreversible island formation the rates for island addition could be enhanced (compared to the rate for adsorption on a bare portion of the substrate) by a mobile precursor "bumping into" or "falling off of" the islands. See Figure 6.1. Invariably it is to be expected that the rates are significantly affected by adatom interactions.

LeBosse et al. (64) have identified four kinds of interactions between identical chemisorbed adatoms. They are (1) direct bonding, (2) indirect bonding, (3) dipole interactions and (4) deformation interactions. The first two interactions involve electron sharing, the first directly between adatoms and the second through the substrate. The third interaction deals with electrostatic forces created by the adatoms and their screening charge on the substrate. The fourth kind of interaction is due to elastic distortion of the substrate by adatoms. Lopez and Allan (65) have discussed deformation interactions in the

Figure 6.1. Enhancement (compared to adsorption on a bare lattice) of island formation by "bumping into" or "falling off of" the islands

oxygen-nickel system and concluded that the effect of this last interaction is small. LeBosse et al. (64) point out that the relative importance of the first three types of interactions depends on the distance of the adatoms from each other and their ionic character. For long distances and neutral adatoms indirect interactions are dominant but, for long distances and ionic adatoms, dipole interactions are most important. For very short distances, independent of the ionic character, direct coupling dominates. Intermediate distances require each case to be individually determined.

As pointed out by Lundqvist et al. (66) a comprehensive theory of adsorption processes should incorporate all of these effects and use a complete description of the surface; but, due to the many complexities of this problem, only the essential characteristics of the process are retained in practical models.

6.1. Surface Processes Requiring Irreversible Models

Some surface processes have irreversible, immobile character and require irreversible kinetic modeling as previously discussed. Such processes are <u>not</u> correctly described by an equilibrium model (67). Below is a list of some of these processes:

(1) <u>Ammonia adsorbed onto γ-alumina (68)</u>. At 50° ammonia adsorbed onto γ-alumina is immoble and will form nonequilibrium adsorbate configurations.

(2) Dehydration of wet γ-alumina oxide (5). Dehydration of wet γ-alumina oxide (see Figure 1.4) takes place in an irreversible, immobile manner for temperatures less than 600°C.

(3) Adsorption of oxygen on a stepped platinum surface (69). The saturation coverage of oxygen adsorbed onto the step, inside edge sites is approximately constant over a broad temperature range. This indicates that the oxygen atoms chemisorbed on these sites are immobile.

(4) Chemisorption of CO on the (210) face of tungsten (70). The chemisorption of CO on the (210) face of tungsten is immobile below 700°K. For chemisorption with both oxygen and carbon in contact with the surface cooperative effects are also present, manifested by a β_1 state which has an occupied n.n. and a more strongly bound β_2 state when n.n. are unoccupied.

(5) Coadsorption of CO and oxygen on the (100) face of tungsten (71). Three β states (two surface sites occupied) and one weekly bound α state (one surface site occupied) are observed for CO coadsorbed with oxygen on the (100) face of tungsten. Sequential filling of these states has been demonstrated. Separate studies (72) show that β-CO is immobile below 600°K on this crystal surface.

(6) Chemisorption of nitrogen on the (100) face of tungsten (73). The next section discusses the chemisorption of nitrogen on the (100) face of tungsten in some detail and shows that an exploration of this process requires an irreversible cooperative model.

6.2. Chemisorption of N_2 onto W(100)

The nitrogen-tungsten system has been extensively studied (3, 73,74-77). In a very thorough discussion by King and Wells (73), it was pointed out that this system is well-suited for analysis because the dissociatively chemisorbed (β) state is formed with a large heat of adsorption compared to the physisorbed and molecularly chemisorbed states. As a result the β state can be assumed not to desorb during the formation of the adlayer. The physisorbed precursor state is expected to exist at very low concentration on the surface. The (100) face of tungsten is also well-characterized making this system a good candidate for theoretical analysis.

6.2.1. Characterization of the process

The basic assumptions used by King and Wells to describe this system are:

(1) The accommodation coefficient, which gives the probability of a molecule incident on the surface being physisorbed, is independent of adlayer coverage and crystal temperature.

(2) A physisorbed molecule can (a) dissociatively chemisorb over a pair of empty nearest neighbor adatom sites, or, (b) hop to a different physisorption site, or, (c) be scattered back into the gas phase. The rates of (b) and (c) depend on whether or not the physisorbed molecule is over filled or empty sites on the lattice.

(3) At all coverages the adatoms in the chemisorbed layer occupy identical sites on the substrate. At temperatures below about 650 K the adatoms in the β overlayer are immobile. Adatom penetration of the substrate and reconstruction of the substrate are precluded.

(4) Newly formed adatoms are mobile because they have excess energy due to the exothermicity of the chemisorption reaction. These "hot" adatoms can hop between adatom sites until they lose sufficient energy to become immobily attached to a particular adatom site.

(5) Surface hopping of the "hot" adatoms leads to a distribution of adatoms on chemisorption sites which is of equilibrium form. Thus P(oo), which is significant in the sticking coefficient expression, can be obtained from an equilibrium Ising model. This quantity is assumed to be determined by a pairwise interaction energy between n.n. adatoms which is strongly repulsive.

The salient experimental facts in support of this model are (73):

(1) Only the accommodation coefficient is affected by the gas temperature. This supports the supposition that the precursor state to the chemisorbed state is a physisorbed state which is energy accommodated with the surface.

(2) Experimentally the accommodation coefficient is independent of surface coverage.

(3) There is very strong evidence, both in the work of King and Wells and that of other investigators (78), that the chemisorbed adlayer is immobile below about 650K on a reasonable time scale of experiment. Above that temperature it becomes increasingly mobile and desorption from the adlayer becomes appreciable above 1000K.

(4) The adlayer "saturates" when the density of the adlayer is equal to about 60% of the surface density of tungsten atoms in the (100) plane. Evidence from LEED indicates that the adlayer is partially ordered in a c(2×2) pattern (75,79). If it is assumed that the number of chemisorption sites is the same as the number of tungsten atoms in the (100) plane (80), then these data suggest that the β state is dissociatively adsorbed and that newly formed adatoms are somewhat mobile.

(5) In desorption experiments, two peaks associated with the β state are observed (67,81). Based on this fact, it is reasonable to assume that adatoms without n.n. are more difficult to desorb than those having n.n.

The King and Wells model is reasonable in most regards and is in good agreement with experiment. However, in that the model assumes an equilibrium spatial distribution of adatoms, it is not physical. If the adatoms are immobile when energy accommodated with the surface, then there is no obvious mechanism for achieving an equilbrium spatial distribution in the adlayer. The experimental evidence is that no such mechanism exists since if f(2), which is discussed in the next section with regard to the sticking coefficient, were an equilibrium quantity

it would be a rather sensitive function of crystal temperature under the assumed condition of strong interaction between adjoining adatoms. However, King and Wells find that, experimentally, it is sensibly independent of temperature over a large temperature range.

As further evidence that f(2) is not an equilibrium property, note that the adlayer seems to saturate (i.e., f(2)=0) at a surface coverage of about 60%. For an equilibrium model with a finite lateral interaction energy, the surface truly saturates only at $\theta=1$, and the point at which saturation is "effectively" complete is somewhat arbitrary, but definitely much higher than 60%. Thus, at very low sticking probability the experimental sticking coefficient curve does not agree with the equilibrium prediction.

Finally, it should be noted that the equilibrium expression for f(oo) used by King and Wells implies that the quantity $f(2)+\theta$, as a function of θ, is symmetric about $\theta=\frac{1}{2}$. However, this quantity, as obtained by fitting the sticking coefficient equation (Equation 6.2.2.1) to experiment, does not exhibit this symmetry.

As indicated above, the experimental observable that may also be theoretically derived is the sticking coefficient. An expression for the sticking coefficient has been previously derived (3) as

$$S(\theta) = S(0)[1+K(1/f(2)-1)]^{-1} \qquad (6.1)$$

where $K=K_d'/(K_c+K_d)$. The constants K_d', K_c and K_d are the rate constants for desorption over a filled or partially filled site, for chemisorption and for desorption over a bare site on the lattice respectively. This

equation was also obtained by Tamm and Schmidt (82) for an adsorption model via a precursor state. Clavenna and Schmidt (77) point out that this equation also follows from the Kisliuk model (83) for random two site adsorption in the limit $K_d = K'_d$.

The concentration dependence of the sticking coefficient arises from the function f(2). The experimental evidence suggests that the formation of n.n. adatom pairs is strongly disfavored. However, since the adlayer saturates at $\theta > \frac{1}{2}$ there must be some disorder in the adlayer. To account for this disorder, King and Wells assume that the adatoms have an equilibrium distribution on the lattice which is governed by a large, but finite, repulsive interaction between n.n. pairs. If this model is correct then the disorder in the adlayer arises from entropic considerations and should therefore increase with increasing crystal temperature. Thus, f(2) should be a function of the temperature of the solid and the saturation coverage should increase with temperature. These predictions are not in agreement with experiment.

For a process with strongly repulsive n.n. interactions, filling in stages will occur as discussed in Section 3.2. In the current system, hot adatoms will first land on sites with no n.n. Since $f(xx) \cong 0$, it follows from conservation of probability that

$$f(2) = 1 - 2\theta \tag{6.2}$$

during this first stage. At some point in the process, all adsorption

sites which have all empty n.n. sites will be gone but empty sites with at least one empty n.n. will remain. Under the assumed mechanism, dissociation can continue to occur because neighboring pairs of empty sites exist (i.e., $f(2)\neq 0$). Since the adatoms which are energy accommodated with the surface are immobile, new adatoms formed must accept sites which have at least one n.n. and f(xx) will no longer remain zero. (This is in contrast to the infinite interaction equilibrium case where the adlayer can simply reorder to keep adatoms apart.) The chemisorption process will continue until $f(2)=0$. Thus, as an inherent feature of the nonequilibrium nature of ordered adlayer formation, the sticking coefficient vanishes and the adlayer saturates at a covering fraction greater than $\theta=\frac{1}{2}$. This result is not dimensionally dependent.

According to the model, the final step which determines the adatom distribution is the loss of energy of the hot adatoms to the lattice which makes them immobily attached to the surface. There is no mechanism by which the immobile adatoms can become spatially equilibrated and hence an equilibrium model for their distribution is basically untenable.

6.2.2. 1-D model and comparison with experiment

The 1-D model with n.n. repulsive cooperative effects incorporates the basic features of the general treatment, yet allows a simplified investigation of the nature of the adlayer disorder and its consequences. The necessary equations are given in Chapter two and the ordered filling limit, which is pertinent here, is described in Section 3.2. By

employing this model, it is tacitly assumed that the rate constants have no "memory" of when adatoms in the environment were immobily fixed. This is consistent with a small hot adatom concentration and rapid equilibration of newly frozen adatoms with the surface.

The relationship between f(2) and θ in the repulsive limit is (see Section 3.2)

$$f(2) = 1 - 2\theta, \quad 0 \leq \theta \leq \theta^*(1) = (1-e^{-2})/2 = 0.432, \quad \text{(filling with no n.n.)},$$

$$= 1 - \theta^*(1) - \theta, \quad \theta^*(1) \leq \theta \leq \theta^*(2) = (1+e^{-2})/2 = 0.568, \quad \text{(filling with one n.n.)},$$

$$= 0, \qquad \theta^*(2) \leq \theta \leq 1, \quad \text{(filling with two n.n.)} \; . \qquad (6.3)$$

In Figure 6.2, the relative sticking coefficient, $S(\theta)/S(0)$, is given for the (100) face of tungsten at a crystal temperature of 300K. The data points are experimental values taken from the work of King and Wells (73). The values of θ have been calculated on the assumption that the density of adsorption sites is equal to the surface density of tungsten in the (100) plane. The solid curve is theoretically derived from Equation 6.1 using the nonequilibrium functional form for f(2) of Equation 6.2. It has one adjustable parameter, k=0.09. The discontinuous slope in the curve results from the face that it was obtained by determining f(2) in the repulsive interaction limit. For small deviations from this limit, the curve is smooth. The dashed curve is the theoretical result given by King and Wells. It is obtained from Equation 6.1 using the equilibrium functional form for f(2) as obtained from the Ising model in the Bethe approximation (50). In this case,

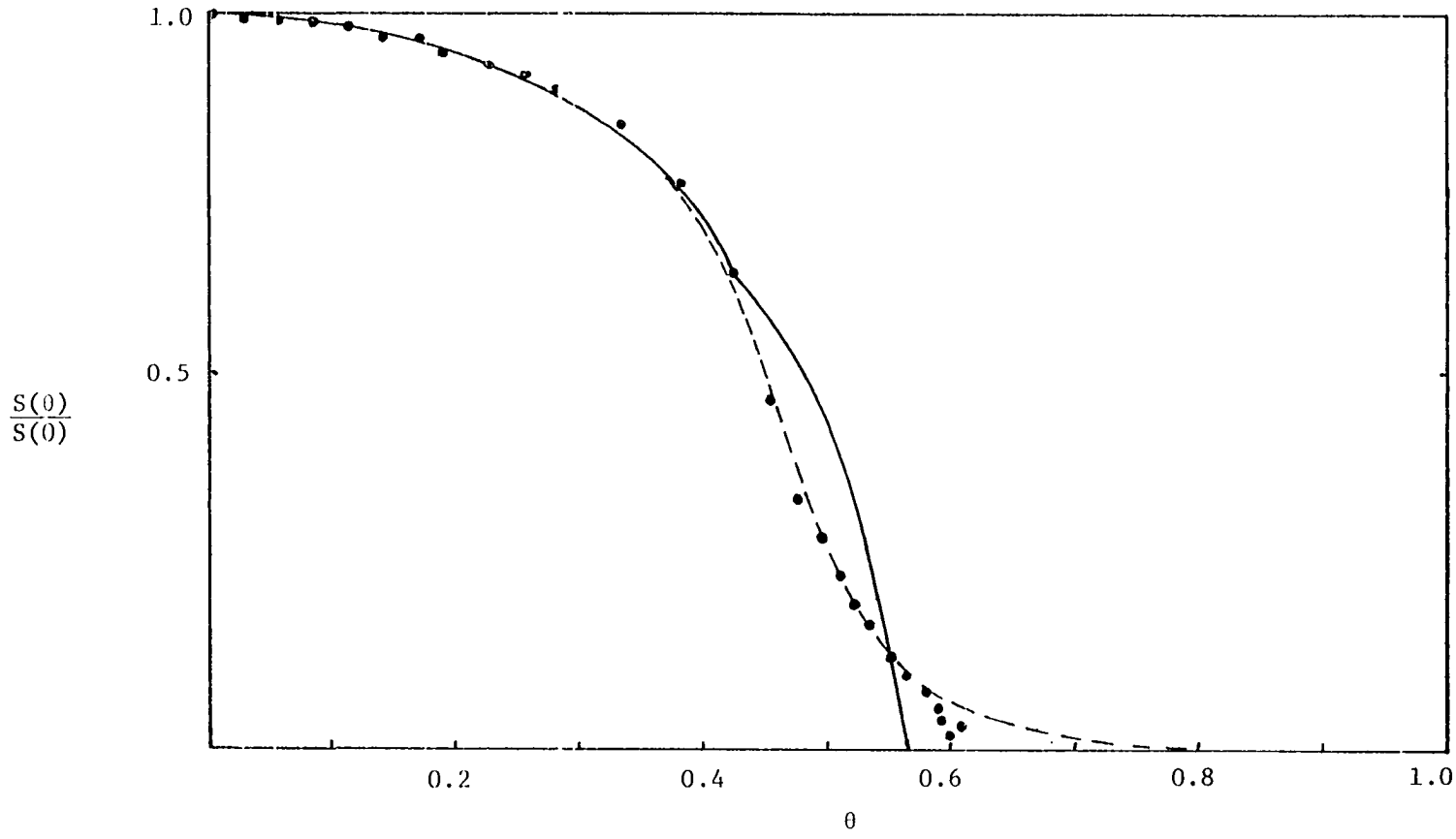

Figure 6.2. The relative sticking coefficient for nitrogen on the (100) face of tungsten at a crystal temperature of 300°K. The data points were experimentally determined by King and Wells (73)

$$f(2) = 1-\theta-2\theta(1-\theta)/\{[1+4\theta(1-\theta)B(T_s)]^{\frac{1}{2}}+1\} \qquad (6.4)$$

where $B(T_s)=\exp(-\omega/kT_s)-1$ and ω is the repulsive interaction energy between n.n. adatoms. King and Wells gave the sticking coefficient as a function of a "sealed" density $\theta'=\gamma\theta$. Thus, the dashed curve of Figure 6.2.2.2 depends on three adjustable parameters, K=0.083, γ=1.05 and B=0.989 where B is the ordering parameter of Equation 6.4.

The figure shows that the equilibrium expression for the sticking coefficient (dashed curve) does not have the saturation behavior exhibited by the experimental points. This, and the fact that the equilibrium expression for f(2) of Equation 6.4 is dependent on the crystal temperature, are two of the principal objections to the equilibrium mode. The nonequilibrium expression for $S(\theta)/S(0)$ (solid curve) does not suffer from these deficiencies since it is based on a temperature independent expression for f(2) and predicts a definite saturation value in the repulsive interaction limit. An effective saturation near this limiting value is also found for a range of strong repulsive interactions. Both of these features are consequences of our general theoretical treatment and are not limited to the 1-D model. The saturation value $\theta_{sat}=\theta^*(2)=(1+e^{-2})/2=0.568$ is independent of any adjustable parameter and is about 5% less than the apparent experimental saturation covering fraction.

In Figure 6.3, the function $f(2)+\theta$ is given as calculated from Equation 6.3 (solid curve) and from Equation 6.4 (dashed curve). The latter has been computed using a value of B=0.989. As previously

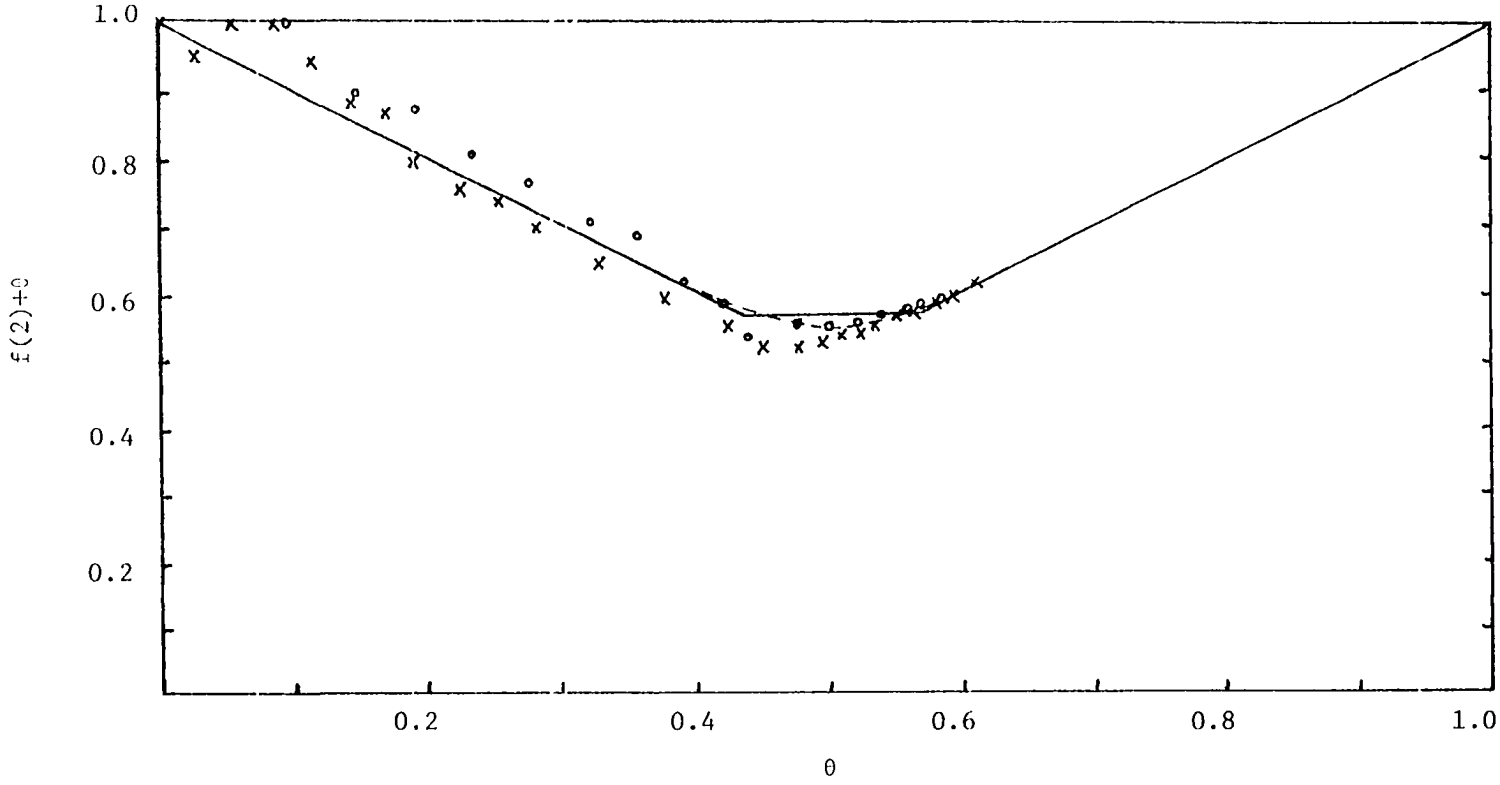

Figure 6.3. f(2)+0 as a function of θ. The theoretical irreversible (——) and equilibrium (----) curves are obtained from Equation 6.3 and 6.4, respectively. The data points are taken from King and Wells (73) and are for temperatures of 300°K (x) and 433°K (o)

mentioned, although the quantity B is theoretically a function of T_s, King and Wells treat it as an adjustable parameter to be determined at each temperature. They found that the constant value of 0.989 fit the data well at all temperatures. Experimental points are also given in Figure 6.3 which have been obtained by inverting Equation 6.4 using sticking coefficient data reported by King and Wells for the crystal temperatures 300 and 433K. These are the two temperatures which the investigators used that lie well below the temperature of adatom mobility (which is somewhere in the range 650 to 750K (65,79)).

Even allowing for the scatter in the experimental points, at low values of θ the apparent slope of $f(2)+\theta$ appears to be less (i.e., a greater negative number) than the theoretical limiting slope of -1. This can be easily rationalized by noting that K in Equation 6.1 is assumed constant. It is reasonable to assume that the rate of the initial chemisorption mechanistic step over a pair of empty sites decreases with increasing surface coverage due to the repulsive interaction of n.n. adatoms. Such an effect would cause K to increase with θ. Only a very slight dependence of K on θ of this kind is required to correct the difficulty cited above and to increase the agreement of theory and experiment significantly in the low θ region.

After accounting for the θ dependence of K, it is still evident that the experimental data is asymmetric while the theoretical models predict symmetry about θ=.5. No explanation for this asymmetry is available from the equilibrium model. However, the following simple

extensions of the basic irreversible model described above do lead to asymmetry:

(1) Relaxation of repulsive n.n. limit. As shown in Section 3.2.3, a perturbation from the repulsive n.n. limit causes asymmetry. Furthermore, $\theta_{min} < \frac{1}{2}$ as required in this case, see Figure 3.12 for an illustration of this effect. Suppose, for the nitrogen on tungsten system being discussed, we may estimate the rates by assuming an Arrhenius form and describing the activation energy by the equilibrium interaction energy. Using the value of ω=0.989 given by King and Wells for the interaction energy results in a plot very close to the infinite interaction limit, thus justifying the analysis just given. We conclude that the experimentally observed asymmetry is not due to relaxation of the repulsive n.n. limit.

(2) Spatial correlations of hot adatoms due to limited mobility. No correlation is assumed between hot adatoms (this is reflected in the source term of the hierarchy). In particular, the possible spatial correlation of hot adatoms which were initially partners in the undissociated molecule has been ignored. Another way to state this assumption, is to say that each adatom is mobile for a time sufficiently long so that it can find an optimum site to immobily chemisorb onto in the adlayer. This ignores the fact that hot adatoms are formed in pairs and it becomes increasingly difficult for both adatoms to find favored sites as the adlayer fills. This spatial correlation of adatom pairs breaks the symmetry of $f(2)+\theta$ as a function of θ. This break in the symmetry may be understood by considering the filling process in the

second stage of filling. During that stage, dimers land on a pair of sites flanked on both sides by occupied sites. According to the theoretical model, the molecule dissociates into two hot adatoms each one then finding sites with only one occupied n.n. For this process, $f(2)$ falls off with a slope of -1 and $f(2)+\theta$ has slope zero (both as functions of θ). As the lattice fills, however, it may physically become more difficult for both adatoms to find sites with only one n.n. occupied site. For the sake of argument, suppose none of the adatoms can migrate sufficiently far to find a second pair of empty sites, then the adsorption of two adatoms will destroy only one pair of empty adjacent sites causing $f(2)$ to fall off with slope $-\frac{1}{2}$ and $f(2)+\theta$ to have a slope of $\frac{1}{2}$. Figure 6.4 illustrates this effect. The true effect is, of course, intermediate between these limits.

Another model which gives qualitatively similar results was presented in Section 3.7. That model predicts asymmetry in the function $f(2)+\theta$ as illustrated in Figure 3.25 for the 1-D, R=1 and d=1 case (infinite repulsion limit).

The experimental evidence suggests that the nitrogen adatoms are in a $c(2\times2)$ pattern on the tungsten surface. This indicates an attractive second n.n. cooperative effect as well as a n.n. repulsion. The effects of an attractive second n.n. in the 1-D irreversible model have been discussed in Section 3.1. This effect, by itself, retains the symmetry of $f(2)+\theta$, but makes the second stage shorter. This moves $\theta^*(1)$ to the right which is in agreement with the experimental data.

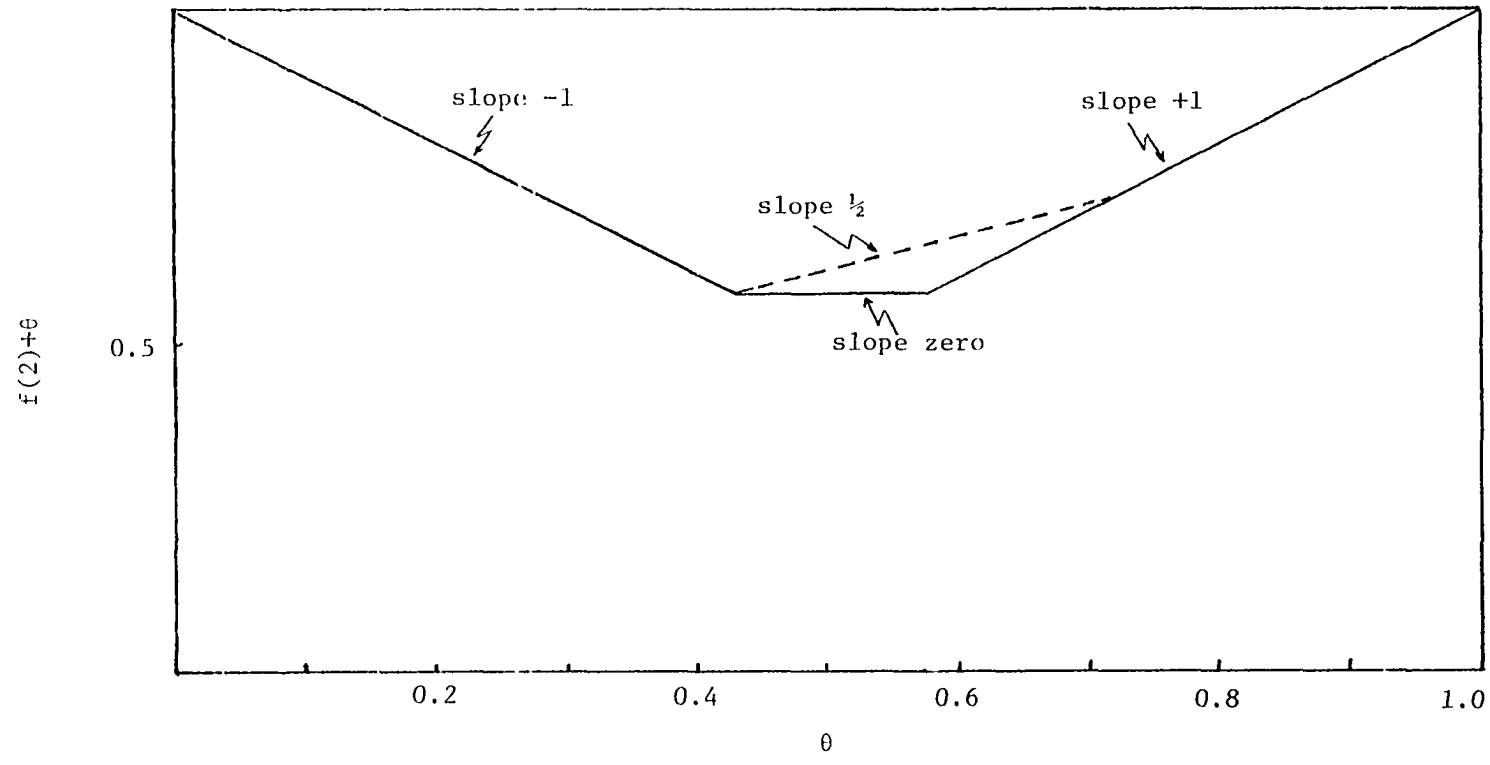

Figure 6.4. f(2)+θ as a function of θ. The solid curve is calculated from Equation 6.3 and the dashed curve is calculated as described in the text. The two curves coincide except in the middle region

It is, of course, possible that all of these effects are occurring in varying degrees and combining to create the experimentally observed behavior. It is true, however, that a 1-D model, even with all of these effects considered, should not be expected to completely describe a 2-D process. At the same time, many of the concepts used in the 1-D model carry over to 2-D and so the same qualitative effects should be observed.

6.2.3. 2-D model

The adlayer adsorption sites on the (100) face of tungsten are in a square lattice geometry, and the most obvious extension of the theory would be to incorporate this geometry into the model. As discussed in Chapter two, the 2-D kinetic equations are not exactly soluble. It is, however, possible to discuss the behavior of f(2) in the repulsive interaction limit (the analogue of the case treated in Chapter four). Table 6.1 describes the filling process for highly repulsive n.n. cooperative effects (the site indicated by • is being filled).

Table 6.1. Filling in stages on a 2-D square lattice for $R^1=R^2=1$

1st stage:	$\overset{o}{o}\bullet\underset{o}{o}$	$d/d\theta\ f(2) = -2$
2nd stage:	$\overset{o}{o}\bullet\underset{x}{o}$	$= -3/2$
3rd stage:	$\overset{o}{o}\bullet\underset{x}{x}$ or $\overset{x}{o}\bullet\underset{x}{o}$	$= -1$
4th stage:	$\overset{o}{x}\bullet\underset{x}{x}$	$= -1/2$
5th stage:	$\overset{x}{x}\bullet\underset{x}{x}$	$= 0$

Both the 1-D model and the 2-D square lattice model exhibit an initial stage with $d/d\theta\ f(oo)=-2$. This is in agreement with experiment, but the detailed behavior of later stages is not. A more realistic model for the adsorption process is described below.

It is clear that the first stage of filling involves occupation of sites with no filled n.n. as assumed above (and leading to $d/d\theta\ f(oo)=-2$). However, experimental observation of a C(2×2) structure indicates that adsorption is enhanced if a diagonal n.n. is occupied (no doubt in part due to an attractive diagonal n.n. interaction). Thus, the end of the first stage should be changed from the previous value of $\theta=0.37$ (for random filling with n.n. blocking) to a somewhat higher value, less than $\theta=0.5$, due to more ordered filling. A horizontal and/or vertical enhancement of rates for second n.n. filled also produces this type of shift (as seen by the previous 1-D analogous case). At $\theta\cong0.475$ the islands have grown together leaving only sites with at least one n.n. occupied. Figure 6.5 illustrates the basic configurations along the island boundaries.

The second "stage" of filling is much more complex and can be associated with a variety of mechanisms. The nitrogen molecules dissociate in the channels on remaining pairs of adjacent empty sites between the islands. If the hot adatoms are uncorrelated, the slope of $d/d\theta\ (f(2)+\theta)$ for adsorption with one filled n.n. in the straight (Figure 6.5b) and "zig-zag" (Figure 6.5c) configurations will be -0.5 and zero, respectively. These are both low compared to the experimental value of approximately 0.6. If the hot adatoms remain correlated after

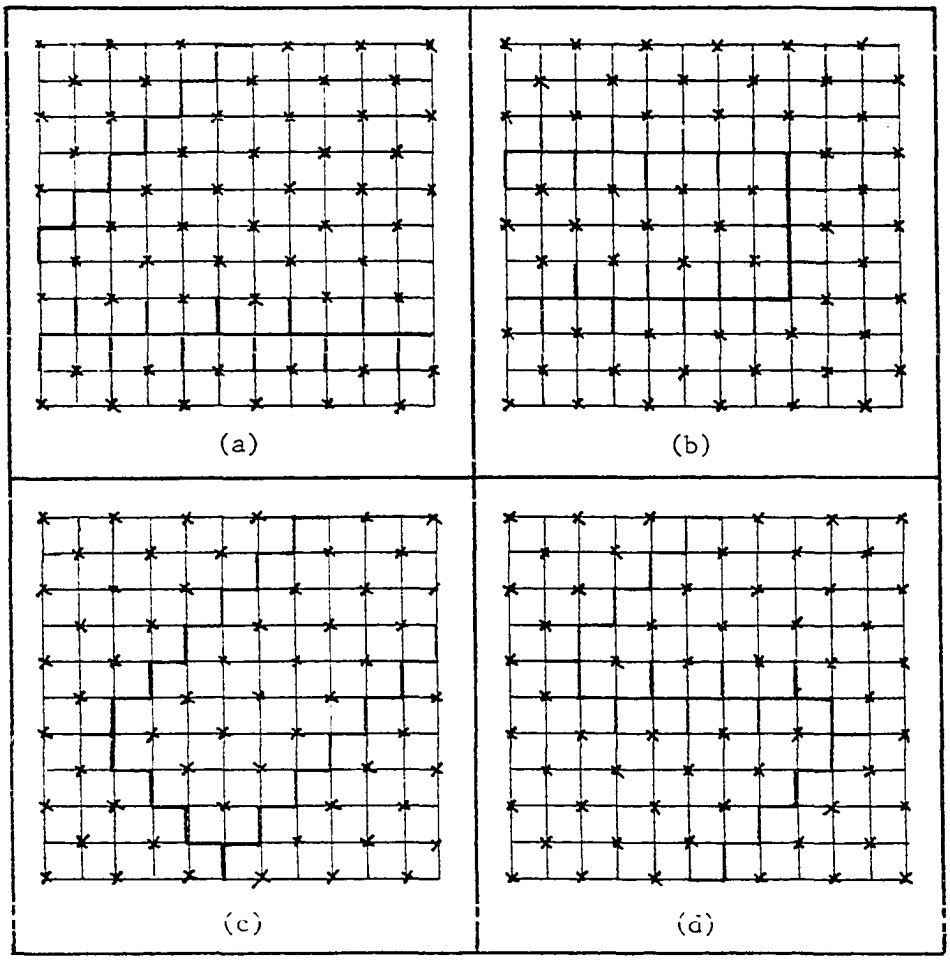

Figure 6.5. Basic configurations along island boundaries

dissociation, the slopes for landing on these sites are -0.25 and 0.25 respectively, more in agreement with experiment. Another possibility is infiltration of hot adatoms into interior sites near the channels. This would not destroy any empty site pairs and thus give $d/d\theta(f(2)+\theta)=1$. Infiltration to interior sites can occur during this process since (a) the hot adatoms would not need to jump over other adsorbed adatoms (they could go diagonally to the desired site) and (b) the tendency for hot adatoms to separate could provide the needed energy for this diagonal movement. A mixture of adatom correlation and infiltration can account for the experimental data, but more detailed study is required to enable an authoritative desorption to be given for the mechanism of this process during the second "stage".

7. APPLICATION TO CRYSTALLINE SOLIDS

The importance of irreversibility has not been fully investigated in many physical processes. In Chapters five and six, some one and two dimensional examples, respectively have been described. There are also, of course, three dimensional processes that occur irreversibly and require the kind of modeling developed in this thesis. Some examples are now given from various areas of chemistry and physics.

(1) Solid state photochemistry. Solid state photochemistry provides many examples of irreversible processes (84). Elgavi et al. (85) give two typical irreversible photochemical processes where the original crystal is composed of monomer units, but upon irradiation bonds are formed between these are shown in Figure 7.1.

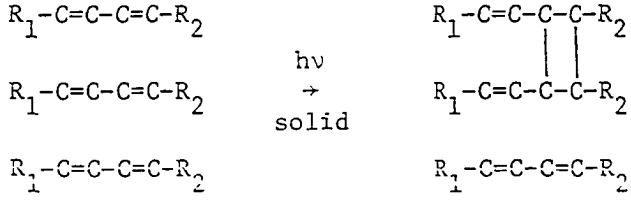

Figure 7.1. Solid State Photodimerization of (a) R_1=2,6-$C_6H_3Cl_2$, R_2=Ph and (b) R_1=2,6-$C_6H_3Cl_2$, R_2=2-thienyl (85)

These solid state, lattice controlled, photocycloaddition reactions take place irreversibly and require models similar to those discussed throughout this thesis. The reactions given in Figure 7.1 can be modeled as random dimer processes. The packing diagram for these crystals is just that shown in Figure 7.1 (85). There is, of course, a 3-D network of the monomer units, but, in these cases, the only distances short enough

for dimerization to occur are along these stack planes (one of which is shown in Figure 7.1). Further, these particular reactions are steriospecific, allowing rings to form next to R_2 groups only. This suggests that the process is really one dimensional along the stack plane (next to the R_2 groups). The experimental work (86) for (a) in Figure 7.1 indicated yields of 80% compared to the theoretically predicted 86% (of Chapter five) for the random dimer model.

When R_1 and R_2 in Figure 7.1 are small groups (e.g., methyl) it is possible for interstack distances to allow dimers to form (87). These reaction, in general, can take place next to either the R_1 or the R_2 groups (separation of the bonds to form eight membered rings apparently seldom occurs (87)) and, therefore, require 3-D models.

The processes discussed above could be monitored using x-ray diffraction techniques since the dimer rings will diffract differently than the monomer units. The short range order (SRO) intensity in terms of the correlation function $C(o\xrightarrow{\underline{r}}o)$ (see Chapter three), for an N-site lattice in which all sites have the same number of neighbors and each site is initially in condition A and then transformed to condition B (with scattering factors f_A and f_B, respectively) is (88)

$$I_{SRO}/N(f_A-f_B)^2 = \sum_{\underline{r}} C(o\xrightarrow{\underline{r}}o)\cos[-2\pi\underline{r}\cdot(s-s_o)/\lambda] \qquad (7.1)$$

where the unit vectors $\hat{s}$ and $\hat{s}_o$ indicate the final and initial direction for the x-radiation and λ is its wavelength.

As an example, the exact 1-D results previously derived in Chapter three are now used to evaluate the 1-D x-ray SRO intensity for a binary

(A→B) system. In 1-D, Equation 7.1 simplifies to

$$I_{SRO}/N(f_A-f_B)^2 = \sum_{j=0}^{\infty} C(o\underline{\underline{j\ell}}o) \cos(4\pi j\ell/\lambda) \ , \qquad (7.2)$$

where ℓ is the lattice spacing. If ℓ is a multiple of λ, the cosine of Equation 7.2 is one and the maximum intensity is obtained. The ratio ℓ/λ is the only variable in the 1-D case for scatterers A and B for a particular choice of cooperative effects. Figure 7.2 shows the irreversible for highly inhibitory and the corresponding highly repulsive equilibrium values of $I_{SRO}/N(f_A-f_B)^2$ as a function of θ. Another method for treating the SRO intensity, using a density expansion technique developed by Hoffman (47), is outlined in Appendix B.

(2) Order-order transformations. Titanium undergoes an order-order transition from a body centered cubic (β) structure to a hexagonal close packed (α) structure at approximately 850°C (89). Water quenching from above 850°C results in wedge-shaped crystals of the α type (90). Nishiyama et al. (90) show that certain boundaries must be completely due to the tranformation process and can not exist in thermal equilibrium. We assume these boundaries are the interfaces between islands that have grown together. This kind of process is described by Equation 1.1 as shown in Chapter three and four.

Hardening of steels, usually accomplished by relatively rapid cooling (quenching), is an important industrial process which often occurs through an order-order transformation (e.g., face centered cubic

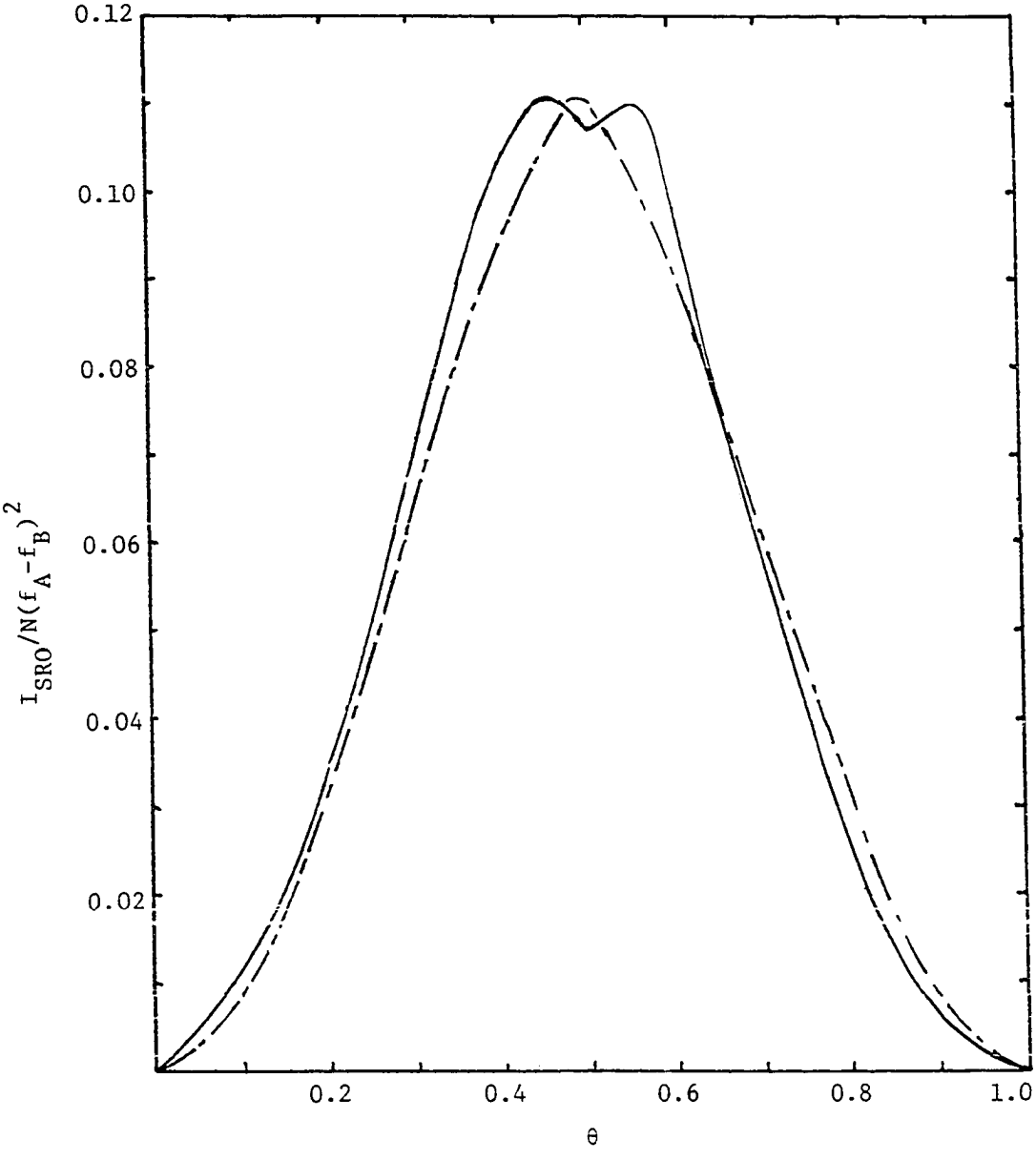

Figure 7.2. 1-D short range order intensity as a function of θ for irreversible (——) and equilibrium (—— - ——) processes for highly inhibitory n.n. ($\tau_{o\cdot x}$=0.01)

austenite transforms to body centered cubic martensite when the carbon content is less than .25% (91,92). These diffusionless Martensitic transformations (transformations that occur by cooperative atomic movements) have been called Shōgidaoshi, a Japanese word meaning "falling one after another in succession" (92). These processes are, also, island building processes and should be modeled in a manner similar to that described in Chapters three and four since the time scale for equilibration is much longer than allowed during quenching. Given the relative rates for initialization and propagation of the process, such a model could, predict the island size and shape distribution.

(3) Disorder-order transformations. Disorder-order transformations also display irreversible character under certain conditions (93). For example, Jaumet and Sutcliffe (94), working with Cu-Au alloys between 15.5 and 34.2 atomic percent gold, say that "incredibly long times" are required to attain thermal equilibrium. If the rate of cooling is fast compared to the rate of transformation, the process will not be able to equilibrate. For example, the quenching and subsequent isothermal transformation of Cu_3Au (95) at the final temperature, has two stages. The first, very fast, stage is associated with development of short range order only (a sort of island formation), while the second slower stage apparently corresponds to development of the long range order (93).

Another process of this type is illustrated by the cooling of carbon monoxide to low temperatures. Carbon monoxide does not orient itself in the most favorable way upon crystallization due to its small dipole

moment. When cooled, the lowest energy state is not realized because the molecules get locked into the original configuration (96). This manifests itself in the entropy at very low temperatures (zero point entropy). For a completely random choice, the difference from perfect order is $R \ln 2 = 1.38$ e.u. The observed change is 1.1 e.u. (96,97), indicating that some ordering has occurred. Quantitative study of this kind of irreversible ordering presumably also requires models of the kind developed in this thesis.

8. LITERATURE CITED

1. P. J. Flory, J. Amer. Chem. Soc. 61 (1939) 1518.
2. N. O. Wolf, Ph.D. thesis, Iowa State University, 1979.
3. N. O. Wolf, D. R. Burgess and D. K. Hoffman, Surface Science 100 (1980) 453.
4. I. R. Epstein, Biophysical Chemistry 8 (1978) 327.
5. J. B. Peri, J. Phys. Chem. 69 (1965) 220.
6. E. R. Cohen and H. Reiss, J. Chem. Phys. 38 (1963) 680.
7. E. S. Page, J. Roy. Stat. Soc. B 21 (1959) 364.
8. R. B. McQuistan and D. Lichtman, J. Math. Phys. 9 (1968) 1680.
9. B. Widom, J. Chem. Phys. 58 (1973) 4043.
10. T. H. K. Barron and E. A. Boucher, Trans. Far. Soc. 65 (1969) 3301.
11. F. Downton, J. Roy. Stat. Soc. B 23 (1961) 207.
12. W. H. Olson, J. Appl. Prob. 15 (1978) 835.
13. E. A. Boucher, J. Chem. Phys. 59 (1973) 3848.
14. M. Gordon and I. H. Hillier, J. Chem. Phys. 38 (1963) 1376.
15. E. A. Boucher, Faraday Trans. II 69 (1973) 1839.
16. J. K. MacKenzie, J. Chem. Phys. 37 (1962) 723.
17. J. B. Keller, J. Phys. Chem. 37 (1962) 2584.
18. T. Alfrey, Jr. and W. G. Lloyd, J. Chem. Phys. 38 (1963) 318.
19. C. B. Arends, J. Chem. Phys. 38 (1963) 322.
20. J. B. Keller, J. Chem. Phys. 38 (1963) 325.
21. D. A. McQuarrie, J. P. McTague and H. Reiss, Biopolymers 3 (1965) 657.
22. B. H. Zimm and J. K. Bragg, J. Chem. Phys. 31 (1959) 526.

23. G. Schwartz, Ber. Bunsen-ges. Phys. Chem. 75 (1971) 40.

24. R. Kikuchi, Ann. Physics 10 (1960) 127.

25. N. Gō, J. Phys. Soc. Jap. 22 (1967) 413.

26. E. A. Boucher, Chem. Phys. Lett. 17 (1972) 221.

27. J. J. Gonzalez, P. C. Hemmer and J. S. Høye, J. Chem. Phys. 3 (1974) 228.

28. E. Klesper, A. Johnsen and W. Gronski, Makromol. Chem. 160 (1972) 167.

29. J. J. Gonzalez and K. W. Kehr, Macromolecules 11 (1978) 996.

30. B. U. Felderhof, J. Stat. Phys. 6 (1972) 21.

31. T. H. K. Barron, R. J. Bawden and E. A. Boucher, J. Chem. Soc. 70 (1974) 651.

32. N. A. Platé, A. D. Litmanovich, O. V. Noah, A. L. Toom and N. B. Vasilyev, J. Polym. Sci. Polym. Chem. Ed. 12 (1974) 2165.

33. N. A. Platé, A. D. Litmanovich and O. V. Noah, Macromolecules 12 (1979) 1230.

34. P. C. Hemmer and J. J. Gonzalez, J. Polym. Sci. Polym. Phys. Ed. 15 (1977) 321.

35. J. J. Gonzalez and P. C. Hemmer, J. Polym. Sci. Polym. Lett. Ed. 14 (1976) 645.

36. J. J. Gonzalez and P. C. Hemmer, J. Chem. Phys. 67 (1977) 2496.

37. J. J. Gonzalex and P. C. Hemmer, J. Chem. Phys. 67 (1977) 2509.

38. J. J. Gonzalez, Macromolecules 11 (1978) 1074.

39. I. R. Epstein, Biopolymers 18 (1979) 765.

40. A. Rényi, Magyar Tudományos Akad. Mat. Kutató Int. Közleményi 3 (1958) 109, also in Selected Transl. Math. Stat. Prob. 4 (1963) 205.

41. J. B. Peri, J. Phys. Chem. 69 (1965) 220.

42. D. R. Rossington and R. Borst, Surface Science 3 (1965) 202.

43. K. J. Vette, T. W. Orent, D. K. Hoffman and R. S. Hansen, J. Chem. Phys. 60 (1974) 4854.

44. B. E. Blaisdell and H. Solomon, J. Appl. Prob. 7 (1970) 667.

45. I. Palasti, Prbl. Math. Inst. Hung. Acad. Sci. 5 (1960) 353.

46. J. L. Jackson and E. W. Montroll, J. Chem. Phys. 28 (1958) 1101.

47. D. K. Hoffman, J. Chem. Phys. 65 (1976) 95.

48. J. W. Evans, D. R. Burgess, N. O. Wolf and D. K. Hoffman, "Random and Cooperative Irreversible Processes on Lattices. I. General Theory", preprint.

49. M. Abramowitz and I. A. Stegun, Handbook of Mathematical Functions (Dover Publications, Inc., New York, 1964).

50. I. S. Gradshteyn and I. M. Ryzhik, Table of Integrals, Series, and Products (Academic Press, New York, 1965).

51. R. Fowler and E. A. Guggenheim, Statistical Thermodynamics (Cambridge University Press, London, 1965).

52. K. Kita, Y. Inaki and K. Takemoto, J. Polym. Sci. PC 18 (1980) 427.

53. Y. Nakanishi, J. Polym. Sci. PC 13 (1975) 1223.

54. H. Hiraoka, E. Gipstein, J. Bargon and L. W. Welsh, Jr., J. Appl. Polym. Sci. 22 (1978) 3397.

55. M. Tanaka, F. Nishimura and T. Shono, Anal. Chim. Acta 74 (1975) 119.

56. H. Kawabe, B. Chem. Soc. J. 48 (1975) 2357.

57. R. M. Fuoss, M. Watanabe and B. D. Coleman, J. Polym. Sci. 48 (1960) 5.

58. P. Rempp, Pure Appl. Chem. 46 (1976) 9.

59. M. Higuchi and R. Senju, Polymer Journal 3 (1972) 370.

60. J. J. Bourguignon and J. C. Galin, Macromolecules 10 (1977) 804.

61. D. B. James, R. E. Wetton and D. S. Brown, Polymer 20 (1979) 187.

62. M. Gordon and J. S. Taylor, J. Appl. Chem. 2 (1952) 493.

63. J. G. Dash, Films on Solid Surfaces (Academic Press, New York, 1975).

64. J. C. LeBosse, J. Lopez and J. Rousseau-Violet, Surf. Sci. 72 (1978) 125.

65. J. Lopez and G. Allan, Surf. Sci. 103 (1981) 456.

66. B. I. Lundqvist, H. Hjelmberg and O. Gunnarsson in Photoemission and the Electronic Properties of Surfaces, Edited by B. Feuerbacher, B. Fitton and R. F. Willis (Wiley, New York, 1978).

67. D. L. Adams, Surf. Sci. 42 (1974) 12.

68. J. B. Peri, J. Phys. Chem. 69 (1965) 231.

69. J. L. Gland and V. N. Korchak, Surf. Sci. 75 (1978) 733.

70. D. L. Adams and L. H. Germer, Surf. Sci. 32 (1972) 205.

71. L. R. Clavenna and L. D. Schmidt, Surf. Sci. 33 (1972) 11.

72. R. A. Armstrong, Can. J. Phys. 46 (1968) 949.

73. D. A. King and M. G. Wells, Proc. R. Soc. Lond. A 339 (1974) 245.

74. D. O. Hayward in Chemisorption and Reaction on Metallic Surfaces, Ed. J. R. Anderson (Academic Press, London, 1971).

75. D. L. Adams and L. H. Germer, Surf. Sci. 26 (1971) 109.

76. D. L. Adams and L. H. Germer, Surf. Sci. 27 (1971) 21.

77. L. R. Clavenna and L. D. Schmidt, Surf. Sci. 22 (1970) 365.

78. G. Erlich and F. G. Hudda, J. Chem. Phys. 35 (1961) 1421.

79. P. J. Estrup and J. Anderson, J. Chem. Phys. 45 (1966) 2254.

80. L. W. Anders, R. S. Hansen and L. S. Bartell, J. Chem. Phys. 62 (1975) 1641.

81. C. G. Goymour and D. A. King, JCS Faraday I 69 (1973) 749.

82. P. W. Tamm and L. D. Schmidt, J. Chem. Phys. 51 (1969) 5352; 52 (1970) 1150.

83. P. Kisliuk, J. Phys. Chem. Solids 3 (1957) 95; 5 (1958) 78.

84. G. M. J. Schmidt in Solid State Photochemistry, Ed. D. Ginsburg (Verlag Chemie, Weinheim, New York, 1976).

85. A. Elgavi, B. S. Green and G. M. J. Schmidt, J. Amer. Chem. Soc. 95 (1973) 2058.

86. M. D. Cohen, A. Elgavi, B. S. Green, Z. Ludmer and G. M. J. Schmidt, J. Amer. Chem. Soc. 94 (1972) 6776.

87. B. S. Green, M. Lahav and G. M. J. Schmidt, J. Chem. Soc. (B) (1971) 1552.

88. B. E. Warren, X-Ray Diffraction (Addison-Wesley Publishing Company, London, 1969).

89. P. Duwez, Trans. AIME 191 (1951) 765.

90. Z. Nishiyama, M. Oka and H. Nakagawa, Trans. JIM 7 (1966) 168.

91. J. T. A. Pollock and H. W. King, J. Mater. Sci. 3 (1968) 373.

92. Z. Nishiyama, Martenistic Transformation (Academic Press, New York, 1978).

93. H. Sato in Physical Chemistry: An Advanced Treatisc, Ed. H. Eyring, D. Henderson and W. Jost (Academic Press, New York, 1970).

94. F. E. Jaumet, Jr. and C. H. Sutcliffe, Acta Mettallurgica 2 (1954) 63.

95. N. W. Lord, J. Chem. Phys. 21 (1953) 692.

96. J. O. Clayton and W. F. Giauque, J. Amer. Chem. Soc. 54 (1932) 2610.

97. D. A. McQuarrie, Statistical Mechanics (Harper and Row, New York, 1976).

98. J. W. Evans and D. K. Hoffman, "Random and Cooperative Irreversible Processes on Lattices. III. Density Expansions", preprint.

9. ACKNOWLEDGMENTS

I would like to thank Dr. Hoffman for his guidance in this research and throughout my graduate career. Dr. Jim Evans has also contributed to this research in a significant way and receives special acknowledgment. All members of Dr. Hoffman's research group (Dave Evans, Nick Wolf, Bob Cole, C. K. Chan and Ross Nord) have been very supportive. I especially recognize Nick Wolf for his support during the early years of my graduate study. The final stages of my graduate career have gone smoothly due to the efforts of an excellent typist, Wanda Lembke, and a special friend, Donna Boschert.

Working with youth and other organizations, I have associated with many good people in the Ames area. Each has touched my life. I am grateful to my parents and family, whose support I have felt throughout my life, and especially during crucial periods of my graduate study. Finally, I acknowledge a loving Heavenly Father, from whom all blessings flow.

10. APPENDIX A: CONDITIONAL PROBABILITIES FOR CB3

1. 
2. 
3. 
4. 
5.
6.
7. 
8.
9. 
10.
11.
12.
13.
14.
15.
16.
17.
18. 
19.
20. 
21. 
22. 
23. 
24. 
25. 
26. 
27. 
28. 
29. 
30. 
31. 
32. 
33. 
34. 
35. 
36. 
37. 
38. 
39. 
40. 
41.
42.
43.
44.
45.
46.
47.
48.
49.
50.
51.
52.
53.
54.
55.
56.
57.
58.
59.
60.
61.
62.
63.
64.
65.

66. 
67. 
68. 
69. 
70. 

71. 
72. 
73. 
74. 
75. 

76. 
77. 
78. 
79. 
80. 

81. 
82. 
83. 
84. 
85. 

86. 
87. 
88. 
89. 
90. 

91. 
92. 
93. 
94. 
95. 

96. 
97. 
98. 
99. 
100. 

101. 
102. 
103.
104. 
105. 

106.
107.
108.
109.
110.

111.
112.
113.
114.
115.

116.
117.
118.
119.
120.

121.
122.
123.
124.
125.

126.
127.
128.

11. APPENDIX B: DENSITY EXPANSION FOR THE SRO X-RAY INTENSITY

Equation 7.1 for the short range order (SRO) intensity can also be written in virial expansion form. The density virial expansion for the probability of finding two transformed sites at a vector $\underline{r}$ from each other, $P_{BB}(\underline{r})$, has previously been given by Hoffman (47) for an Arrhenius choice of rates with pairwise additive activation energies. A generalization of the technique has also been developed for arbitrary rates (98). Following Hoffman

$$P_{BB}(\underline{r}) = A_2(\underline{r})\ \theta^2 + A_3(\underline{r})\ \theta^3 + A_4(\underline{r})\ \theta^4 + \cdots \tag{11.1}$$

where the θ independent coefficients are exactly obtainable and can be written in a form involving Mayer cluster diagrams. Then,

$$C(x\xrightarrow{\underline{r}}x) = (A_2(\underline{r})-1)\ \theta^2 + A_3(\underline{r})\ \theta^3 + A_4(\underline{r})\ \theta^4 + \cdots \tag{11.2}$$

and

$$I_{SRO}/N(f_A-f_B)^2 = \sum_{\underline{r}} \{[A_2(\underline{r})-1]\ \theta^2 + A_3(\underline{r})\ \theta^3 + A_4(\underline{r})\ \theta^4 + \cdots] \times \cos\left[\frac{-2\pi i}{\lambda}\ \underline{r}\cdot(\hat{S}-\hat{S}_o)\right] . \tag{11.3}$$

The following definitions are then made:

$$\underline{h} = (\hat{S}-\hat{S}_o)$$

$$C_2(\underline{h}) = \sum_{\underline{r}} [A_2(\underline{r})-1] \cos(-2\pi\ \underline{r}\cdot\underline{h})$$

$$C_3(\underline{h}) = \sum_{\underline{r}} A_3(\underline{r}) \cos(-2\pi\ \underline{r}\cdot\underline{h})$$

$$C_4(\underline{h}) = \sum_{\underline{r}} A_4(\underline{r}) \cos(-2\pi\ \underline{r}\cdot\underline{h})$$

$$\vdots \qquad (11.4)$$

Equation B.3 then transforms to

$$I_{SRO}(\underline{h})/N(f_A-f_B)^2 = \theta^2[C_2(\underline{h})+C_3(\underline{h})\theta+C_4(\underline{h})\theta^2+\cdots] \qquad (11.5)$$

which is the desired virial expansion for the SRO intensity as a function of $\underline{h}$.